Autismus-assoziierte Mutationen beeinträchtigen die Funktion des N-Terminus von Shank3 in der postsynaptischen Signaltransduktion

Dissertation

zur Erlangung der Würde des
Doktors der Naturwissenschaften (Dr. rer. nat.)
an der Fakultät für Mathematik, Informatik und Naturwissenschaften
des Fachbereichs Biologie
der Universität Hamburg

vorgelegt von

Fatemeh Hassani Nia
aus dem Iran

Hamburg 2019

Datum der Disputation: 03.05.2019

Gutachter der Dissertation:

1. Gutachter: Prof. Dr. Hans-Jürgen Kreienkamp
2. Gutachter: Prof. Dr. Christian Lohr

Autism-associated mutations interfere with the function of the Shank3 N-terminus in postsynaptic signaling pathways

DISSERTATION

SUBMITTED FOR THE DOCTORAL DEGREE
DEPARTMENT OF BIOLOGY
UNIVERSITY OF HAMBURG

By

Fatemeh Hassani Nia
from Iran

Hamburg 2019

The experimental part of the present work was carried out in the Institute for Human Genetics at the University Medical Center Hamburg-Eppendorf (UKE) under supervision of Prof. Dr. Hans-Jürgen Kreienkamp in the period of July 2015 to March 2019.

Date of disputation: 03.05.2019

Reviewer of the dissertation:

Prof. Dr. Hans-Jürgen Kreienkamp (Supervisor)

Prof. Dr. Christian Lohr (Advisor)

For

My Guardian Angels

Vajiheh & Meyfar

Abstract

Autism Spectrum Disorders (ASDs) are neurodevelopmental disorders characterized by deficits in social communication as well as repetitive behaviors. The analysis of genetic causes for ASDs has identified a significant contribution of risk genes that mainly encode proteins involved in synapse formation, development and function, suggesting that ASDs may be described as synaptopathies.

The *SHANK3 gene,* coding for the postsynaptic scaffold protein Shank3, was one of the first genes shown to be associated with ASDs. A variety of mutations in this gene have been identified in association with an autism phenotype. Loss of one copy of the *SHANK3* gene located on chromosome 22 leads to 22q13 deletion/Phelan-McDermid syndrome, which is associated with severe intellectual disability and autism. Interestingly, several missense mutations associated with ASDs affect the N-terminal part of Shank3 which contains the highly conserved Shank/ProSAP N-terminal (SPN) and Ankyrin repeat (Ank) domains. Still the relevance of these mutations for Shank3 function and autism pathogenesis is unclear.

The SPN domain is engaged in an intramolecular interaction with the Ank domain. Importantly, it also constitutes a high affinity binding site for several Ras family G-proteins, including active, GTP-bound variants of Ras and Rap1. The ability of Shank3 to bind to active small G-proteins via its SPN domain might affect signal transduction at synapses in different ways. Either Shank3 could be a downstream effector of Ras signaling in a so far unidentified pathway, or it could function as a negative regulator of pathways that require small G-proteins by sequestering and thus limiting their availability.

Interestingly, two autism-associated mutations in *SHANK3* (L68P and R12C) disrupt the interaction between Shank3 and the small G-proteins of the Ras family. In addition, L68P directly affects Ank domain interactions by disrupting the regulatory effect of the SPN domain on the Ank repeats.

This study represents an attempt to clarify the role of the Shank3 N-terminus in the functioning of synapses and to determine the mechanisms in which the molecular interactions of the Shank3 N-terminus and ASD-associated mutations in this part contribute to the development of autism.

Super resolution imaging applied for the investigation of the spatial distribution of Shank3 in the postsynaptic density revealed that Shank3 co-clusters with the synaptic marker PSD95 in distinct nanodomains within a same synaptic unit.

Activation of the Ras/MAPK pathway in a human cell line, and overexpression of active GTP-bound Ras in neurons showed that the Ras-SPN interaction causes a significant attenuation of the interaction of Shank3 with SAPAP1, another postsynaptic scaffold protein. This subsequently results in separation of Shank from the synaptic PSD95/SAPAP/Shank complex, which constitutes the core of the postsynaptic density, and leads to colocalization of Shank3 with active Ras.

Further experiments revealed that overexpression of Shank3 WT in neurons suppresses filopodia formation and neurite outgrowth by sequestering active Rap1 and inhibiting the integrin activation pathway.

Several approaches were taken in this study to identify new interaction partners of the N-terminus of Shank3; initial work in a human cell line revealed that the Ank domain of Shank3 is a high affinity

binding site for RNA binding proteins such as DDX5 which might be functionally relevant in a Shank3 isoform-dependent manner. More importantly for the synaptic function of Shank3, two members of the Catenin family, β-Catenin and δ-Catenin, were identified as novel interaction partners of Shank3 at postsynaptic sites. These two proteins appeared to target distinct binding domains on Shank3. β-Catenin binds to the PDZ domain of Shank3, most likely through a putative internal PDZ ligand, whereas δ-Catenin binds to the Shank3 Ank domain via its Armadillo-repeat domain. Further investigations revealed that the lack of Shank3 proteins containing an N-terminal Ank domain results in loss of postsynaptic δ-Catenin. On the other hand, the L68P mutation in the Shank3 SPN domain, that causes an open conformation of the Shank3 N-terminus according to the results of FRET analyses in this study, significantly increased the interaction of Shank3 with δ-Catenin.

The data presented in this thesis show that Shank3 is integrated in small G-protein as well as Catenin dependent signaling pathways which may be disrupted in autistic patients due to mutations in *SHANK3*.

Abbreviations

aa.	amino acid
Ank	Ankyrin repeat region
AMPA	α -Amino-3-hydroxy-5-Methyl-4-isoxazole Propionic Acid
ASD	Autism Spectrum Disorder
bp	base pair(s)
BSA	Bovine Serum Albumin
°C	degree Celsius
CamKII	Ca^{2+}/calmodulin-dependent protein Kinase II
cm	centimeter
CNS	Central Nervous System
CREB	cAMP Response Element-Binding protein
C-terminal	Carboxy terminal
Dapi	4',6-Diamidino-2-phenylindole
ddH2O	double distilled water
DMEM	Dulbecco's Modified Eagle's Medium
DNA	Deoxyribonucleic Acid
dNTP	deoxyribonucleoside 5'-TriPhospate
E. coli	Escherichia Coli
EGF	Epidermal Growth Factor
EGFP	Enhanced Green Fluorescence Protein
EPSC	Excitatory Post Synaptic Current
ERK	Extracellular signal-Regulated Kinase
F-actin	Filamentous actin
FBS	Fetal Bovine Serum
g	gram(s)
GABA	γ-Aminobutyric Acid
GKAP	Guanylate-Kinase Associated Protein
GTP	Guanosine-5'-triphosphate
hr	hour(s)
HBSS	Hank's Balanced Salt Solution
HCN1	Hyperpolarization-activated Cyclic Nucleotide-gated cation channel1
HEK	Human Embryonic Kidney
kb	kilobase(s)
kDa	kilo Dalton
KO	Knockout
L	liter(s)
LB	Lysogeny Broth
LTD	Long-Term Depression
LTP	Long-Term Potentiation
M	Molar

Map2	Microtubule-associated protein 2
MAPK	Mitogen-Activated Protein Kinase
MEM	Minimum Essential Medium
mGluR	metabotropic Glutamate Receptor
µ	micro
min	minute(s)
mRFP	monomeric Red Fluorescent Protein
mRNA	messenger Ribonucleic Acid
mTOR	mammalian Target Of Rapamycin
n	nano
NLS	Nuclear Localization Signal
NMDA	N-Methyl-D-Aspartate
N-terminal	amino terminal
NHS	N-Hydroxy-Succinimidyl
OD	Optical Density
PALM	Photo-Activated Localization Microscopy
PBS	Phosphate-Buffered Saline
PCR	Polymerase Chain Reaction
PDZ	PSD-95/DLG/ZO1
PLL	Poly-L-Lysine
PMSF	Phenyl-Methyl-Sulfonyl Fluoride
Proline-rich	Proline-rich region
PSD	Post Synaptic Density
RIPA	Radioimmunoprecipitation Assay
rpm	revolutions per minute
sec	second(s)
SAM	Sterile Alpha Motif
SAPAP	SAP90/PSD-95-Associated Protein
SH3	Src Homology 3
Shank	SH3 and multiple ankyrin repeats
SDS	Sodium Dodecyl Sulfate
SPN	Shank/ProSAP N-terminal
STED	STimulated Emission Depletion
TAE	Tris-Acetate/EDTA
TBS-T	Tris-Buffered Saline-Tween20
TEMED	N,N'N,N'-Tetra-Methyl-Ethylene-Diamine
TNIK	TRAF2 and NCK-Interacting protein Kinase
U	Unit(s) of enzyme activity

Table of Contents

Chapter 1

Introduction

1.1 Synapse

1.1.1 Neurons

The human brain contains approximately 85–100 billion highly complex cells known as nerve cells or neurons that form a network of connectivity throughout the brain via specialized structures called synapses (Lin and Man, 2013). Neurons consist of a cell body (or soma) containing cell organelles and long branching neurites called axons and dendrites (figure 1.1). The single axon is a dominating neurite that conducts signals from the cell body to presynaptic terminals, whereas dendrites are branched processes that receive synaptic input from other neurons and conduct signals to the integration site, which is often the cell body (Chklovskii, 2004, Franze and Guck, 2010).

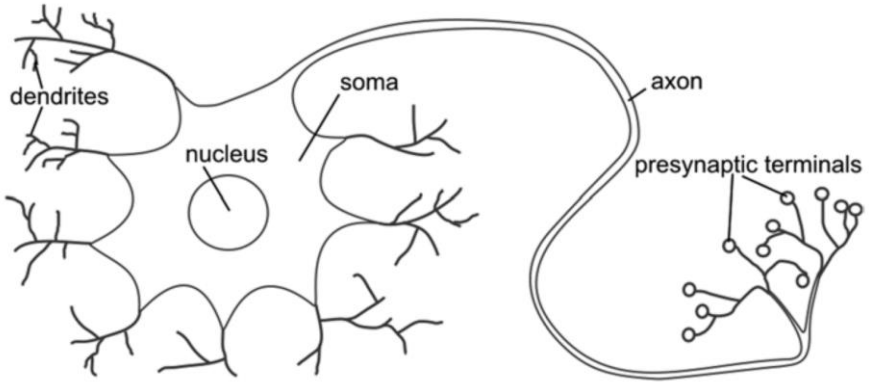

Figure 1.1 Typical morphology of a neuron. Typical neurons consist of a cell body containing nucleus and other organelles, an axon and multiple dendrites. From (Franze and Guck, 2010).

1.1.2 Synapses

Synapses are intercellular junctions specialized to transfer information. Synapses occur where a signal is transferred from a neuron to a target cell which is usually another neuron, via a contact between a presynaptic axon and a postsynaptic dendrite (Südhof, 2008, Sheng and Hoogenraad, 2007). The two major types of the brain's synapses are known as excitatory and inhibitory synapses. Excitatory, glutamatergic synapses form through contact between glutamate-releasing axon terminals and postsynaptic sites containing glutamate receptors which include ionotropic glutamate receptors such as N-methyl-D-aspartat (NMDA) and α -amino-3-hydroxy-5-methyl-4-isoxazole propionic acid (AMPA) receptors as well as metabotropic glutamate receptors (mGluRs). Inhibitory synapses form through contact between postsynaptic specializations containing GABA or glycine receptors with the presynaptic terminals positive for GABA or glycine (Sheng and Kim, 2011, Fogarty et al., 2016, Levinson and El-Husseini, 2005). The number and integration of excitatory and inhibitory synaptic inputs regulates the likelihood of firing action potentials and mediates neuronal signal processing to maintain neural networks in a balanced state (Schummers et al., 2002).

The morphology of inhibitory and excitatory synpases is depicted in figure 1.2. Inhibitory synapses form on the dendritic shafts, whereas excitatory synapses are often localized on dendritic spines which are small membranous actin rich protrusions harbouring the postsynaptic apparatus of glutamatergic receptors and other postsynaptic components. A gap of 20 to 25 nm called the synaptic cleft separates the pre- and postsynaptic sites. (Franze and Guck, 2010, van Spronsen and Hoogenraad, 2010).

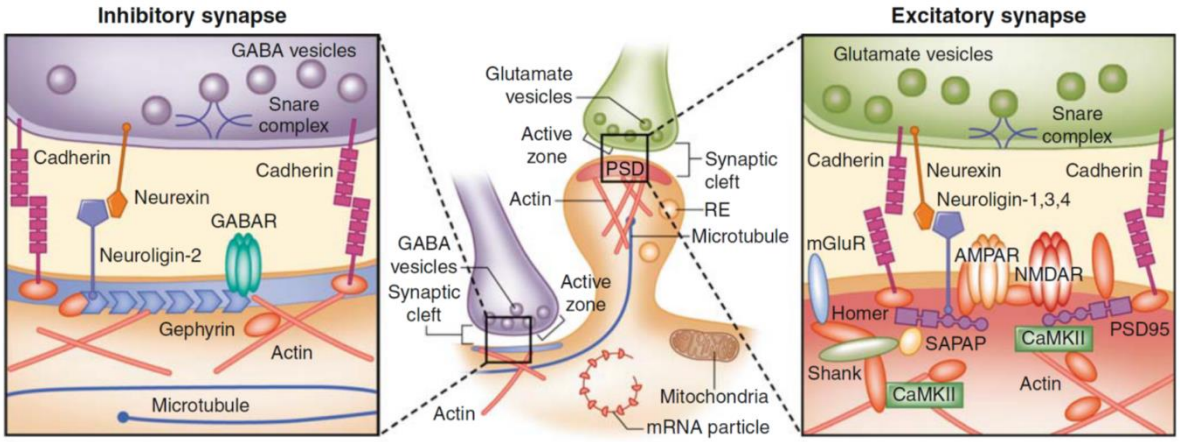

Figure 1.2 Molecular architecture of inhibitory and excitatory synapses. The microanatomy of the inhibitory and excitatory synapses and their organization of proteins and protein–protein interactions are depicted in the left and right panels, respectively. From (van Spronsen and Hoogenraad, 2010).

1.1.3 The postsynaptic density

The postsynaptic density (PSD) is a highly complex protein network in dendritic spines typically located on the head of the spine that closely opposes the presynaptic active zone. It contains a large number of proteins including receptors, scaffolds, and signal transduction molecules (figure 1.2). As clusters of synaptic vesicles containing neurotransmitters are docked to the presynaptic active zone which are ready to release the neurotransmitters to the synaptic cleft via vesicle exocytosis, the PSD guarantees a successful synaptic transmission by organizing the neurotransmitter receptors opposite to active zones (Nimchinsky et al., 2002, Meyer et al., 2014, van Spronsen and Hoogenraad, 2010).

The PSD appears as an electron-dense thickening of the postsynaptic membrane under electron microscopy. However, recent studies using super-resolution imaging techniques have investigated the molecular architecture of synapses and revealed that the major postsynaptic proteins are organized into nanoclusters in the postsynaptic density (MacGillavry et al., 2013, Nair et al., 2013, Fukata et al., 2013).

1.1.4 Synaptic plasticity

The synaptic connections between neurons can undergo long-lasting changes in strength (Ramiro-Cortés et al., 2013). The bidirectional ability of synapses to strengthen or weaken in response to a persistent pattern of synaptic activity is known as synaptic plasticity, which is thought to be the cellular basis of learning and memory. These changes that occur locally at individual synapses can be experimentally observed as long-term potentiation (LTP) or long-term depression (LTD) (Bailey et al.,

2015, Diering and Huganir, 2018). LTP is a persistent increase in synaptic strength induced by brief high-frequency stimulation which is associated with increasing synapse size as well as insertion of AMPA receptors, whereas LTD is a persistent decrease in synaptic strength induced by longer episodes of low-frequency stimulation that results in shrinkage or loss of synapses (Zhou et al., 2004, Bailey et al., 2015, Han et al., 2017, Makino and Malinow, 2009). Since the imbalance of excitatory/inhibitory (E/I) synapses underlies several neurological diseases including epilepsy and ASDs, the size and number of excitatory and inhibitory synapses is tightly regulated, and the long-term plasticity of glutamatergic and GABAergic synaptic transmission occurs in a concerted manner in order to adjust the balance of E/I synaptic transmission (Bourne and Harris, 2011, Bonansco and Fuenzalida, 2016).

1.2 Synaptopathy

Both synaptogenesis and synaptic plasticity are highly complex processes which are subject to precise regulatory mechanisms to maintain neuronal homeostasis and proper functioning of the brain. Impairing the function of a single component in this system can lead to a group of brain diseases arising from synaptic dysfunction which have been termed synaptopathies. Synaptopathies are believed to be the major determinant of several neurodevelopmental and neurodegenerative diseases such as autism spectrum disorders (ASD), epilepsy, Alzheimer and Parkinson disease (Grant, 2012, Lepeta et al., 2016).

1.2.1 Autism Spectrum Disorders (ASDs)

Autism Spectrum Disorders (ASDs) are a heterogeneous group of neurodevelopmental disorders characterized by deficits in social interactions, poor language development, stereotyped behaviours and restricted patterns of interest and activities. According to the Diagnostic and Statistical Manual of Mental Disorders (DSM-IV), ASD encompasses three different pervasive disorders including autistic disorder, Asperger disorder, and pervasive developmental disorder not otherwise specified (PDD-NOS) (American Psychiatric Association, 2013). In 2003 autism spectrum disorders have been defined as a form of synaptopathies caused by an E/I imbalance (Rubenstein and Merzenich, 2003), but still the causes of autism are largely unknown.

Molecular genetic studies have shown a high genetic contribution. In particular, chromosomal rearrangements, rare *de novo* copy-number variants and *de novo* coding-sequence variants have been found to contribute to up to 25% of ASD cases (Geschwind, 2009, Huguet et al., 2013).

Contrary to the wide genetic landscape of ASD, the genes associated with this disorder are mainly involved in a limited number of biological pathways including chromatin remodelling, protein translation, actin dynamics, and synaptic functions (Bourgeron, 2009, Huguet et al., 2013, Toro et al., 2010). In several cases, the proteins encoded by ASD risk genes have been shown to be involved in synapse formation, development and function (Kelleher et al., 2012). These include cell adhesion proteins of the Neuroligin and Neurexin families (Jamain et al., 2003); proteins involved in signaling (e.g., regulators of small G-protein signaling such as Epac or SynGAP (Clement et al., 2012, Woolfrey et al., 2009)); and scaffold proteins of excitatory, glutamatergic synapses, including all three members of the Shank family (Berkel et al., 2010, Durand et al., 2007, Gauthier et al., 2009, Moessner et al., 2007) (figure

1.3). These studies confirm the theory considering ASDs as synaptopathies which result from an aberrant synaptic transmission affecting specific brain circuits (Leblond et al., 2014, Martella et al., 2018).

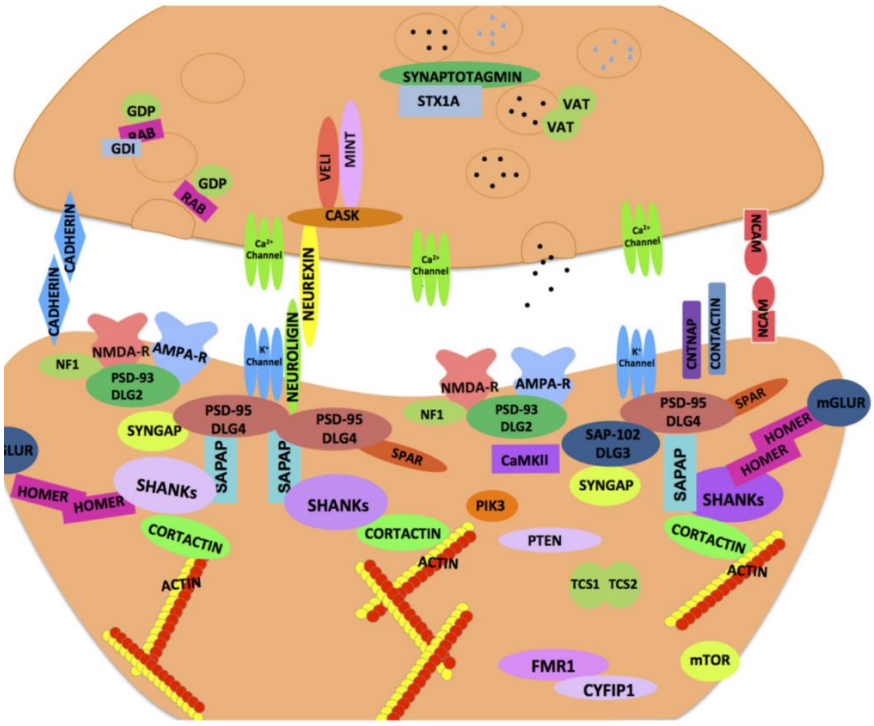

Figure 1.3 Synaptic proteins implicated in neurodevelopmental and neuropsychiatric disorders. A schematic illustration of an ensemble of pre- and postsynaptic proteins. The majority of these proteins are highly conserved across species and thought to confer susceptibility to a host of neurodevelopmental and neuropsychiatric disorders including ASD. From (Banerjee et al., 2014)

1.3 Shank

SH3 and multiple Ankyrin repeats (Shank) proteins are 'master' scaffolding proteins in the postsynaptic density of excitatory synapses that integrate intermediate scaffolding proteins, and their proper performance is critical for synaptic development and function. These multiple domain proteins with around 2000 residues in length encoded by the three genes *SHANK1*, *SHANK2,* and *SHANK3* and share 63-87% homology in their sequences (Guilmatre et al., 2014, Sheng and Kim, 2000). Deletions, duplications and coding mutations in the *SHANK* genes have been repeatedly reported in patients with ASD (Leblond et al., 2014).

Shank genes show distinct patterns of expression. In the adult rat, *Shank1* is exclusively expressed in brain, *Shank2* mRNA is expressed not only in brain but also at lower levels in kidney and liver and *Shank3* is predominantly expressed in brain, spleen and heart. In the brain, *Shank1* is expressed in hippocampus, cortex, amygdala, substantia nigra, and thalamus. *Shank2* and *Shank3* share a common expression in different brain regions, including hippocampus and cortex. In the cerebellum, *Shank1* and *Shank2* are expressed in Purkinje cells, whereas *Shank3* is expressed in the granular cell layer (Lim et al., 1999, Zitzer et al., 1999, Boeckers et al., 1999).

All three members of the Shank family share a similar set of domains including a Shank/ProSAP N-terminal (SPN) domain, a set of multiple ankyrin repeats (Ank), a Src homology 3 (SH3) domain, a PSD-95/DLG/ZO1 (PDZ) domain, a long Proline-rich region (Proline-rich) and a C-terminal sterile alpha motif (SAM) domain (Sheng and Kim, 2000) (figure 1.4). Through these domains Shank proteins bind to a

large number of postsynaptic proteins and have the potential to establish an indirect interaction between the glutamate receptors and the actin cytoskeleton. Several transcript variants are generated through alternative splicing and the use of alternative promoters, leading to omission of individual protein interaction motifs. Thus only the Shank2 proteins expressed in epithelial cells, but not those expressed in brain, possess N-terminal SPN and Ank domains (McWilliams et al., 2004).

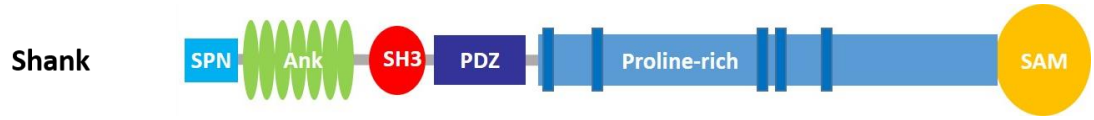

Figure. 1.4 Domain organization of Shank family proteins. All three members of the Shank family share a similar set of domains. The binding sites for the interaction partners of the Prolin-rich region (including Abi-1, IRSp53, Homer, Dynamin and Cortactin) have been depicted by rectangles.

Well characterized interaction partners of the Shank PDZ domain are members of the GKAP (also known as SAPAP) protein family that mediate an indirect interaction between Shank proteins and the NMDA receptors through binding to postsynaptic scaffold proteins of the PSD-95 family (Naisbitt et al., 1999, Boeckers et al., 1999). Homer, an interaction partner of the Proline-rich region of Shank, binds to metabotropic glutamate receptors (mGluRs) and IP3 receptors (Tu et al., 1999, Xiao et al., 1998). Cortactin, another interaction partner of the Proline-rich region, is an actin binding protein that along with the other interaction partners such as IRSp53, Abi-1 and α-Fodrin connects Shank proteins to the actin cytoskeleton (Du et al., 1998, Wu and Parsons, 1993, Bockmann et al., 2002, Proepper et al., 2007, Boeckers et al., 2001, Soltau et al., 2002). The SAM domain of Shank that has an essential role in synaptic targeting of Shank proteins (Boeckers et al., 2005, Baron et al., 2006) , in fact enables them to multimerize in a tail-to-tail manner and allows cross-linking of multiple sets of Shank-associated protein complexes at postsynaptic sites (Sheng and Kim, 2000). Interestingly the SAM domain of Shank2 and Shank3 (but not Shank1) is Zn^{2+} sensitive. Therefore, the synaptic targeting and the postsynaptic level of these two proteins is dependent on the SAM domain and regulated via Zn^{2+} ions, respectively (Baron et al., 2006, Grabrucker, 2014). In contrast, the postsynaptic localization of Shank1 is mediated by the PDZ domain binding to SAPAP and follows the formation of the PSD 95/GKAP complexes (Sala et al., 2001, Romorini et al., 2004).

		SHANK1	*SHANK2*	*SHANK3*
DNA	chromosome	19q13.3	11q13.3	22q13.3
	damaging mutations in Controls	1.02%	2.66%	1.07%
	truncating mutations in Controls	0%	0%	0%
RNA & Proteins	mRNA localization in neurons	soma and dendrites (hippocampal & Purkinje cells)	soma and dendrites (Purkinje cells)	soma and dendrites (hippocampal neurons)
	expression pattern	high in cortex	broad in brain (cerebellar Purkinje cells)	high in striatum (cerebellar granule cells)
Synapses	localization	glutamatergic synapses	glutamatergic synapses	glutamatergic synapses
	expression dynamics	3rd Shank at the synapse	1st Shank at the synapse	2nd Shank at the synapse
	effect loss	decrease in GKAP & Homer	increase in NMDAR NR1	decrease in NMDAR NR1 and AMPAR
	zinc dependence	independent	dependent	dependent
Spines	effect of loss	decreased size of spine heads	decreased number of mature spines	decreased number of mature spines
	effect of gain		increased number of mature spines	increased number of mature spines
	effect of mutation in ASD		reduction of synaptic density affect spine induction & morphology	reduction of synaptic density affect spine induction & morphology
Synaptic currents	effect of loss	normal NMDA and AMPA	increase/decrease NMDA*	decrease NMDA and AMPA
Mouse behavior	social interactions	reduced	reduced	reduced
	vocal behaviors	abnormal	abnormal	abnormal
	activity	reduced	increased	reduced
	stereotypies		increased	increased
	learning	enhanced (but reduced memory)	reduced	reduced
Truncating mutations	ASD	0.04%	0.17%	0.69%
	ASD (IQ>70)	0.12%	0.30%	0%
	ASD (IQ≤70)	0%	0.33%	2.12%
IQ	ASD	95±11	62±17	30±8
Penetrance	males	high	high	high
	females	incomplete	not reported	high

Table 1.1 Summary of the functions of Shank proteins and of the main findings obtained for patients with ASDs. From (Leblond et al., 2014).

1.4 Shank3

SHANK3 was the first gene in the *SHANK* family which was shown to be associated with ASDs. Loss of one copy of the region on chromosome 22 including the Shank3 gene leads to 22q13 deletion/Phelan-McDermid syndrome, which is associated with severe intellectual disability and autism (Bonaglia et al., 2006). Animal models of *Shank3* loss or mutation show several circuit defects in a wide range of brain regions and various degrees of synaptic dysfunction and autistic-like behaviours (Bozdagi et al., 2010, Kouser et al., 2013, Peca et al., 2011, Tatavarty et al., 2018, Wang et al., 2011). In addition, duplication of the *SHANK3* gene in patients or overexpression of *Shank3* in mice leads to synaptic dysfunction and a neurological phenotype that highlights a *SHANK3* gene dosage effect (Han et al., 2013). A variety of insertions, deletions, nonsense, splice site and missense mutations have been identified in this gene in autistic patients (Leblond et al., 2014) (figure 1.5). In 2010 *SHANK3* was reported as a common gene between ASDs and schizophrenia (SCZ) by identifying two *de novo* mutations (R1117X and R536W) in the gene coding for this postsynaptic scaffolding protein in patients

ascertained for SCZ. The non-sense mutation (R1117X) results in a severely truncated Shank3 variant, leading to childhood-onset of schizophrenia and intellectual disability (Gauthier et al., 2010).

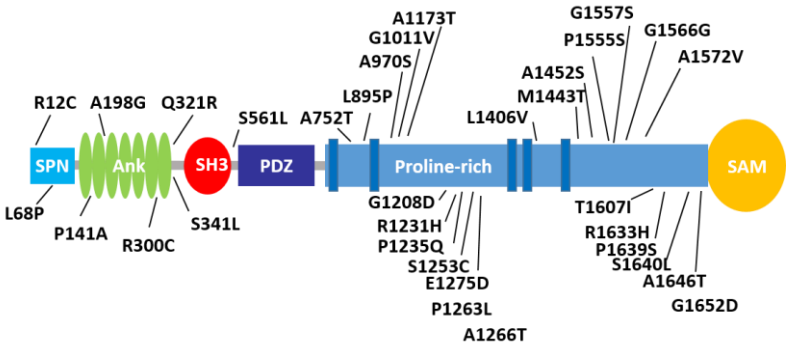

Figure 1.5 Shank missense variants found in patients with ASD. Adapted from (Leblond et al., 2014).

Through alternative splicing and intragenic promoters *Shank3* undergoes a complex transcriptional regulation in brain that results in diverse Shank3 isoforms. These isoforms are expressed in a cell type, developmental, and activity-dependent manner and display different subcellular distribution and differential effects on dendritic spine morphology (Wang et al., 2014) (figure 1.6).

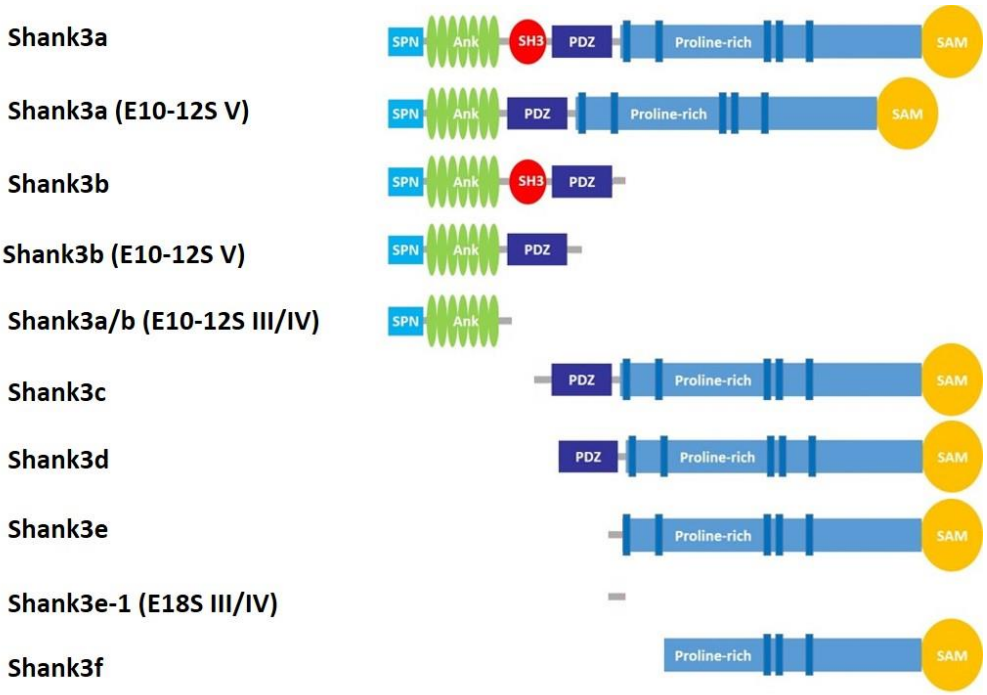

Figure 1.6 Diverse Shank3 isoforms result from intragenic promoters and alternative splicing. The predicted Shank3 protein isoforms were deduced from the combination of intragenic promoters and alternative splicing of mRNAs. Interestingly, the alternatively spliced exons are concentrated in the conserved SH3, proline-rich, and SAM domains of Shank3 and result in protein species with different combinations of the five functional domains. Some of these splice variants result in truncated isoforms only containing the N-terminal portion and some produce C-terminal truncated Shank3 isoforms lacking the SAM domain which most likely cannot be targeted to the synapses, very similarly to the already reported Shank3 variants resulted from truncating mutations. E stands for exon and S represents splice variants. Adapted from (Wang et al., 2014).

1.4.1 The structure and function of the Shank3 N-terminus

In 2013 Mameza et al. reported that in the long variants of Shank1 and Shank3 the N-terminal Ank repeats are preceded by a highly conserved domain termed the Shank/ProSAP N-terminal (SPN) domain which is affected by two autism-associated mutations (L68P and R12C) in *SHANK3* (Mameza et al., 2013). Further analysis of a SPN-Ank containing fragment of Shank3 using X-ray crystallography showed that the SPN domain is in a ubiquitin like (ubl) fold, very similar to the F0 domain of Talin (Lilja et al., 2017). In this three-dimensional structure, the seven ankyrin repeats of Shank3 are linked (by a 19 amino acid long linker region) to the 90 amino acid conserved SPN domain (figure 1.7). This structure confirms biochemical data indicating that the Shank3 SPN domain is engaged in an intramolecular interaction with Ank and forms a large interface with this region (Mameza et al., 2013).

1.4.2 Mutations affecting the Shank3 N-terminus

The N-terminal part of Shank3 is affected by seven missense mutations found in patients with ASDs (figure 1.7). The relevance of these mutations for Shank3 function and autism pathogenesis is still unclear (Boccuto et al., 2013, Durand et al., 2007, Gauthier et al., 2009, Moessner et al., 2007). Among these mutations, P141A and Q321R are *de novo* mutations (Boccuto et al., 2013, Moessner et al., 2007), whereas the rest are inherited, mainly from healthy parents (A198G, R300C and S341L) (Durand et al., 2007, Moessner et al., 2007). The two mutations that affect the SPN domain are inherited from an epileptic father (L68P) and a mother with social phobia (R12C) (Durand et al., 2007, Gauthier et al., 2009).

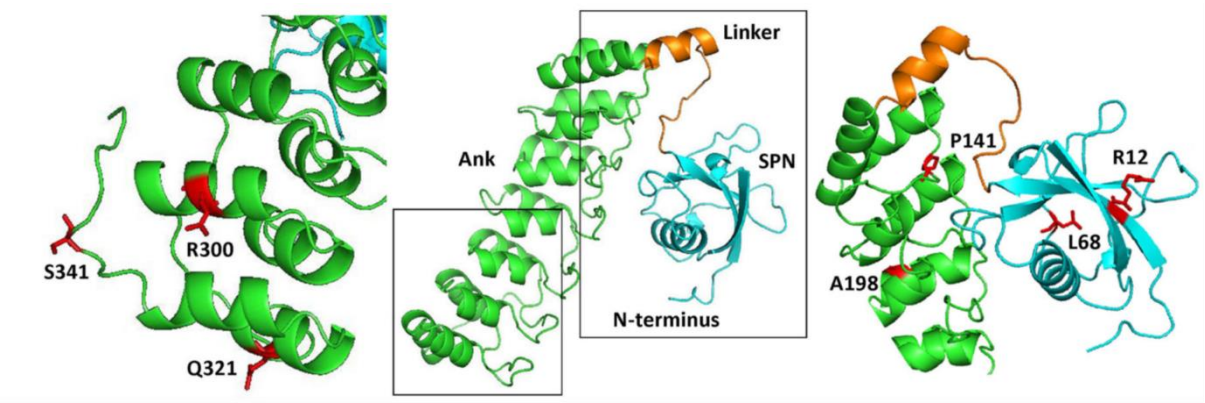

Figure 1.7 Three-dimensional structure of the N-terminus of Shank3, comprising the SPN and Ankyrin repeat (Ank) domains. The central part shows an overview, where both the SPN domain and the set of seven Ankyrin repeats can be clearly seen as individual domains connected by a short linker. Both the linker region and SPN domain are engaged in an extensive intramolecular contact with the Ank domain. To the right and left, enlarged and slightly rotated pictures show in red the positions and side chains of residues which have been shown to be altered in autistic patients. From (Hassani Nia and Kreienkamp, 2018).

1.4.3 The molecular interactions of Shank3 N-terminus

In 2001 two interaction partners for the Ank domain of Shank proteins were reported. First, the signalling protein Sharpin showed an interaction with the Shank Ank domain via its ubiquitin like domain. Sharpin was described to colocalize with Shank in the excitatory synapses (Lim et al., 2001). Furthermore, the actin-binding protein α-Fodrin provides another link to the actin cytoskeleton by a direct interaction with the Shank Ank repeats (Bockers et al., 2001). Yi et al. in 2016 reported the ion channels of the hyperpolarization-activated cyclic nucleotide-gated cation channel (HCN) family as novel interaction partners for the Shank3 Ank domain. HCN proteins form the I_h current, and mutation in SHANK3 was shown to cause an I_h-channelopathy (Yi et al., 2016). The Ank domain also has the intramolecular interaction partner SPN domain that blocks access of Ank domain ligands α-Fodrin and Sharpin (Mameza et al., 2013). Intriguingly, these interactors do not share any common sequence motifs which might predict a common way of binding to the Ank domain.
The SPN domain exhibits structural similarity to Ras binding/Ras association domains such as F0 domain of Talin (figure 1.8 A). Subsequent interaction studies confirmed that the SPN domain of Shank3 is in fact a novel Ras association domain that constitutes a high affinity binding site for several Ras family G-proteins, including active GTP-bound forms of Ras and Rap proteins (Lilja et al., 2017) (figure 1.8 B).

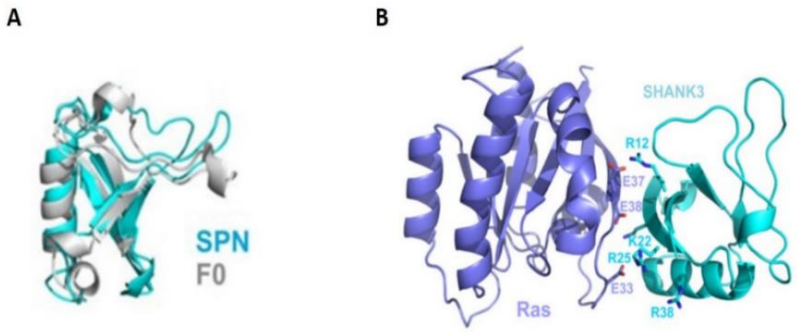

Figure 1.8 Structural analysis of the Shank SPN domain. A. Superposition of Shank3 SPN (cyan) and talin F0 (grey) domain structures. **B.** Model of the Shank3 SPN domain in complex with Ras based on the structure of RalGDS/active H-Ras complex. From (Lilja et al., 2017).

1.4.4 The functional relevance of mutations affecting the Shank3 N-terminus

Several studies have shown that the normal synaptic targeting of Shank3 is not affected by the mutations in the N-terminus (Arons et al., 2012, Durand et al., 2012, Mameza et al., 2013). Although overexpression of Shank3 WT in primary hippocampal neurons significantly increases dendritic spine density, the expression of N-terminal mutant variants show a moderate effect on the spine formation (Arons et al., 2012, Durand et al., 2012).
Shank3 WT (but not the N-terminal mutant variants) is shown to be involved in spine maturation by forming spines with larger heads (Durand et al., 2012). However, these results have been obtained using confocal microscopy and it is not clear whether the N-terminal mutations affect the spine morphology by changing the nanoscale organization of the Shank3 proteins in the postsynaptic density.

In 2013 Mameza et al. showed that the L68P mutant variant supports normal excitatory synaptic transmission by restoring the reduced mEPSC frequency in Shank3 knockdown neurons (treated with shShank3) to the control levels, similar to Shank3 WT (Mameza et al., 2013) . In another study, overexpression of Shank3 WT in hippocampal neurons significantly increased mEPSC frequency compare to the control neurons transfected with GFP, while missense mutations (R12C, R300C, Q321R) slightly increased mEPSC frequency but not as much as WT (Durand et al., 2012).

Shank3 has been reported to affect not only the excitatory postsynaptic but also presynaptic function by directly interacting with the cytoplasmic tails of Neuroligins (Meyer et al., 2004). Arons et al. showed that ASD-associated mutations in Shank3 (R12C, R300C and Q321R) interfere with the role of Shank3 in transsynaptic signalling. Unlike the overexpressed Shank3 WT, these three mutants failed to increase the level of postsynaptic Homer1 and presynaptic VGLUT1. In addition, the size of the total recycling pool (TRP) of synaptic vesicles (SVs) at presynaptic sites contacting dendritic profiles of neurons expressing these mutant variants of Shank3 significantly decreased compare to Shank3 WT neurons. Also, the authors observed that the amplitude of both AMPAR and NMDAR EPSCs dramatically decreased, and the synaptic failure rate highly increased when these mutant forms of Shank3 were compared to Shank3 WT (Arons et al., 2012).

A study in 2011 showed that the R12C mutant variant impairs the regulatory effects of Shank3 on the mGluR5 pathway. Using DHPG as an agonist of group I metabotropic glutamate receptors, the authors observed that upon loss of Shank3 the signaling pathway of mGluRs and subsequently phosphorylation of ERK1/2 and CREB was impaired. While reexpression of Shank3 WT and also of mGluR5 was able to rescue the DHPG-induced ERK1/2 phosphorylation, Shank3 R12C was not able to rescue the ERK1/2 phosphorylation induced by DHPG (Verpelli et al., 2011).

Interestingly, the two inherited mutations affecting residues in the Shank3 SPN domain (L68P and R12C) disrupt the interaction between Shank3 and the small G-proteins of Ras family. As predicted from the structural analysis, Arg 12 is involved in forming an ion pair with Glu 37 of Ras (figure 1.8 B). The side chain of Leu 68 is one of the key residues of the hydrophobic core and is involved in the proper folding of the SPN domain (figure 1.7). By disrupting any of these ion-pair and hydrophobic interactions, these two mutations interfere with Shank3 binding to the small G-proteins (Lilja et al., 2017). Moreover, the L68P mutation but not R12C was shown to disrupt the blockade of Ank by the SPN domain and improve the interaction of Shank3 with three Ank ligands (Sharpin, α-Fodrin and exogenous SPN), suggesting that this mutation most likely represents a permanent open conformation of the Shank3 N-terminus that not only dysregulates Ank domain function but also hinders Shank3 of interaction with small G-proteins of Ras family (Mameza et al., 2013, Lilja et al., 2017).

1.5 Aim of the project

The Shank3 N-terminus is the target of several missense mutations associated with ASDs. Intriguingly, the functional relevance of these mutations on a structural, molecular and cell biological level is poorly understood. So far, it has been clarified that two of these N-terminal mutations, R12C and L68P affect molecular interactions of the Shank3 protein. Both R12C and L68P mutations located in the SPN domain of Shank3 disrupt the interaction between Shank3 and the small G-proteins of Ras family. In addition, L68P directly affects Ank domain interactions by disrupting the regulatory effect of the SPN domain on the Ank repeats. How this may contribute to the autistic phenotype in the patients is unclear. More importantly, the effect of the other five mutations which alter residues in the Ank domain is completely unknown on a molecular level. It seems likely that the proper functioning of the Shank3 N-terminus and subsequently the full-length Shank3 protein is dependent on a precise cooperation between the SPN domain and Ank-repeat region which itself is regulated through an intramolecular interaction between these two domains.

In this study, I sought to determine the mechanisms in which the molecular interactions of the N-terminus of Shank3 contributes to the function of the Shank3 protein, and how this is altered by the ASD-related mutations affecting this part of the protein.

In this regard one important aspect was to define the relevance of the Shank3 N-terminus interaction with G-proteins of the Ras family for synaptic function, and for the development of autism. We assume that Shank3 is part of a synaptic Ras GTPase dependent signalling pathway which is disrupted by mutations in the N-terminal part of Shank3. Therefore, I aimed to clarify on a molecular level how the small G-proteins of Ras family affect the interactions and scaffolding capabilities of Shank3 and also, to assess the role of WT and mutant forms of Shank3 in mediating the effects of Ras on synapse formation. Along with this, I aimed to determine which interaction partners of the Shank3 N-terminus play a role in the CNS and more specifically, in the postsynaptic density. This also required finding so far unknown interaction partners of this part of the protein in neurons.

Additionally, since there is not much information about the spatial distribution of the Shank3 protein in the postsynaptic density, I aimed to resolve the nanoscale organization of Shank3 using super-resolution microscopy.

Chapter 2
Materials and Methods

2.1 Materials

2.1.1 Chemicals

All the chemicals used in this project were purchased from Merck, Sigma or Carl Roth unless otherwise indicated.

2.1.2 Microbial Strains, Laboratory Animals and Cell Lines

Organism	**Name**	**Source**
Bacterial E. Coli strains	Top10F' NEB Stable BL21 (DE3)	Thermo Fisher Scientific New England BioLabs New England BioLabs
Cell lines	HEK293-T U2OS	ATCC ATCC
Laboratory animals	*Rattus norvegicus* Shank3 KO Mice	Envigo Tobias Böckers, Ulm

2.1.3 DNA Plasmids

2.1.3.1 Basic Vectors

Name	**Remarks**	**Source**
pEGFP-C1	CMV promotor, green fluorescent protein, Kan^R	Clontech
pEGFP-C3	CMV promotor, green fluorescent protein, Kan^R	Clontech
pET SUMO	Bacterial expression; His_6-SUMO-tag, Kan^R	Thermo
pmRFP N1	CMV promotor, monomeric red fluorescent protein, Kan^R	RG Kreienkamp
pmRFP N3	CMV promotor, monomeric red fluorescent protein, Kan^R	RG Kreienkamp
pFRET	N-terminal GFP, C-terminal mCherry sequence, Kan^R	RG Kreienkamp
PMT2sm -HA	CMV promoter with HA tag, Amp^R	RG Rosenberger

2.1.3.2 Full length Shank3 Vectors

EGFP pHAGE- Shank3 WT	RG Kreienkamp
EGFP pHAGE- Shank3 L68P	RG Kreienkamp
EGFP pHAGE- Shank3 R12C	RG Kreienkamp
pmRFP- Shank3 WT	RG Kreienkamp
pmRFP- Shank3 L68P	RG Kreienkamp
pmRFP- Shank3 R12C	RG Kreienkamp
pmRFP- Shank3 P141A	RG Kreienkamp
MYC His- Shank3 WT	RG Kreienkamp
MYC His- Shank3 L68P	RG Kreienkamp
MYC His- Shank3 R12C	RG Kreienkamp
MYC His- Shank3 R300C	RG Kreienkamp
MYC His- Shank3 Q321R	RG Kreienkamp
MYC His- Shank3 A198G	RG Kreienkamp
MYC His- Shank3 S341L	RG Kreienkamp

2.1.3.3 Δ-Shank3 Vectors

pmRFP- Shank3 WT aa. 1-1334	RG Kreienkamp
pmRFP- Shank3 WT aa. 1-979	RG Kreienkamp
pmRFP- Shank3 WT aa. 1-934	RG Kreienkamp
pmRFP- Shank3 WT aa. 1-835	RG Kreienkamp
pmRFP- Shank3 WT aa. 1-782	RG Kreienkamp
pmRFP- Shank3 WT aa. 1-698	RG Kreienkamp
pmRFP- Shank3 WT aa. 1-676	RG Kreienkamp
pmRFP- Shank3 WT aa. 1-576	RG Kreienkamp
pmRFP- Shank3 WT aa. 1-538	RG Kreienkamp
pmRFP- Shank3 WT aa. 1-376	RG Kreienkamp
pmRFP- Shank3 WT aa. 1-339	RG Kreienkamp
pmRFP- Shank3 L68P aa. 1-339	RG Kreienkamp
pmRFP- Shank3 R12C aa. 1-339	RG Kreienkamp
pmRFP- Shank3 P141A aa. 1-339	RG Kreienkamp
pFRET- Shank3 WT aa. 1-339	RG Kreienkamp
pFRET- Shank3 L68P aa. 1-339	RG Kreienkamp
pFRET- Shank3 R12C aa. 1-339	RG Kreienkamp
pET SUMO- Shank3 WT aa. 1-348	RG Kreienkamp
pET SUMO- Shank3 WT aa. 99-348	RG Kreienkamp

2.1.3.4 Expression Vectors for Interaction Partners

Name	Source
pEGFP- Abi1	Tobias Böckers, Ulm, Germany
mRFP- N-Cadherin	RG Kneussel, ZMNH, Hamburg, Germany
pEGFP- α-Catenin	Addgene
Emerald- β-Catenin	Addgene
pEGFP- δ-Catenin	Kenneth Kosik, UC Santa Barbara, California, US
pEGFP- Cortactin	RG Kreienkamp
pEGFP- Densin-180	RG Kreienkamp
pEGFP- Fodrin	Tobias Böckers, Ulm, Germany
pEGFP- HCN1	R. Bender, UKE, Hamburg, Germany
pEGFP- Homer	RG Kreienkamp
pEGFP- IRSp53	RG Kreienkamp
HA- Rap1a G12V	RG Rosenberger, UKE, Hamburg, Germany
HA- Rap1a S17N	RG Rosenberger, UKE, Hamburg, Germany
HA- HRas WT	RG Rosenberger, UKE, Hamburg, Germany
HA- HRas G12V	RG Rosenberger, UKE, Hamburg, Germany
HA- HRas S17N	RG Rosenberger, UKE, Hamburg, Germany
pEGFP- SAPAP1	Stefan Kindler, UKE, Hamburg, Germany
pEGFP- Sharpin	RG Kreienkamp
HA- TNIK	Ken-ichi Kariya, Okinawa, Japan
HA- TNIK KM	Ken-ichi Kariya, Okinawa, Japan

2.1.3.5 Shank1 Vectors

pET SUMO- Shank1 N-terminal	RG Kreienkamp
MYC His- Shank1B	RG Kreienkamp

2.1.3.6 Δ-δ-Catenin Vectors

GFP- δ-Catenin aa. 518-1225	RG Kreienkamp
GFP- δ-Catenin aa. 934-1225	RG Kreienkamp
GFP- δ-Catenin aa. 1014-1225	RG Kreienkamp
GFP- δ-Catenin aa. 1040-1225	RG Kreienkamp
GFP- δ-Catenin aa. 1084-1225	RG Kreienkamp

2.1.3.7 β-Catenin Vectors

GFP- β-Catenin T779A	RG Kreienkamp
GFP- β-Catenin Δ PDZ ligand	RG Kreienkamp

2.1.4 Sequencing Primers

Name	Sequence (5' → 3')
GFP-n- fwd	AATGTCGTAACAACTC
pmRFP fwd	CCTACAAGACCGACATCAAG
pmRFP rev	GTCACCTTCAGCTTGGCG
SVPA2 rev	ATTCATTTTATGTTTCAGGTTCAG
T7	TAATACGACTCACTATAGGG

2.1.5 Antibodies and Toxins

Primary Antibodies	WB	ICC	Source
rb anti- Actin	1:200	1:80	Sigma #A2066
ms anti- N-Cadherin	1:3000	1:1000	BD Trans. Lab #610921
ms anti- β-Catenin	1:1000		Cell Signaling #2698
ms anti- δ-Catenin	1:250		BD Trans. Lab
rb anti- δ2-Catenin	1:1000	1:500	Abcam #ab 184917
rb anti- Densin 180	1:2000	1:200	RG Kreienkamp
rb anti- DDX3X	1:500		Bethyl Laboratories
rb anti- DDX5	1:2500	1:250	Bethyl Laboratories
rb anti- DHX9	1:2000		Bethyl Laboratories
rb anti- (ERK1/2) p44/42 MAPK	1:1000		Cell Signaling #9102S
rb anti-phospho-(ERK1/2) p44/42 MAPK (Thr202/Tyr204)	1:1000	1:400	Cell Signaling #9101S
ms anti- GFP	1:5000		Covance MMS-118P
rb anti- GFP	1:1000	1:2000	Abcam #ab6556
ms anti- HA	1:1000	1:200	Sigma Aldrich #H9658
rb anti- HA	1:1000	1:200	Sigma Aldrich #H6908
rb anti- hnRNP-H	1:10000		Bethyl Laboratories
ms anti- hnRNP-U (3G6)	1:2000		Antibodies Online
ms anti- Homer	1:1000	1:500	Synaptic Systems #160011
chk anti- MAP2	1:20000	1:1000	Antibodies Online
rb anti- c-MYC	1:5000	1:200	Sigma #C3956
rb anti- NONO	1:2000		Bethyl Laboratories
Phalloidin 546		1:40	MoBiTec
Phalloidin 488		1:40	MoBiTec
ms anti- PSD 95	1:2000	1:500	Thermo Fisher #MA1-046
rb anti- HRas	1:1000	1:50	Thermo Fischer #PA5-14863
rat anti- RFP	1:1000		Chromotek (5F8)
gp anti- Shank3	1:1000	1:500	Synaptic Systems # 162 304
ms anti- α Tubulin	1:5000		Abcam #ab7291

Secondary Antibodies	WB	ICC	Source
HRP Goat anti- ms IgG	1:2500		Jackson ImmunoResearch
HRP Goat anti- rb IgG	1:2500		Jackson ImmunoResearch
HRP Goat anti- rt IgG	1:2500		Jackson ImmunoResearch
HRP Goat anti- gp IgG	1:2500		Jackson ImmunoResearch
Alexa 633 goat anti-chk IgG		1:1000	Invitrogen
Alexa 405 goat anti-chk IgG		1:1000	Abcam
Alexa 448 goat anti-ms IgG		1:1000	Invitrogen
Alexa 633 goat anti-ms IgG		1:1000	Invitrogen
Alexa 594 goat anti-ms IgG		1:250	Invitrogen
Alexa 555 goat anti-gp IgG		1:1000	Life Technologies
Alexa 633 goat anti-rb IgG		1:1000	Life Technologies
Cy3 goat anti-rb IgG		1:1000	Dianova
Abberior STAR RED goat anti-gp IgG		1:250	Abberior
Abberior STAR RED goat anti-ms IgG		1:250	Abberior
Abberior STAR RED goat anti-rb IgG		1:250	Abberior
Abberior STAR RED Phalloidin		1:250	Abberior

2.1.6 Enzymes

The FastDigest restriction enzymes were purchased from Thermo Fisher Scientific.

2.1.7 Commercial Kits

Commercial Kits	Manufacturer
Nucleofection kit for rat neurons	Lonza
NucleoBond Xtra Midi Kit	Macherey-Nagel
GeneJet Gel Extraction Kit	Thermo Fisher Scientific

2.1.8 Oligonucleotides

The custom synthesized oligonucleotides were purchased from Sigma Aldrich and reconstituted with ddH2O to the working dilution of 10 µM for PCR or 1 µM for sequencing.

2.2 Methods

2.2.1 Molecular Biology Methods

2.2.1.1 Transformation of Competent Cells

Competent *E. coli* cells of the Top10F'strain were slowly thawed on ice. The DNA mixture was prepared by diluting 10 µl of DNA plasmid or the product of a ligation reaction with 20 µl 5x KCM buffer followed by adding 70 µl ddH2O (final volume of 100 µl). 100 µl of thawed competent cells were added and the reaction was incubated on ice for 20 min. The cells were heat-shocked at 42°C for 20 sec and immediately after that were placed on ice for 2 more minutes. 1 mL of pre-warmed LB medium without selective antibiotics was added to the cells and cells were incubated in a shaker-incubator at 37°C for 1 hr at 300 rpm. The transformation reaction was then centrifuged at 13000 rpm for 30 sec and the supernatant was discarded. The pellet was resuspended in 100 µl of LB medium and plated on a pre-warmed LB-agar plate containing selective antibiotic followed by an overnight incubation at 37°C.
The NEB stable competent cells (recommended for isolation of plasmid clones containing repeat elements and unstable inserts) were used to prepare Shank3 pHAGE constructs, according to the manufacturer's instructions.

Cultures of single colonies were prepared in LB medium containing selective antibiotic and incubated in a shaker-incubator at 37°C, 200 rpm overnight.

5x KCM buffer

KCl	500 mM
CaCl2	150 mM
MgCl2	250 mM

LB (Luria Broth) medium

Bacto Yeast Extract (pH 7.6)	5 g/L
NaCl	171 g/L
MgSO4	4 mM
KCl	10 mM

LB agar

Bacto Yeast Extract (pH 7.5)	5 g/L
Bacto-Peptone	10 g/L
NaCl	10 g/L
Agar	15 g/L

Antibiotics

Ampicillin	100 µg/mL
Kanamycin	50 µg/mL

2.2.1.2 DNA Mini Preparation

Mini preparation of plasmid DNA was performed using buffers from the NucleoBond Xtra plasmid purification kit. 1 mL of the E. coli culture grown overnight was centrifuged in an Eppendorf tube at 13000 rpm for 30 sec. The supernatant was discarded, and the pellet was resuspended in 100 µL of resuspension buffer containing RNase, followed by adding 100 µL lysis buffer. The tube was inverted a few times and incubated for 2 min at RT. 100 µL of neutralization buffer was added to the reaction and the tube was centrifuged for 20 min at 13000 rpm at RT. The supernatant containing DNA was collected and mixed with 70% (V/V) isopropanol. Samples were centrifuged for 20 min at 13000 rpm. The supernatant was discarded, and the pellet was washed twice with 500 µL 70% ethanol in a 5 min centrifugation step at 13000 rpm. After discarding the supernatant, the pellet was dried at RT for 15 min and then resuspended in 50 µL ddH2O. The purified DNA was further analysed by a restriction enzyme digest or sequencing.

2.2.1.3 DNA Midi Preparation

For the purpose of large-scale plasmid purification, Midi preparation was performed according to the manufacturer's instructions of NucleoBond Xtra Midi kit from 100 mL cultures. The purified DNA was dissolved in an appropriate volume of buffer TE for 1 hr at RT and the DNA concentration was determined using Epoch ™ Multi-Volume Spectrophotometer System.

2.2.1.4 Restriction Digestion

Restriction digestion was performed using appropriate restriction endonucleases that recognize short, specific DNA sequences and cleave double-stranded DNA (dsDNA) at specific sites within or adjacent to their recognition sequences. To control the correctness of a purified DNA plasmid or create fragments for a ligation reaction, 1 µg of DNA plasmid was mixed with 2 µL of 10x Fast Digest buffer and 1 µL of each corresponding Fast Digest restriction enzymes. The reaction was then filled up to 20 µL with ddH2O and incubated at 37°C for 45 minutes. To avoid the vector re-closure by intramolecular ligation, 5'-phosphate groups were in some cases removed using the alkaline phosphatase FastAP. For this, 1 µL FastAP was added to the digestion reaction 10 min prior to the end of incubation time.

2.2.1.5 Agarose Gel Electrophoresis

The DNA fragments generated by restriction enzymes were further analysed using agarose gel electrophoresis. 6 µL of Midori green DNA stain was added to 100 mL of 1 or 1.3% agarose-TAE solution prior to the gel casting. The samples were then mixed with the appropriate volume of loading buffer and loaded into the solidified agarose gel. The gel was electrophoresed in 1x TAE buffer at 100 V for 20 min, leading to separation of DNA fragments according to their molecular weight. The size of DNA fragments was determined using a 1kb DNA marker. The DNA bands were detected by a UV transilluminator.

TAE buffer (pH 8.0)

Tris-Acetat	40 mM
EDTA	2 mM

6x DNA-loading buffer (pH 7.6)

Tris-HCl (pH 7.6)	10 mM
Bromophenol blue	0.03 % (v/v)
Xylen-Cyanol FF	0.03 % (w/v)
Glycerol	60 % (v/v)
EDTA	60 mM

2.2.1.6 Extraction of DNA Fragments

The separated DNA fragment of interest was excised from the agarose gel under UV light and purified using GeneJet Gel Extraction kit according to the manufacturer's instruction.

2.2.1.7 Ligation

In order to subclone a DNA fragment (insert) into a new vector, the ligation reaction was performed using T4 DNA ligase. For this, insert and vector were mixed in a 3:1 ratio and 1 µL T4 DNA ligase was added. The reaction was made up to 20 µl by a ligation buffer containing 1 mM ATP and was incubated overnight at 16°C.

2.2.1.8 DNA Sequencing

The sequencing reactions to define the arrangement of nucleotides in DNA plasmids were performed using the Sanger method, using BigDye Terminator Cycle Sequencing Kit (Thermo Scientific). The sequencing reaction was set up as follows:

PCR Reaction

DNA plasmid	1 µg
5x sequencing buffer	2 µL
Big Dye	1 µL
Primer	1 µL
ddH2O	Up to 10 µL

The reaction tubes were placed in the PCR machine to pass through thermal cycles as follows:

Thermal Cycles

Step	Temperature	Time	Number of cycles
Initial denaturation	96°C	1 min	1
Denaturation	96°C	10 sec	25
Primer annealing	50°C	5 sec	
Extension	60°C	4 min	
Final extension	60°C	4 min	1

This was followed by a Sodium Acetate Precipitation Reaction:

Sodium Acetate Precipitation Reaction

PCR product	10 µL
3M NaAc (pH 5.5)	2 µL
100% EtOH	50 µL
ddH2O	10 µL

After a brief mixing, the precipitation reaction was incubated at RT for 15 min, followed by a 20 min centrifugation at RT at 4000 rpm. The supernatant was carefully discarded, and the pellet was washed with 70% EtOH in a 10 min centrifugation step at RT at 4000 rpm. The supernatant was discarded, and the pellet was dried at RT for 15 min. The precipitated DNA was then dissolved in 20 µL HiDi (highly deionized) formamide and analysed by capillary electrophoresis performed at the diagnostic department of the UKE Institute for Human Genetics.

2.2.2 Cell Biology Methods

2.2.2.1 Cell Culture

Human embryonic kidney 293T (HEK293T) cells were cultured in 10 cm plates with growth medium and passaged every 2-4 days using Versene buffer to rinse the cell layer, followed by 3 min trypsinization with 1 mL Trypsin 1x (in Versene). Dissociated cells were then re-plated with fresh growth medium in the intended passage ratio.

Growth Medium

DMEM with high glucose and pyruvate	450 mL
Fetal Bovine Serum	50 mL
Penicillin/Streptomycin (100x)	5 mL

Versene (pH 7.4)

NaCl	137 mM
Na_2HPO_4	8.8 mM
KCl	2.7 mM
KH_2PO_4	0.7 mM
EDTA	1 mM

2.2.2.2 Transient Transfection of Cells

Transient transfection of HEK293T cells was performed using TurboFect Transfection Reagent (Thermo Scientific). For this, 5 µg of DNA were diluted in 1 mL of serum-free DMEM. 18 µL of TurboFect were added, followed by immediate mixing. After 10 minutes incubation at room temperature, the transfection mixture was drop-wise added to the 10 cm cell plate and the plate was gently rocked to achieve an even distribution. The transfected cells were then incubated overnight at 37°C in a CO_2 incubator, followed by the subsequent analysis.

2.2.2.3 Cell Starvation and EGF Stimulation Assay

To activate the Ras/Raf/MAP kinase pathway, an EGF stimulation assay was performed in transfected HEK293T cells. 4 hours after transfection, cells were split into two plates and cultured overnight in starvation medium (DMEM+ 0.1% FBS). On the following day, one plate was stimulated by adding 10 ng/mL EGF to the medium 20 min before lysis and the other plate remained non-stimulated as control plate.

2.2.2.4 Primary Hippocampal Neuron Culture

Pregnant animals (rats at day E18 of pregnancy/mice at E16) were sacrificed by anesthesis with CO_2, followed by decapitation. The embryos were removed and collected in a 90-mm Petri Dish containing cold dissection medium. Under sterile conditions, pups were decapitated with a pair of sterile surgical scissors; after removing head skin and the skull under the dissecting microscope the hippocampi were separated from the cortex and collected in a 15 mL falcon tube containing cold dissection medium. The hippocampi were trypsinized by adding Trypsin to the dissection medium and incubated at 37°C in the water bath for 15 min. The enzymatic solution then was discarded, and the hippocampi were washed in 8 mL plating medium 4-5 times. During the last wash, the hippocampi were completely dissociated into a single cell suspension using Pasteur pipettes. The dissociated hippocampal neurons were plated on poly-L-lysine (PLL) coated coverslips in plating medium. The plating medium was then removed one day after dissection (DIV 1), and cells were grown in complete Neurobasal medium at 37°C, 5 % CO_2.

PLL Buffer (pH 8.5)

Boric acid	100 mM
Poly-L-Lysin	100 mg

Dissection Medium

HBSS	500 mL
Penicillin/Streptomycin (100x)	5 mL

Plating Medium

DMEM + GLUTAMAX	450 mL
Horse Serum	50 mL
Penicillin/Streptomycin (100x)	5 mL

Complete Neurobasal Medium

Neurobasal	500 mL
B27	10 mL
Glutamax	5 mL
Penicillin/Streptomycin (100x)	5 mL

2.2.2.5 Neuron Transfection

Neurons were transfected on DIV 7 using the calcium phosphate method. One hour before transfection, the complete Neurobasal medium was collected from the multi-well plate and replaced by 500 µl of pre-warmed transfection medium (MEM+Glutamax) per well. To prepare the transfection reaction, a maximum of 10 µg of plasmid DNA was diluted in 80 µl of ddH_20 and mixed with 10 µl of 2.5 M $CaCl_2$ (final volume of 100 µl). 100 µl of 2× HBS were then added drop-wise to the reaction tube under continuous vortexing. The transfection reaction was incubated at RT for 30 min. 100 µl of this mixture was added to each well. The cells were incubated at 37°C in a humidified atmosphere of 5% CO_2 for another 2 hours. The cells were washed 7 times with 1×HBSS and after the last wash, the previously collected Neurobasal medium was added to the cells.

HBS 2X (pH: 7.05 adjusted with NaOH)

NaCl	274 mM
KCl	10 mM
Na_2HPO_4	1.4 mM
D-Glucose	15 mM
Hepes	42 mM

2.2.2.6 Nucleofection

Nucleofection was performed according to manufacturer's instructions using the Amaxa nucleofection kit before the plating of neurons. Coverslips were coated with ornithine and laminin and incubated with 300 µL complete Neurobasal media before plating of the neurons. 500 µL of neuron plating medium per each coverslip was pre-incubated in the incubator. Approximately, 4–5 x 10^6 freshly dissociated primary neurons for each reaction were centrifuged at 80 g for 5 min at RT. The supernatant was removed, and the pellet was gently resuspended in 100 µL nucleofection solution (already mixed with supplement solution). The cell suspension was mixed with 3 µg plasmid DNA and transferred into a certified cuvette (sample covered the bottom of the cuvette without air bubbles). The cuvette was placed into the Amaxa-Nucleofector cuvette holder and program 0-03 was applied. Immediately after finishing the program, the cuvette was taken out of the holder. 500 µl of the pre-incubated plating medium were added to the cuvette and the sample was gently transferred into the plate with the coated coverslips. 4 hours later the plating medium was replaced by complete Neurobasal media and incubated overnight at 37C.

2.2.3 Biochemical Methods

2.2.3.1. Cell Lysis and Co-Immunoprecipitation (Co-IP)

The transfected HEK cells were washed twice with ice-cold 1x PBS and incubated with 1mL IP buffer containing protease inhibitors for 15 min on ice. The lysed cells were collected in 1.5 mL Eppendorf tubes and centrifuged at 20,000 g for 20 min at 4°C. Then the supernatant was collected, and immune-precipitation was performed using GFP/RFP trap beads. 80 µL of supernatant were kept as whole cell

lysate (input) sample and the rest was incubated with 20 µL of beads for 2hrs at 4°C on a rotator. The beads were collected by centrifugation at 1000g for 1min at 4°C and the supernatant containing unbound proteins was removed. To avoid non-specific binding, the beads were washed 5 times with 500 µL of lysis buffer, followed by centrifugation at 1000g for 1 min at 4°C. After the last wash, the supernatant was discarded, and the precipitated beads were treated with 50 µL of 1x Laemmli buffer, heat denatured at 94°C for 5 min followed by incubation on ice for 2 min. After a brief spinning, 15 µL of the prepared sample were loaded into each well of an SDS gel and subsequent experiments were carried out.

1x PBS (pH 7.4)

NaCl	140 mM
KCl	2.7 mM
Na_2HPO_4	10 mM
KH_2PO_4	1.8 mM

IP buffer (pH 8.0)

Tris	50 mM
NaCl	120 mM
NP40	0.5 %
EDTA	1 mM

1x Laemmli buffer (pH 6.8)

Glycerine	10% (v/v)
DTT	20 mM
SDS	1.5 % (w/v)
Tris/HCl	60 mM
Coomassie G-250	0.05 %

2.2.3.2 RNA Digestion

To remove RNA from the cell lysate, an RNase treatment was performed using RNAase One (Ambion). After 2hrs incubation of cell lysate with beads and prior to the final washing steps the lysate was treated with 1U/µL RNAase and incubated at RT for 30 min on a rotator.

2.2.3.3 Expression of His-tagged Proteins

Aliquots of competent BL21 (DE3) *E. coli* cells were slowly thawed on ice and incubated with β-mercaptoethanol (dilution 1:40) for 10 min. 1 µL of a bacterial expression plasmid (1 µg/µL) was added to 40 µL of cells and incubated on ice for 30 min. The samples were then heat-shocked at 42°C for 20 sec and again incubated on ice for 2 min. 300 µL of pre-warmed SOC medium were added to each reaction. The samples were incubated in a shaker-incubator at 300 rpm for 1 hour at 37°C. 60 µL of each transformation reaction were plated onto a pre-warmed LB plate containing the appropriate antibiotic for plasmid selection. The plates were incubated overnight at 37°C. Individual colonies were

picked and incubated in 3mL of LB medium containing the appropriate selective antibiotic in a shaker-incubator at 37°C and 200 rpm overnight. Then, cultures were added to 100 mL complete TB medium (90 mL TB, 10mL TB 10x salts and appropriate antibiotic) and incubated at 37°C 200rpm. 6-8 hours later, protein expression was induced with 100 µL IPTG, and the culture was incubated at 20 °C overnight at 200rpm.

SOC Medium (pH 7.0)

Tryptone	20 g/L
yeast extract	5 g/L
NaCl	0.5 g/L
KCl	2.5 mM
MgCl2	10 mM
Glucose	20 mM

TB (Terrific Broth) Medium

Tryptone	12 g/L
yeast extract	24 g/L
glycerol	5 g/L

10X TB Salts

0.17 M KH_2PO_4	23.1 g/L
0.72 M K_2HPO_4	125.4 g/L

2.2.3.4 Purification and Covalent Coupling of His-tagged Proteins

For purification of His-tagged SUMO-Shank3 fusion proteins, the bacterial culture was centrifuged at 5000 rpm for 10 min at 4°C. The supernatant was discarded, and the pellet was resuspended in 10 mL native purification buffer (1 x native buffer + 10 mM Imidazole). 20 mg lysozyme were added, and cells were incubated for 30 min on ice. The cells were then lysed with two cycles of ultra-sonication (3 times, each time 10 sec) followed by a rapid freezing (at -80°C)/ thawing. The lysate was centrifuged at 12.000 rpm for 20 min at 4°C. The supernatant was collected and incubated with 0.5 mL Ni-NTA-Agarose at 4°C for 1 hour on a rotator. The samples were centrifuged at 1500 g for 2min at 4°C and the supernatant was discarded. The beads were washed 3 times using 10 mL native wash buffer (1 x native buffer + 20 mM Imidazole) followed by 2 min centrifugation and aspirating the supernatant. With the last wash, the beads were resuspended in 3 mL of supernatant and poured into small columns. The unbound proteins were washed out and the purified proteins were eluted from the columns using 2.5 mL native elution buffer (1 x native buffer + 250 mM Imidazole).

5x Native Buffer (pH 8.0 adjusted with NaOH)

NaH_2PO_4	250mM
NaCl	2.5M

Imidazole (pH 6.0)

Imidazole	3 M
NaCl	500 mM
NaH_2PO_4	20 mM

In order to remove the Imidazole from the affinity-purified protein solution and exchange the buffer, a gel filtration chromatography was performed using NAP™ 25 columns containing Sephadex™ G-25 DNA Grade equilibrated in coupling buffer. The solution of affinity-purified proteins (2.5 mL) was applied to the column. Then 3.5 mL coupling buffer were added to the columns to elute the proteins. The protein solution was then incubated with N-hydroxy-succinimidyl (NHS) activated sepharose which allows for covalent coupling of proteins. The NHS-sepharose was pre-washed with cold 1 mM HCl to prevent hydrolysis of the active ester group. Samples collected during the purification process were analyzed using SDS gel electrophoresis and Coomassie blue staining.

Coupling Buffer (pH: 7.8)

$NaHCO_3$	0.1 M
NaCl	0.2 M

2.2.3.5 Brain Lysis and Pulldown Assay

To prepare whole brain lysate, adult mice were sacrificed by anesthetizing with CO_2, followed by decapitation. Brains (without the cerebellum) were homogenized in ice-cold lysis buffer (4mL per each brain) containing protease and phosphatase inhibitors using a potter, followed by centrifugation at 17000 rpm for 20 min at 4°C. The supernatant was collected and incubated with pre-washed beads for 2hrs at 4°C on rotator. The magnetic beads attached to the protein of interest (His-tagged SUMO-Shank fusion proteins) were washed 5 times using magnetic stands while washing the sepharose beads was performed by centrifugation, as previously described for RFP/GFP trap. After the last wash, the precipitated beads were treated with 50 µL of 1x Laemmli buffer, heat denatured at 94°C for 5 min and incubated on ice for 2 min. After a short spin, 15 µL of the prepared sample was loaded into each well of SDS gel and subsequent experiments were carried out.

RIPA buffer (pH 8.0)

Tris	50 mM
NaCl	120 mM
NP40	1%
Na-Deoxycholate	0.5%
EDTA	5 mM
SDS	0.1%

DOC buffer (pH 9.0)

Tris	50mM
Na-Deoxycholate	1%
NaF	50mM
Na-Orthovanadate	1mM

2.2.3.6 Preparation of Samples for Mass Spectroscopy Analysis

To provide the samples for mass spectroscopy analysis, the samples from Co-IP or pulldown assays were loaded into SDS gel wells under a keratin-free condition. Electrophoresis was performed at 100V for 10min, until the samples passed the first cm of the resolving gel. Then 1 cm of resolving gel together with 2 mm of the lower part of the stacking gel was cut out and transferred to an Eppendorf tube to perform the mass spectrometric analysis at UKE mass spectrometry facility.

2.2.3.7 Preparation of Post Synaptic Density (PSD)

Adult mice (27-39 weeks old) were anesthetized with CO_2 and then decapitated. After removing the skull bones, the brain was extracted, and the cerebellum was removed. Then the rest of brain tissue was mechanically homogenized in 3 mL of solution A using a potter. The homogenate was centrifuged at 1400 g for 10 min at 4 °C. The supernatant was collected, and the pellet was resuspended in 3 mL of solution A and centrifuged again at 1400 g and 4°C for 10 min. The supernatants were combined and centrifuged for 10 minutes at 710 g at 4 ° C. The supernatant was centrifuged at 13800 g and 4°C for 15 min to sediment the cellular membranes including synaptosomes and mitochondria. The pellet was resuspended in 3 mL of solution B and applied on a freshly-made sucrose gradient consisting of 3 mL each of 1.2 M, 1.0 M and 0.85 M sucrose solutions in an ultracentrifugation tube. Ultracentrifugation was performed at 82,500 g for 2 hrs at 4°C. The synaptosome fraction (the white fraction between the 1.0 M and 1.2 M sucrose layers) was recovered using a disposable Pasteur pipette. It was filled up to 5 mL with solution B and then 5 mL of solution C were added to make a total volume of 10 mL. The solution was rotated at 4 ° C for 15 minutes and then centrifuged at 32800 g and 4°C for 20 min. The pellet containing the PSD was resuspended in 150 µL solution B and stored at -80 ° C in 20 µL aliquots for further analyses. The protein concentration was determined using DC™ protein assay (Bio Rad) according to the manufacturer's instruction.

Solution A (pH 7.4)

Hepes	4 mM
Saccharose	0.32 M
MgCl2	1mM
CaCl2	0.5 mM
Pepstatin	2 µg/mL
Leupeptin	10 µg/mL
PMSF	40 µg/mL

Solution B (pH 7.4)

Hepes	4 mM
Saccharose	0.32 M
Pepstatin	2 µg/mL
Leupeptin	10 µg/mL
PMSF	40 µg/mL

Solution C (pH 8.1)

Tris-HCl	12 mM
Saccharose	0.32 M
Triton X 100	1%
Pepstatin	2 µg/mL
Leupeptin	10 µg/mL
PMSF	40 µg/mL

2.2.3.8 SDS-Polyacrylamide-Gel-Electrophoresis (SDS-PAGE)

The electrophoretic separation of proteins was performed in 1x running buffer using a Mini-PROTEAN II System (BioRad). According to the molecular weight of the proteins, 8-12% polyacrylamide SDS-PAGE gels comprising resolving and stacking gels were cast and used for the protein separation. The appropriate volume of denatured protein samples (treated with 1× Laemmli buffer and incubated at 94°C for 5 min) were loaded into the gel wells and electrophoresed at 100-150 V. The molecular weight of the proteins was determined by loading a pre-stained protein marker.

10x Tris/Glycine buffer (pH 8.3)

Tris	250 mM
Glycine	1.92 M

Running buffer

SDS	0.1 % (w/v)
1x Tris/Glycine	Up to volume

SDS Gels

	Resolving gel			**Stacking gel**
	8%	**10%**	**12%**	**5%**
ddH2O	4.5 mL	3.9 mL	3.2 mL	2.8 mL
30% Acrylamid	2.7 mL	3.3mL	4.0 mL	0.7 mL
1.0 M Tris-HCl, pH 6.8	0.0 mL	0.0 mL	0.0 mL	0.5 mL
1.5 M Tris-HCl, pH 8.8	2.6 mL	2.6 mL	2.6 mL	0.0 mL
10% SDS	0.1 mL	0.1 mL	0.1 mL	0.04 mL
TEMED	0.007 mL	0.007 mL	0.007 mL	0.003 mL
10% APS	0.1 mL	0.1 mL	0.1 mL	0.04 mL

2.2.3.9 Western Blotting

For the detection of specific proteins electrophoretic transfer of proteins from SDS gels on nitrocellulose membranes was performed in transfer buffer using a BioRad MINI PROTEAN II ™ system at 100 V for 100 min. The membrane was then incubated in blocking solution for 30 min at room temperature and subsequently incubated with primary antibodies (diluted in blocking solution) at 4°C overnight on a tube rotator. The membrane was washed 3 times (10 min each) with TBS-T solution and incubated with secondary antibodies (diluted in TBS-T solution) for 1 hour at RT. Before imaging, the membrane was washed 3 times (10 min each) with TBS-T solution and shortly incubated with Western Bright ™ ECL solution. The labelled bands were detected using ChemiDoc™ MP Imaging System and images were processed and further analyzed using Image Lab Software.

Transfer buffer

Methanol	20 % (v/v)
SDS	0.02 % (w/v)
1x Tris/Glycin	Up to volume

TBS-T (pH 8.0)

Tris/HCl	10 mM
NaCl	150 mM
Tween 20	0.1 % (v/v)

Blocking solution

Milk powder	5% (w/v)
TBS-T	Up to volume

2.2.3.10 Immunocytochemistry

To perform ICC, cells grown on coverslips were first rinsed three times with ice-cold 1xPBS and fixed using fixation buffer (4% paraformaldehyde in PBS + 4% w/v sucrose) for 15 min at room temperature. The coverslips were then washed 3 times with 1xPBS, followed by permeabilization with 0.1% Triton-X in PBS for 3-5 min at RT. After three fast washes with 1x PBS the cells were blocked in 10% Horse serum in PBS for 1 hour at RT. Appropriate primary antibodies were diluted in 2% Horse serum in PBS and 100 µl of each was then spotted on parafilm. The coverslips were inverted on the drops of antibodies and incubated overnight at 4°C in a humidified dark chamber. On the following day, the coverslips were again placed in plate wells and washed 3 times with 1x PBS for 5 min at RT. Corresponding secondary antibodies were diluted in 1x PBS and incubated with coverslips for 1 hour at RT. After washing 3 times with 1x PBS for 5 min at RT, the coverslips were mounted onto glass microscopic slides using ProLong™ Diamond Antifade mounting medium. The mounting medium was dried overnight at RT and then the slides stored at 4°C before microscopic imaging.

2.2.4 Microscopic Imaging Methods

2.2.4.1 Confocal and Super-resolution Microscopy

Confocal microscopy was performed using Leica SP5 microscope. Super-resolution imaging was performed using a STED microscope from Abberior at UKE microscopy imaging facility (UMIF).

2.2.4.2 Live FRET Imaging

The live FRET imaging was performed using Leica SP5 confocal microscope at UMIF.

2.2.5 Quantitative Analysis and Statistics

The quantitative evaluation of the images obtained by confocal and STED microscopy was performed using the ImageJ Fiji software. The profile analysis was done by ZEN. The evaluation of the fluorescence resonance energy transfer (FRET) was carried out using Bitplane Imaris software. Statistical significance was determined using the Graph Pad Prism program.

Chapter3
Results

3.1 Shank3 in the postsynaptic density

3.1.1 Shank3 colocalizes with the synaptic marker PSD95 in hippocampal neurons

To investigate the localization of Shank3, rat embryonic hippocampal neurons were transfected (DIV7) with the pHAGE-GFP Shank3 plasmid. The neurons were fixed (DIV14) and stained for the endogenous synaptic marker PSD95 and the dendritic marker Map2. Using confocal microscopy, I observed that the overexpressed Shank3 is colocalized with PSD95 at the tip of the dendritic spines (figure 3.1)

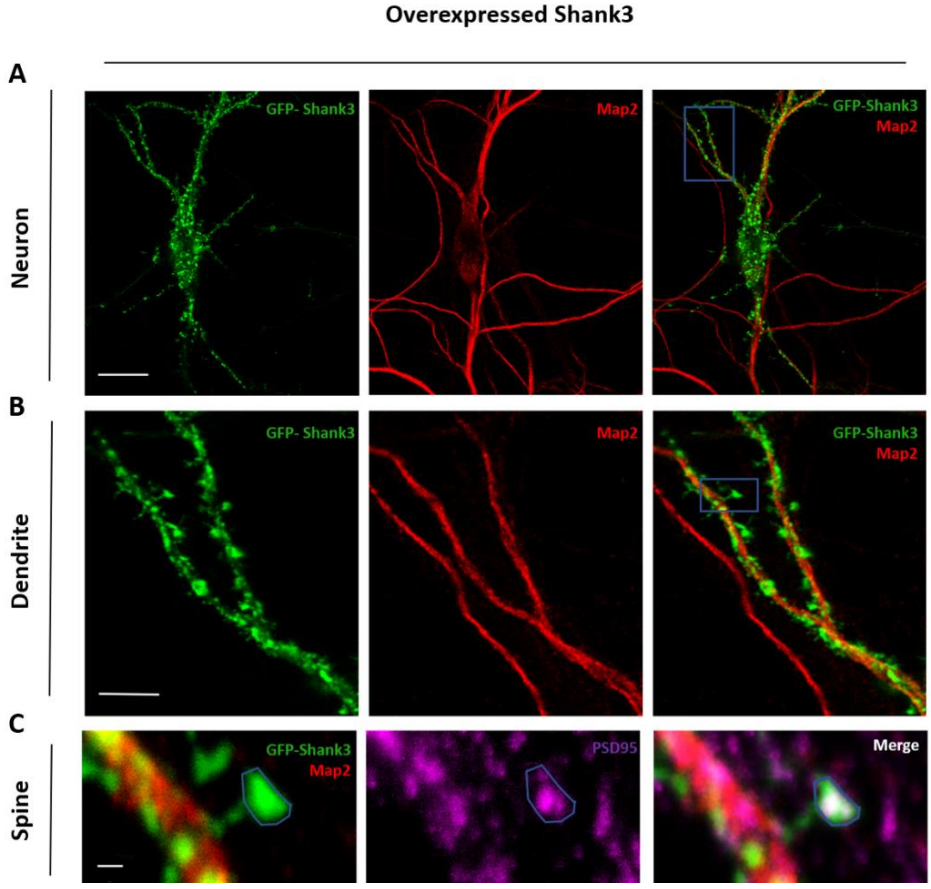

Figure 3.1 Shank3 from three different views. A. An overview image of a transfected neuron with GFP-Shank3 (scale bar 20 µm). **B.** A dendrite with noticeable spines (scale bar 5 µm). **C.** A single dendritic spine with Shank3 at the head, where Shank3 colocalizes with the synaptic marker PSD95 (scale bar 0.5 µm). The head of the spine is indicated in a blue frame.

3.1.2 Shank3 and PSD95 belong to distinct nanodomains at the postsynaptic sites

To study the nanoscale organization of Shank3 clusters in the postsynaptic density, super-resolution imaging was performed using a STED microscope. Primary rat hippocampal neurons were fixed (DIV14) and stained for endogenous proteins Shank3, PSD95 and the dendritic marker Map2. Interestingly, despite the colocalization of Shank3 and PSD95 in the micrometer scale of the confocal

microscope, these two proteins appeared in distinct nanodomains in nanoscopic images (Figure 3.2 A, B). To quantitatively investigate the observed differences between microscopic and nanoscopic images, I performed a profile analysis using ZEN software. Drawing a line across the same part of the spine head in the confocal images and their respective STED images to analyse the signal intensity of both channels (red PSD95 and gray Shank3) showed that, in the confocal images the intensity of both signals (PSD95 and Shank3) follows the same pattern across the line, whereas in the nanometer scale the signals diverge and the overlap between signals of two channels decreases to the point that we can see the distinct nanodomains of two postsynaptic proteins across the same line (Figure 3.2 C, D). This might indicate the fact that Shank3 and PSD95 are indirectly interacting at the postsynaptic sites (Naisbitt et al., 1999, Boeckers et al., 1999), therefore they seem to be belong to the same synaptic unit but do not cluster in the same nanodomains.

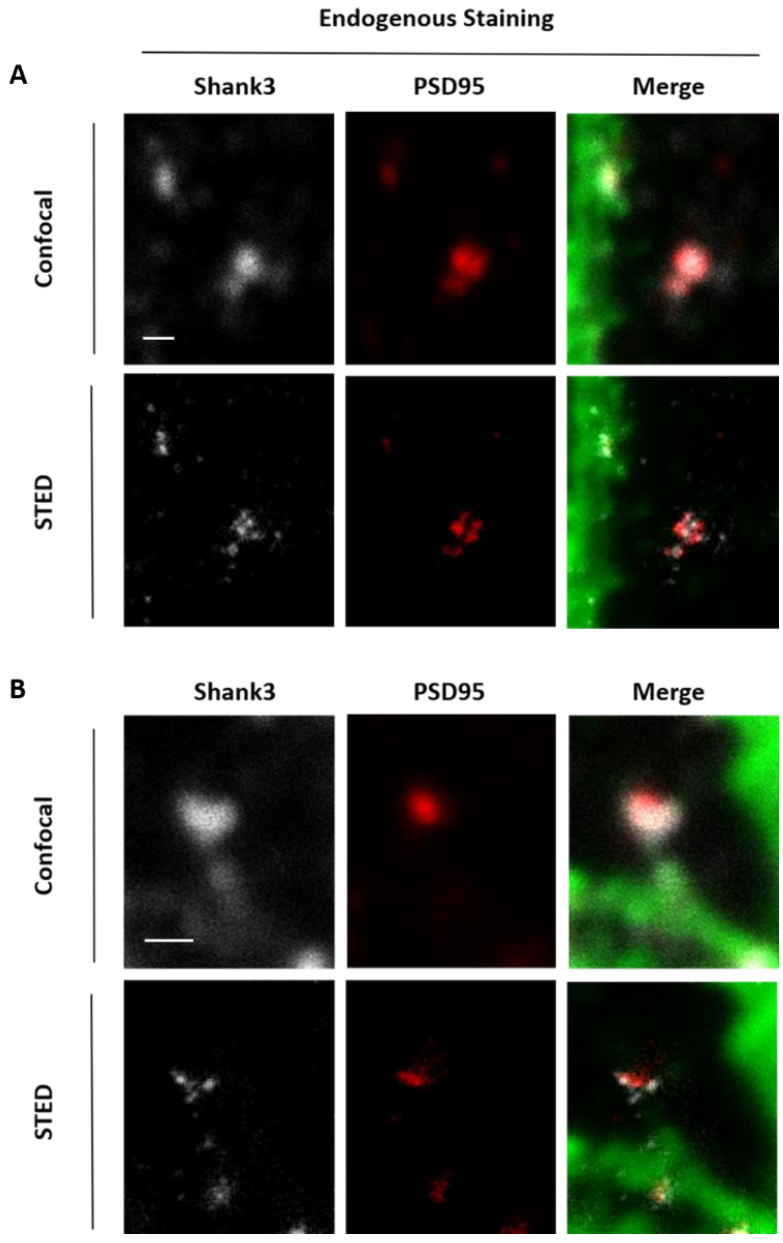

Figure 3.2 Nanoscale organization of Shank3 clusters in the postsynaptic density. A, B. Single spines showing endogenous Shank3 (gray), PSD95 (red) and Map2 (green) (scale bar 0.5µm). **A.** Shank3 and PSD95 resolved in distinct nanoclusters within a same synaptic unit. **B.** A mushroom spine shows a unique arrangement of Shank3 and PSD95 nanoclusters. A single cluster of PSD95 seemed to be surrounded by multiple clusters of Shank3 within a synapse. **C, D.** The profile analysis of the spine A. and spine B. respectively. The left panels show the result of analysis of the confocal images and the right panels represent the analysis results of their respective STED images. The line applied for measuring the signal intensity in each image is indicated in yellow.

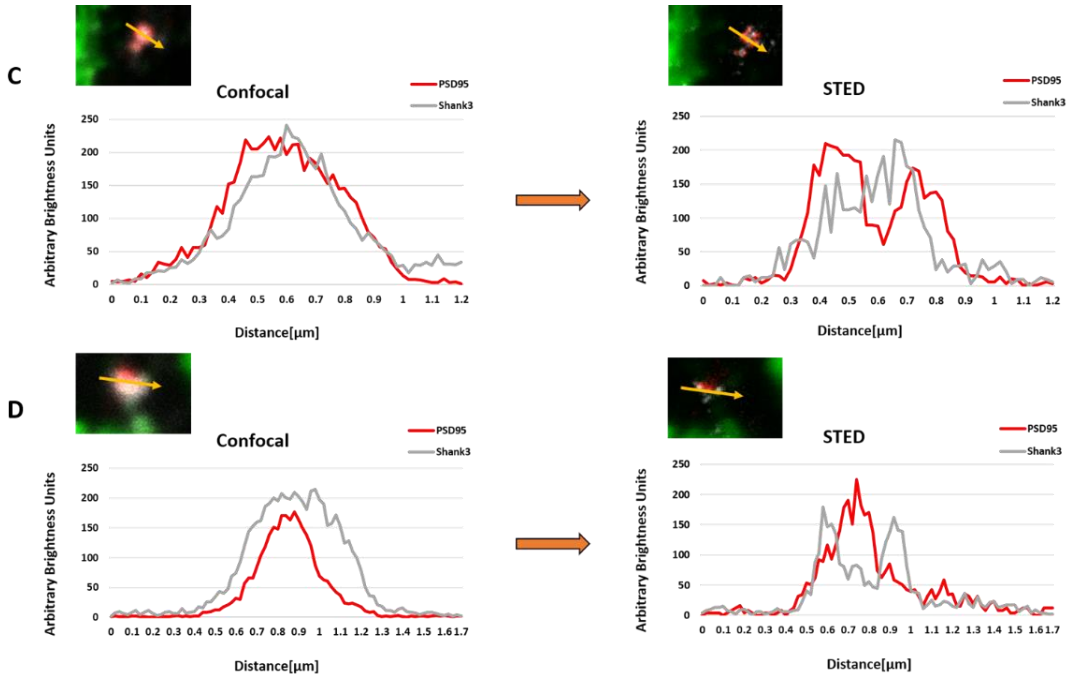

3.1.3 Shank3 nanoclusters form Y shape structures in mushroom spines

Since the postsynaptic localization of Shank3 is a result of Shank3 multimerization via the C-terminal SAM domain (Mangus et al., 2013, Grabrucker, 2014), the synaptic localization of N-terminal mutant variants remains unaffected (Durand et al., 2012, Arons et al., 2012, Mameza et al., 2013). Shank3 WT has been reported to affect spine maturation by forming spines with larger heads while some of the N-terminal missense mutations disrupt the role of Shank3 on spine maturation (Durand et al., 2012). Here, using super-resolution microscopy, I observed that overexpression of Shank3 increases the number of mushroom spines. Interestingly, both WT and L68P mutant forms of Shank3 which were similarly targeted to dendritic spines, often tend to form Y shape structures with their nanoclusters in the postsynaptic density of the mushroom spines. Although, in some cases the WT Shank3 seemed to be able to make ultra-structures of nanoclusters at the postsynaptic sites (figure 3.3).

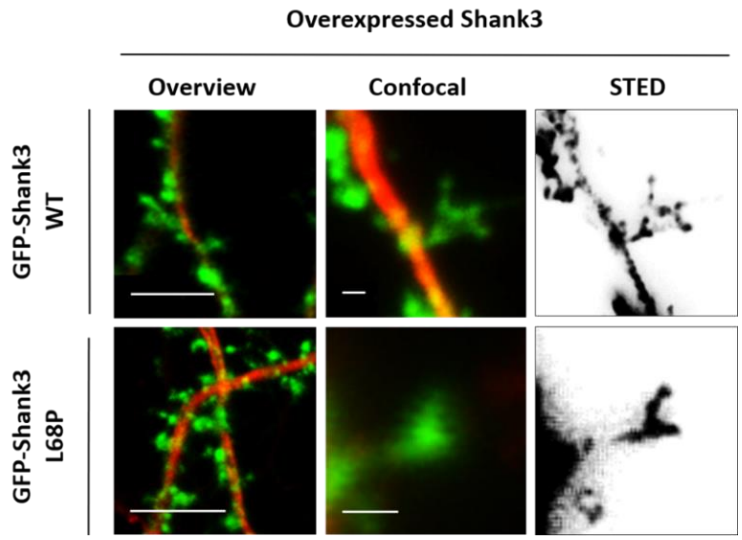

Figure 3.3 The overexpressed Shank3 nanoclusters. Rat embryonic hippocampal neurons overexpressing GFP-Shank3 WT or L68P were fixed (DIV14) and stained for Map2 (red) as dendritic marker and GFP for detecting overexpressed Shank3. STED imaging showed that both WT and L68P Shank3 were targeted to dendritic spines, where the Shank3 nanoclusters often formed Y shape structures within mushroom spines (scale bar 5 µm for overview and 0.5 µm for enlarged images).

3.2 Shank3 and the small G-proteins of Ras family

3.2.1 Activation of Ras pathways affects Shank3 interactions

To define the relevance of the interaction of Shank3 with small G-proteins of Ras family for the synaptic interaction partners of Shank3, an EGF stimulation assay was performed using 293T HEK cells co-expressing RFP-tagged Shank3 with its known GFP-tagged interaction partners. The cells were overnight incubated in a serum starvation condition. On the following day, the cells were stimulated with 10ng/mL EGF (which binds to the EGF receptor and thereby stimulates the Ras/Raf/MAP kinase pathway) 20 min before lysis. At least one interaction partner for each domain of Shank3 was included in this experiment. Since the Ank domain is in a close connection with the SPN domain (which is the binding motif for small G-proteins), the interaction partners of the Ank domain were of particular interest here. Surprisingly, I could not detect specific binding between Shank3 and HCN1 (see below; figure 3.18), which had been reported to interact specifically with the Ank domain of Shank3 (Yi et al., 2016). Using co-immunoprecipitation, I quantified the effects of Ras activation on the interaction of Shank3 with its partners (figure 3.4 A). Surprisingly, the binding of a PDZ domain interaction partner, SAPAP1, was significantly decreased, whereas α-Fodrin, the interaction partner of the Ank domain showed a slight increase in binding to Shank3 after activation of the Ras pathway (figure 3.4 B).

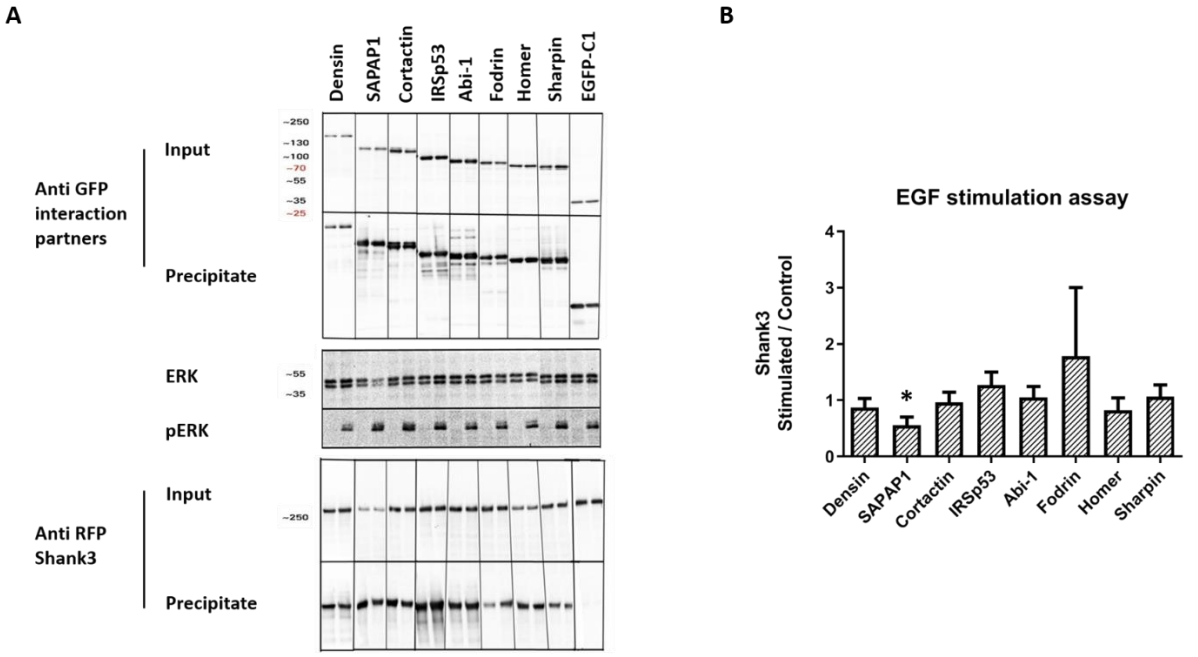

Figure 3.4 EGF stimulation assay. A. 293T cells were transfected with mRFP-Shank3 and GFP-tagged interaction partners, as indicated. After stimulation for 20 min with EGF, cells were lysed and the overexpressed GFP-tagged Shank3 interaction partners were immunoprecipitated from cell lysates (Input) using GFP-trap. Input and precipitate samples were analysed by Western Blot for GFP- and RFP-tagged proteins. Cell lysates were also analysed with ERK and pERK specific antibodies; positive pERK lanes represent stimulated samples in comparison to the control samples with no pERK band. **B.** The effect of stimulation with EGF was determined as the ratio of coprecipitated Shank3 band intensities from stimulated to non-stimulated samples. The result show that activation of Ras pathways significantly decreases the amount of Shank3 bound to SAPAP1, whereas the interaction with Fodrin slightly increases after stimulation (N= 4, paired T-test, *p= 0.01, mean ± SD).

3.2.2 SPN-Ras interaction downregulates binding to SAPAP1

To investigate whether the decrease in the Shank3-SAPAP interaction is a general effect of MAPK pathway activation or due to the binding of active Ras to the SPN domain of Shank3, I performed the EGF stimulation assay comparing Shank3 WT and two Shank3 mutant variants of the SPN domain that are not able to bind to the active Ras (figure 3.5 A). Whereas the interaction of Shank3 WT with SAPAP1 was again reduced upon EGF treatment, the two SPN mutant variants of Shank3 did not show any significant changes in their interaction with SAPAP1. However, the results of the L68P mutant were affected by high variability (figure 3.5 B). These findings indicate that the SPN domain mediates the effect of Ras on Shank3 interaction with SAPAP1 protein and the changes observed in the performed assay is most likely the result of direct interaction between the SPN domain of Shank3 and the active Ras proteins.

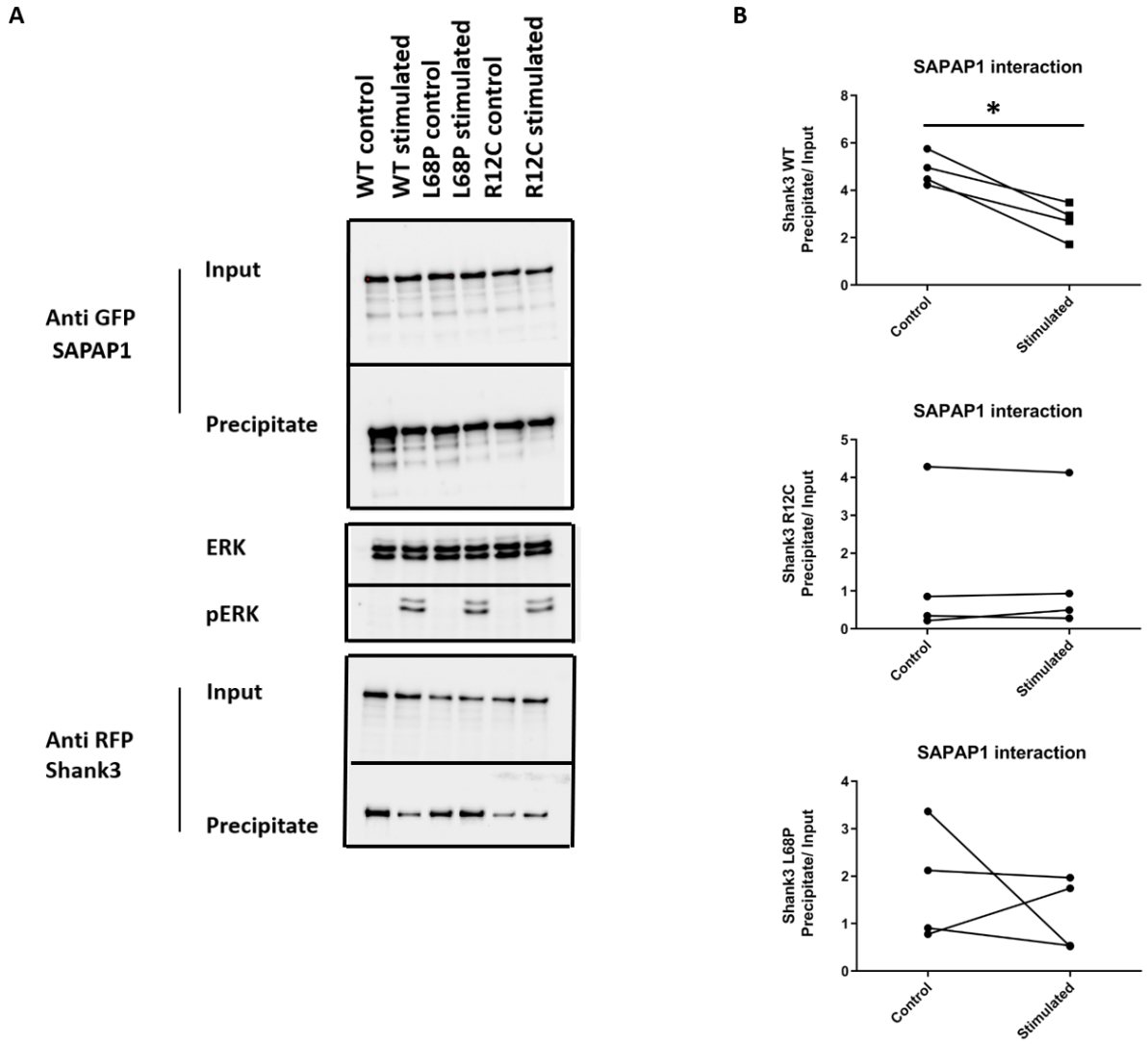

Figure 3.5 EGF stimulation assay with Shank3 mutants. A. Cells expressing Shank3 WT and the SPN mutants with GFP-SAPAP1 were treated with EGF; cell lysates were analysed by immunoprecipitation and Wstern blot as before (Fig. 3.4) **B.** Individual graphs representing the Shank3 variants pattern of interaction with SAPAP1 (N= 4, paired T-test, *p= 0.01, mean ± SD).

3.2.3 SPN-Ras interaction alters the conformation of Shank3 N-terminal

Activation of the MAPK pathway in the EGF stimulation experiments increased the interaction between Shank3 and Fodrin. In 2013, Mameza et al. reported that the SPN domain interacts with the Ank domain in an intramolecular manner, and the L68P mutation unfolds the SPN domain and exposes the Shank3 Ank domain to its ligands. Since the SPN domain is the binding motif for the active form of Ras and activation of the Ras pathway improved binding to α-Fodrin (an interaction partner of Ank), I asked whether the binding to Ras can change the conformation of the Shank3 N-terminus. To address this question, I performed an intra-molecular FRET assay using Shank3 N-terminal FRET constructs (WT, L68P and R12C) coding for amino acids 1- 339 of Shank3, including an N-terminal GFP and a C-terminal mCherry sequence. Based on the three-dimensional structure of the Shank3 N-terminus (Lilja et al., 2017) we assumed that in the WT form of the Shank3 N-terminus, the SPN and Ank domains might be close enough to transfer energy from the GFP donor to the mCherry acceptor and create an intramolecular fluorescence resonance energy transfer (FRET) that can be detected and measured by confocal microscopy. Accordingly, this method might enable us to clarify the effect of SPN domain mutations (L68P and R12C) on the eventual conformational changes in the N-terminus.

To perform intra-molecular FRET, 293T cells were transfected with WT or mutant FRET constructs. On the following day, cells were starved in a serum starvation medium for 4 hrs and then imaged live for 20 min. 2 min after starting the imaging, the cells were stimulated with 10 ng/mL of EGF to activate endogenous Ras proteins. After imaging, the Imaris software was used to process data and determine FRET efficiency. The FRET coefficient was calculated after spectral unmix the acceptor channel (mCherry). The Fret coefficient was calculate point by point in the image by making the following operation between channels: FRET coeffficient= channel acceptor unmixed/ (channel donor+ channel acceptor unmixed). FRET coefficient values range between 0 and 1. To display them as 8-bit images, these values were rescaled ranging between 0 and 255. The values 1(255) represents maximum FRET efficiency while 0 is equivalent to no FRET.

The results showed that in a basal condition the SPN and Ank domain of Shank3 are in an optimal distance and orientation to create a FRET signal (figure 3.6 A) and that the efficiency of this signal is very similar for WT (43%) and R12C (36%) forms of Shank3 N-terminus whereas the L68P mutation (17%) clearly affects the intensity of FRET signal most likely through disrupting the intramolecular interaction between SPN and Ank domains reported by (Mameza et al., 2013). Interestingly, in some cases the cells transfected with the L68P FRET construct showed a high FRET signal which stemmed from protein aggregates inside the cell. This might indicate an intermolecular FRET signal (55%) (figure 3.6 B). Furthermore, comparing the FRET signal intensity before (1 min) and after activation (20 min) of the Ras pathway with EGF revealed that the cells transfected with the WT FRET construct, in total show a signal intensity decay around 2% whereas both L68P and R12C FRET signals remained quite stable during 20 min of imaging (figure 3.6 C). Altogether, these data might indicate a conformational change in the Shank3 WT N-terminus due to binding of the SPN domain to active GTP-bound Ras. While the L68P mutant variant has a constitutive open conformation due to an unfolded SPN domain and R12C shows a closed conformation of the Shank3 N-terminus in which SPN domain is not able to interact with active Ras, the WT Shank3 represent an intermediate state between L68P and R12C that can switch from closed to open conformation through binding to Ras.

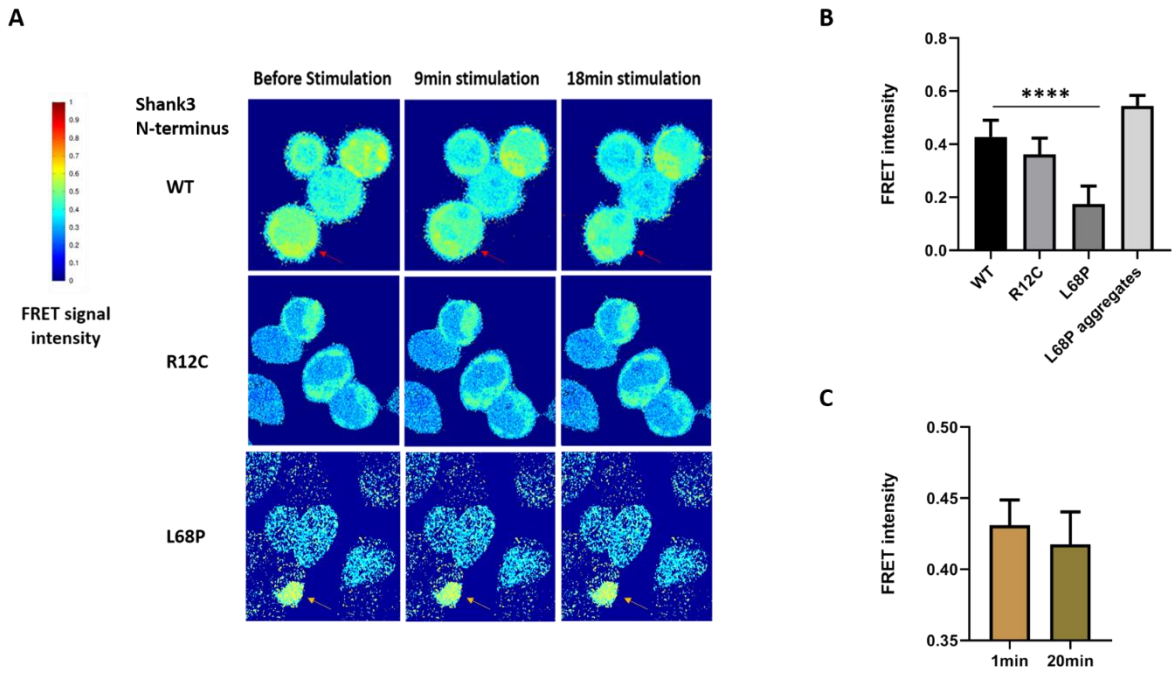

Figure 3.6 Live FRET imaging. A. 293T cells transfected with Shank3 N-terminal FRET constructs (WT, R12C and L68P variants) were first starved and then treated with EGF 2 min after starting the imaging (using a FRET imaging program). The images are selected for three different time points, two minutes (before stimulation), at a middle time point of stimulation (9 min) and during the last few minutes of stimulation (18 min). The color-coded FRET signal intensity represents a low FRET signal (FRET = 0) with the dark blue color and a very high FRET signal (FRET = 1) with the dark red color. A cell showing a FRET decay is indicated by red arrow and a L68P protein aggregate is indicated by yellow arrow. **B.** The FRET efficiency shows a significant decrease in the cells transfected with L68P variant compare to WT and R12C (N= 12-15 cells per each condition from three independent experiments, one-way ANOVA with Dunnett's Test, ****p< 0.0001, mean ± SD). **C**. The cells transfected with WT FRET construct show a signal intensity decay around 2% during 20 min of imaging (N= 12 cells from three independent experiments, mean ± SEM).

3.2.4 WT Shank3 shows colocalization with active HRas in cultured neurons

To analyze the effect of active Ras activity on Shank3 in neurons, primary dissociated hippocampal neurons isolated from embryonic (E18) rats were co-transfected (DIV7) with constructs coding for HA-tagged G12V mutant HRas (i.e. a constitutively active, GTP bound variant) and GFP-Shank3 WT. The cells were then fixed (DIV14) and stained for HA and Map2 as dendritic marker; Shank3 was visualized through the GFP fluorescence. The overexpressed HRas protein showed a membrane associated localization in the neurons. Interestingly, the result of a colocalization analysis revealed that G12V HRas is highly co-localized with Shank3 WT (figure 3.7); note that this pattern for Shank3 is different from the conventional pattern of Shank3 WT clustering in dendritic spines (as shown in 3.1 to 3.3).

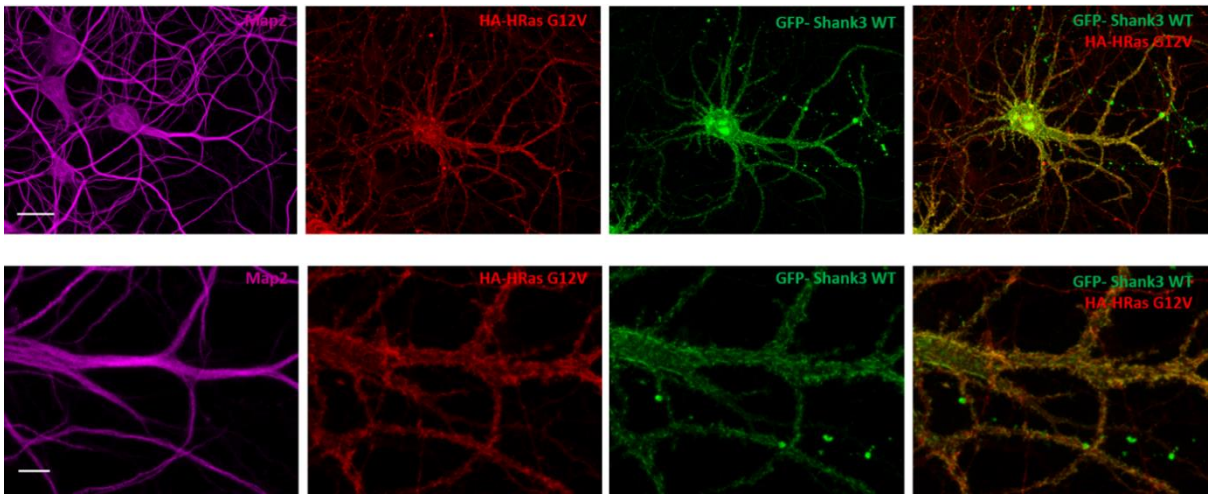

Figure 3.7 Localization of overexpressed HRas and Shank3 in primary cultured neurons. Upper panel shows an overview image of a neuron co-expressing Shank3 WT and active HRas (G12V) (scale bar 20 µm). Lower panel shows a zoomed in image of a dendritic region (scale bar 5 µm). The overexpressed constitutively active form of HRas (G12V) shows a membrane associated pattern of localization in the neurons. Shank3 WT is highly colocalized with active GTP-bound HRas along the dendrite membrane.

Further investigation, comparing the colocalization of Shank3 WT and L68P variant with either the active (G12V) or dominant negative variant (S17N) of HRas showed that only Shank3 WT (but not L68P) colocalizes with the G12V Ras (but not S17N) and as a result Shank3 WT seems to be removed from the postsynaptic clusters and follow the pattern of active Ras in dendrites (figure 3.8).

To see whether the alteration of the Shank3 pattern is due to a general disruption of synaptogenesis caused by overexpression of active HRas, the transfected neurons were also stained for the endogenous synaptic marker PSD95 in the presence of overexpressed HRas. The results show that PSD95 is still present at the postsynaptic sites of G12V-HRas expressing neurons with a normal distribution pattern, indicating no significant alteration in synaptogenesis upon overexpression of active Ras. Comparing the localization of Shank3 WT and the L68P variant with the postsynaptic marker PSD95 showed that in the presence of G12V-HRas Shank3 WT colocalizes with Ras while the L68P variant remains colocalized with PSD95 in synaptic clusters (figure 3.9). In fact, there is no difference between neurons transfected with G12V-HRas and WT Shank3 and those transfected with G12V-HRas and L68P Shank3 in the pattern of PSD95 clustering in dendritic spines. The only variable factor seems to be the distribution pattern of Shank3 WT in the presence of active Ras. This observation indicates that, due to interaction between an intact SPN domain of the WT Shank3 and an active form of the Ras protein, the localization of Shank3 in the postsynaptic density changes, whereas the L68P mutation in the SPN domain results in a resistance to the Ras-induced changes in localization.

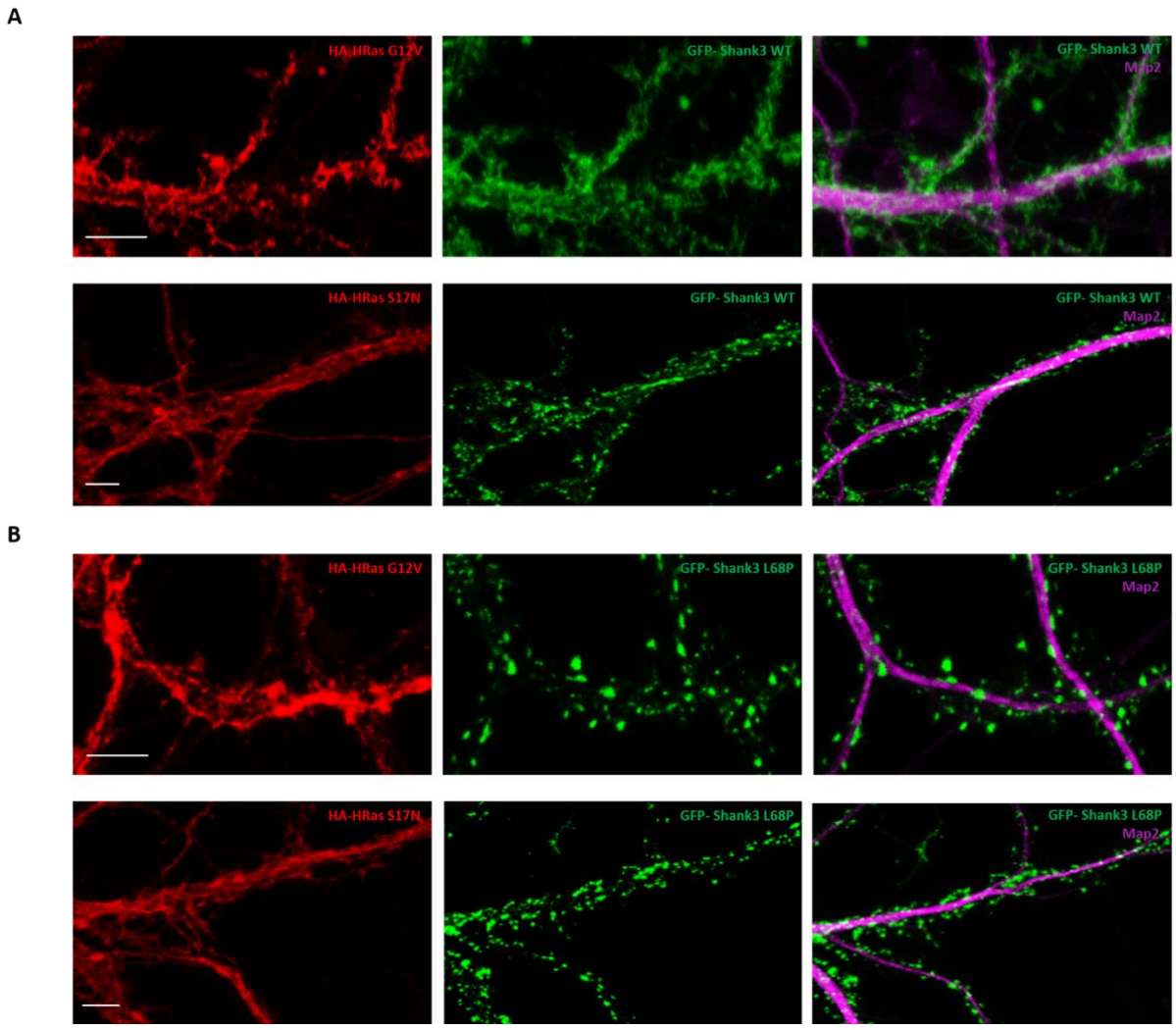

Figure 3.8 Localization of Shank3 variants in the presence of HRas in cultured neurons. A. Neurons overexpressing Shank3 WT with either active (G12V) or inactive (S17N) variants of HRas were stained for HA (red) and the dendritic marker Map2 (magenta). Shank3 WT shows a high degree of colocalization with active G12V (but not S17N) HRas and subsequently changes in the synaptic clustering pattern. **B.** The overexpressed L68P Shank3 shows a punctate pattern of postsynaptic clustering in the presence of both active and inactive forms of HRas (scale bar 5µm).

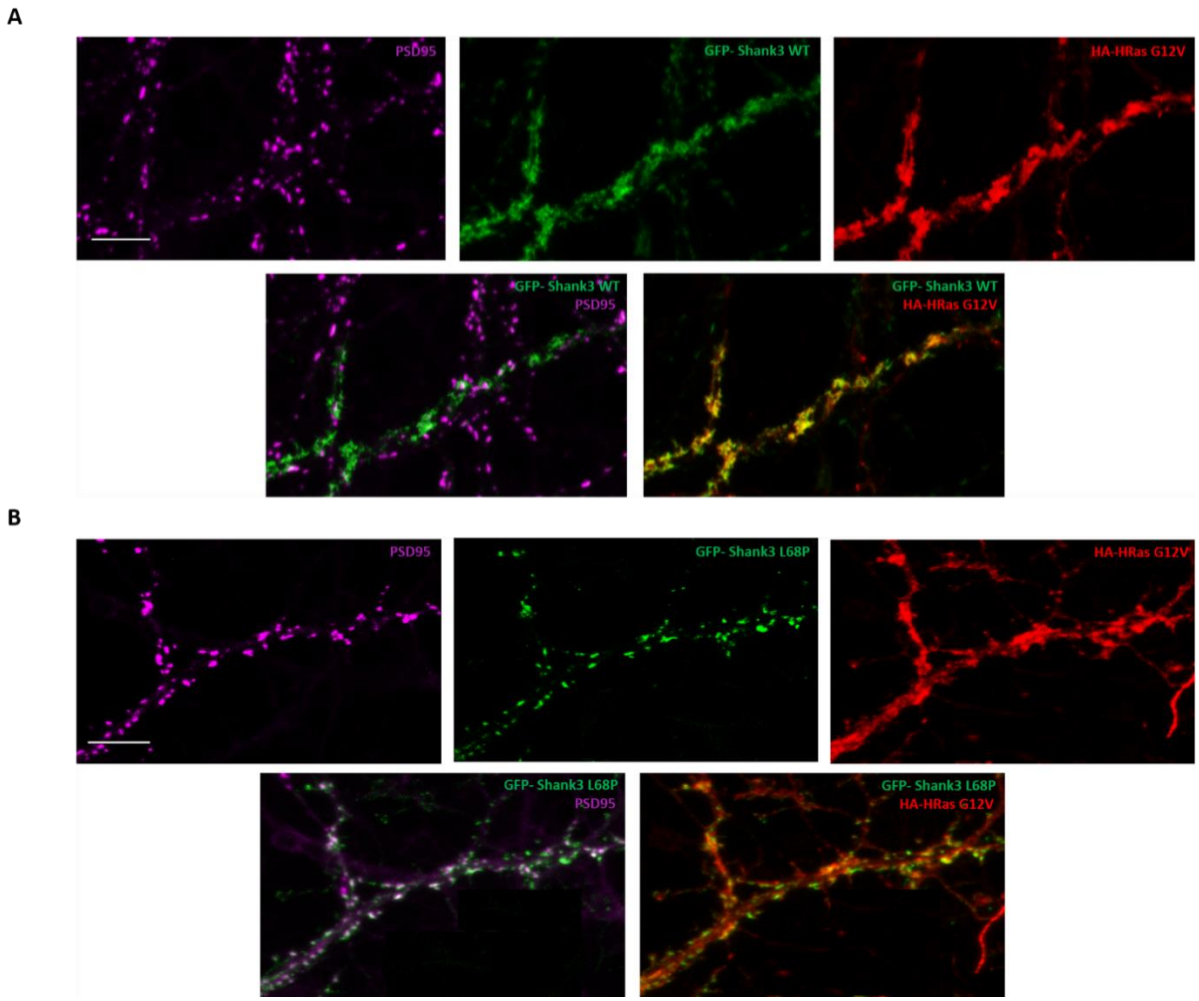

Figure 3.9 The pattern of PSD95 distribution in the presence of active Ras. A, B. Neurons were transfected with constructs coding for GFP-tagged Shank3 WT (A) or L68P mutant (B) in combination with HA-tagged HRas G12V. Cells were stained for HA (red) and the endogenous PSD95 (magenta). In the presence of HRas endogenous PSD95 shows a punctate localization. **A.** The overexpressed WT Shank3 shows a higher colocalization with active HRas compared to PSD95. **B.** The Shank3 L68P variant remains colocalized with PSD95 in the presence of active HRas (scale bar 5µm).

3.2.5 Shank3 regulates small G-protein pathways

The ability of Shank3 to bind to active, GTP-bound small G-proteins via its SPN domain might affect signal transduction at synapses in different ways. Either Shank3 could be downstream effector of Ras signaling in a so far unidentified pathway, or it can function as a regulator of the pathways that require small G-proteins for a proper function. One of the pathways that could be indirectly regulated by Shank3 is the integrin activation pathway which requires active, GTP-bound Rap1 proteins; Rap1 belongs to the Ras family of small G-proteins and exhibits a high affinity for binding to Shank3 in its GTP-bound active form (Lilja et al., 2017). To investigate the effect of Shank3 on this pathway, we targeted a well-known integrin function in neurons, which is enhancing the neurite outgrowth and filopodia formation (Plantman et al., 2008). For this purpose, freshly dissociated rat hippocampal neurons were nucleofected with GFP-Shank3 plasmids (either WT or L68P) using the Amaxa

nucleofection kit and were plated on coverslips coated with laminin as an integrin ligand. The neurons were fixed (DIV1) and stained for F-actin and Map2. Here we observed that the filopodia density in Shank3 L68P transfected neurons was significantly higher than in Shank3 WT transfected neurons (these data were obtained in collaboration with Johanna Lilja and the group of Prof. Johanna Ivaska from Turku, Finland) (figure 3.10). These data suggest that WT Shank3, but not the L68P mutant is able to inhibit integrin activity by sequestering active Rap in the neurons and as a result the formation of filopodia would be suppressed in the presence of this protein (Lilja et al., 2017).

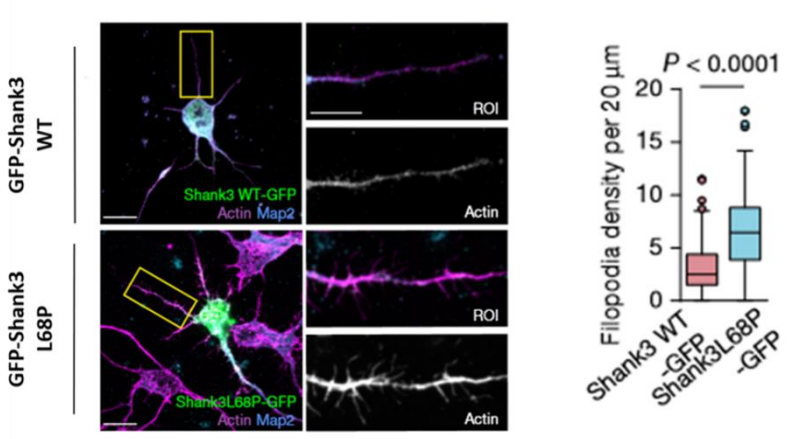

Figure 3.10 The effect of Shank3 on filopodia formation. Representative confocal images and quantification of filopodia in rat hippocampal neurons comparing Shank3 WT and L68P variant (N = 176 (WT), 120 (L68P) from two independent experiments, scale bar 20 µm). ROI represents 10 µm of the dendrite length (Lilja et al., 2017).

3.3 Novel interaction partners of Shank3

Previously, HCN1, Fodrin and Sharpin have been reported as potential interaction partners of the Shank1 and Shank3 Ank domain (Yi et al., 2016, Bockers et al., 2001, Lim et al., 2001). However, Sharpin is hardly present in the postsynapse, and is probably not relevant for the postsynaptic functions of Shank proteins. α-Fodrin was identified in a two-hybrid screen using a truncated Ank fragment. HCN1 is present in the postsynaptic densityand might be a good candidate; however, it seems likely that additional postsynaptic proteins bind to the Ank domain which have so far not been identified. Therefore, to further investigate the role of Shank3 SPN-Ank domain in synaptogenesis and synaptic function, I aimed to identify further interaction partners of the Shank3 N-terminus. For this, I used two different approaches. First, expressing a Shank3 N-terminal fragment in 293T cells and purifying endogenous interaction partners using a co-immunoprecipitation assay, considering the fact that HEK293 cells and human brain share 90% of expressed genes (Ascano et al., 2012) and many neuronal and also actin binding proteins are expressed in this cell line. Second, purification of interaction partners directly from an isolated postsynaptic fraction using an isolated Shank3 N-terminal fragment.

3.3.1 RNA binding proteins interact with Shank3

In order to identify novel interaction partners for the extended Shank3 N-terminus (aa. 1-538) including the SH3 domain (SPN-SH3) and investigate the effect of active Ras on the potential

interactions, I performed a co-expression experiment in 293T cells using a deletion construct coding for the N-terminus of Shank3 and an active Ras variant (HRas G12V). The cells were lysed, and the Shank3 fragment was purified using RFP-trap, followed by a brief electrophoresis step using SDS-PAGE. Gel pieces containing purified proteins were analysed via mass spectrometry. Surprisingly, the result appeared as a list of RNA-binding proteins. Many of these are known nuclear proteins; neither actin binding nor synaptic proteins were found, while Shank3 is known as a synaptic protein. In addition, none of these putative interaction partners was significantly affected by the presence of active Ras in the cells (table 3.1).

Protein names	**Gene names**
SH3 and multiple ankyrin repeat domains protein 3	*SHANK3*
Splicing Factor Proline/Glutamine-Rich	*SFPQ*
Non-POU Domain Containing Octamer Binding protein	*NONO*
Tetratricopeptide Repeat Domain 21A	*TTC21A*
Probable ATP-dependent RNA helicase DDX5	*DDX5*
Nucleolin	*NCL*
Nucleophosmin 1	*NPM1*
60S Ribosomal Protein L3	*RPL3*
60S Ribosomal Protein L4	*RPL4*
ATP-dependent RNA helicase DDX3x	*DDX3X*
Heterogeneous Nuclear Ribonucleoprotein U	*HNRNPU*
40S Ribosomal Protein S3A	*RPS3A*
ATP-dependent RNA helicase A	*DHX9*
40S Ribosomal Protein S8	*RPS8*
60S Ribosomal Protein L7A	*RPL7A*
Heterogeneous Nuclear Ribonucleoprotein A1	*HNRNPA1*
40S Ribosomal Protein S2	*RPS2*
Histone Cluster 1 H1 Family Member C	*HIST1H1C*
Nuclease sensitive element binding protein 1	*YBX1*
60S Ribosomal Protein L6	*RPL6*
60S acidic Ribosomal Protein P0	*RPLP0*
Heterogeneous Nuclear Ribonucleoprotein H1	*HNRNPH1*
40S Ribosomal Protein S4X	*RPS4X; RPS4Y1*
Probable ATP-dependent RNA helicase DDX17	*DDX17*
60S Ribosomal Protein L15	*RPL15*

Table 3.1. Mass Spectrometric analysis result of screening for Shank3 N-terminus interaction partners in 293T cells. RFP-tagged proteins were isolated by immunoprecipitation from lysates of cells expressing an RFP-Shank3 (1-538) (with or without Ras G12V) or RFP as a negative control. All three sets of samples were analysed by mass spectrometry. The label free quantification (LFQ) intensity signals obtained from the negative control samples were subtracted from the LFQ intensity signals obtained from the Shank3 containing samples. Precipitated proteins are ranked in the table above starting with the highest residual LFQ intensity signals. The RNA binding proteins are highlighted in yellow.

3.3.1.1 Identification of a nuclear localization signal in Shank3

Many of the putative interaction partners of Shank3 identified above are nuclear proteins. To investigate the possibility of an interaction between Shank3 and these proteins, I expressed different deletion constructs of Shank3 in 293T cells and performed immunocytochemistry. The results showed that in fact all truncated Shank3 proteins localize in the nucleus, with the exception of the shortest fragment containing residues 1-339 (figure 3.11 A). A closer inspection of the Shank3 protein sequence using the NLStradamus software (available at: http://www.moseslab.csb.utoronto.ca/NLStradamus/) and cNLS Mapper (available at: http://nls-mapper.iab.keio.ac.jp/cgi-bin/NLS_Mapper_form.cgi) as well as previously published data by (Grabrucker et al., 2014) indicated that Shank3 contains four putative nuclear localization signals (NLS) (figure 3.11 B). Here, I show that the first NLS signal located right after the Ank repeats is sufficient for nuclear localization of truncated Shank3 proteins; therefore, as long as this NLS is present, the protein is completely recruited to the nucleus upon expression in 293T cells. Only the shortest Shank3 fragment lacking any NLS shows a diffuse signal in the cell cytosol and nucleus. Interestingly, the full length Shank3 protein quite often appears in small nuclear clusters or forms large clusters mostly around nucleus in 293T cells (figure 3.11 A).

A

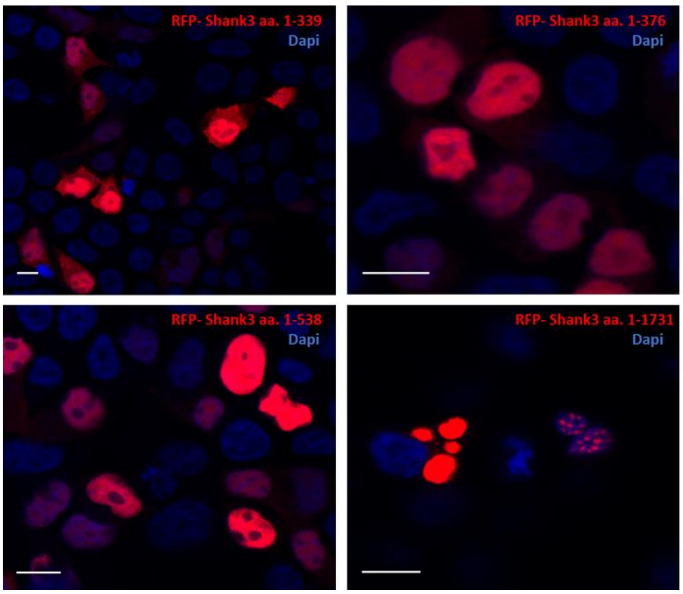

Figure 3.11 Localization of truncated Shank3 variants in 293T cells. A. Shank3 fragments (aa 1-538) containing SPN-Ank-SH3 domains and (aa 1-376) containing SPN-Ank and the NLS1 in the linker region between Ank and SH3 domain show nuclear localization, While the Shank3 N-terminus SPN-Ank (aa 1-339) lacking any NLS sequence shows a diffuse signal in the cell cytosol as well as in the nucleus, the full length Shank3 either appears in small nuclear clusters or more often forms large cytosolic clusters mostly around the nucleus (scale bar 10µm). **B.** Summary of the localization of Shank3 truncated proteins in 293T cells.

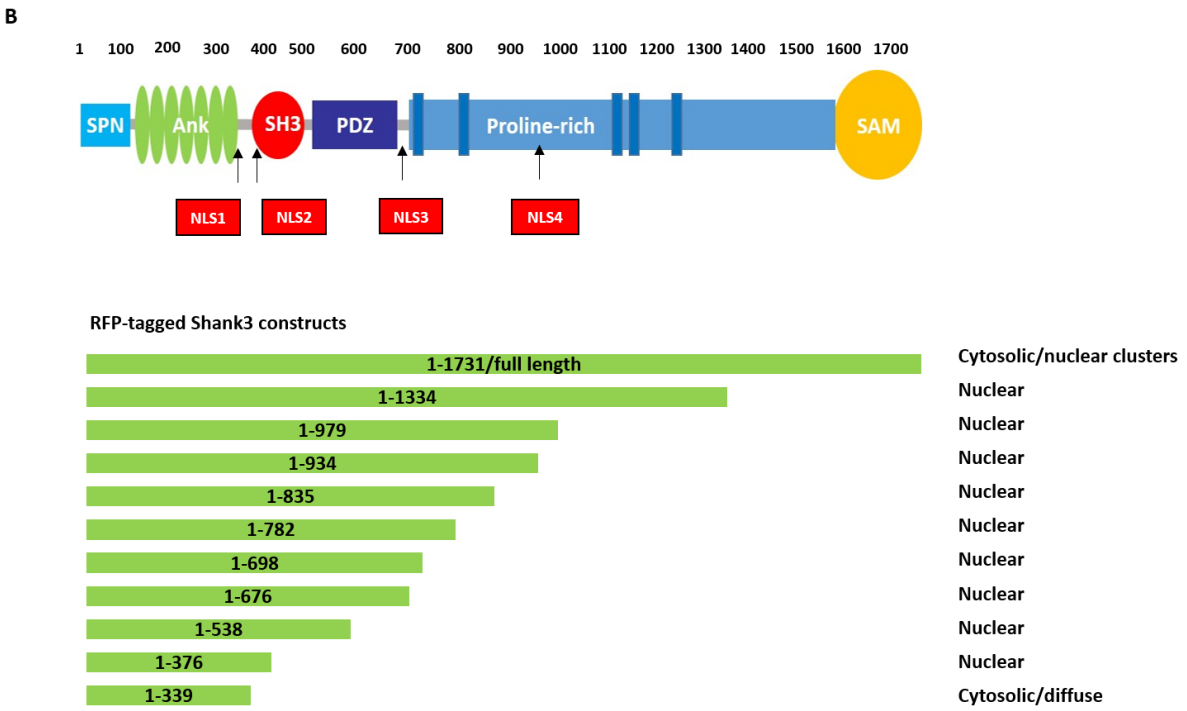

3.3.1.2 Shank3 Ank domain is a binding site for RNA binding proteins

To verify the interaction of RNA binding proteins with Shank3, different RFP-tagged Shank3 deletion constructs were expressed in 293T cells. mRFP-Shank3 variants were precipitated using RFP-trap, and the endogenous RNA binding proteins were detected in input and precipitate samples by Western blotting using specific antibodies. The results show that some of the RNA binding proteins are indeed coprecipitated with Shank3. Since they were all precipitated with the shortest truncated Shank3 protein containing only SPN and Ank domains, they appear to be interaction partners of the Shank3 N-terminus (figure 3.12).

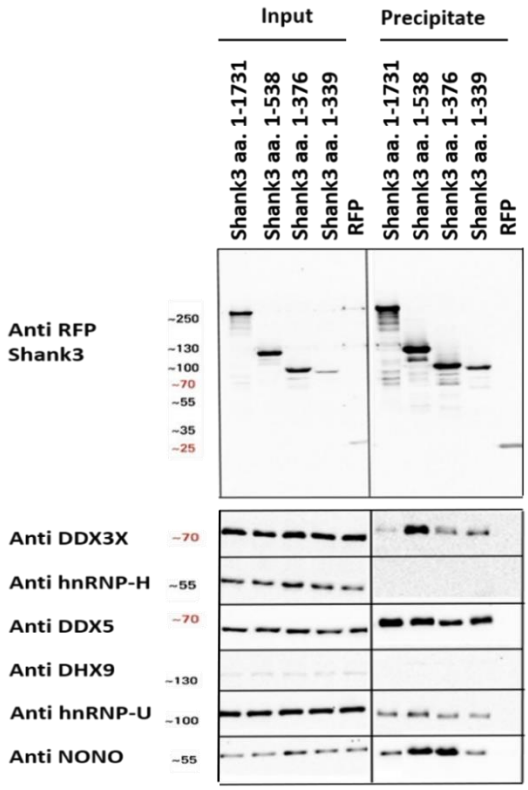

Figure 3.12 Verification of the interaction between RNA-binding proteins and Shank3 in tissue culture. Different RFP-Shank3 deletion constructs were transfected into 293T cells, and RFP-tagged proteins were precipitated using RFP-trap. The results of detection with specific antibodies for six different RNA-binding proteins found in the mass spectrometry analyses show that DDX3X, DDX5, hnRNP-U and NONO are able to specifically interact with Shank3 via the N-terminal SPN-Ank domains.

3.3.1.3 The interaction of Shank3 with DDX5 and hnRNP-U is RNA-independent

Since the RNA binding proteins are likely to be in a complex with RNA, their interaction with Shank3 could be RNA dependent. Using an RNA digestion assay in 293T cells I showed that the interaction of NONO and DDX3X with Shank3 is dependent on the presence of RNA, while DDX5 and hnRNP-U stay bound to Shank3 after digestion of RNA (figure 3.13).

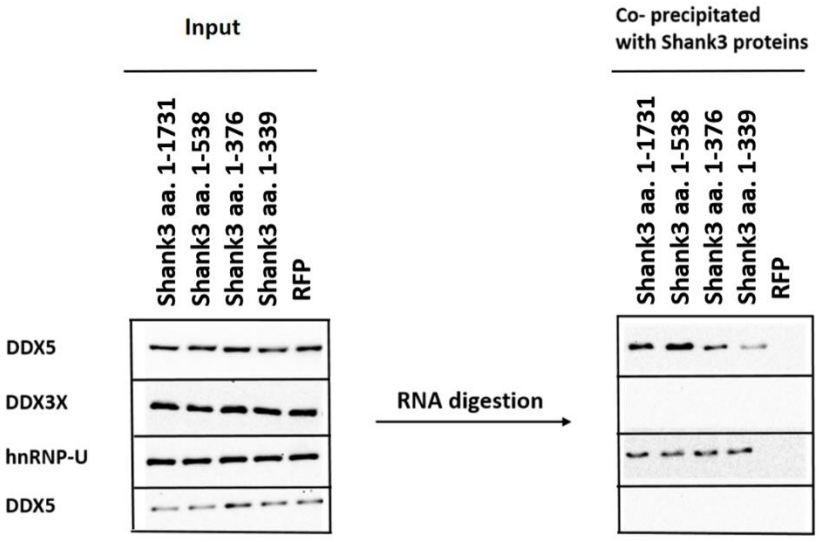

Figure 3.13 RNA digestion assay. Co-immunoprecipitation of RNA-binding proteins after performing an RNA digestion show that the interaction of DDX5 and hnRNP-U with Shank3 is not RNA dependent whereas NONO and DDX3X most likely bind to Shank3 in an RNA-dependent manner.

3.3.1.4 The SPN domain does not affect the Shank3- RNA binding proteins interactions

Using co-expression and co-immunoprecipitation I showed that the mutations in the SPN domain do not affect the interaction between Shank3 and RNA binding proteins (figure 3.14 A). To determine the effect of the Ras binding to Shank3 on the interaction of RNA-binding proteins with Shank3, I also performed an EGF stimulation assay. Activation of the Ras pathway by a 20 min stimulation with 10 ng/µL EGF in 293T cells overexpressing full length Shank3 showed that the interaction between Shank3 and RNA binding proteins is not altered by Ras activity (figure 3.14 B).

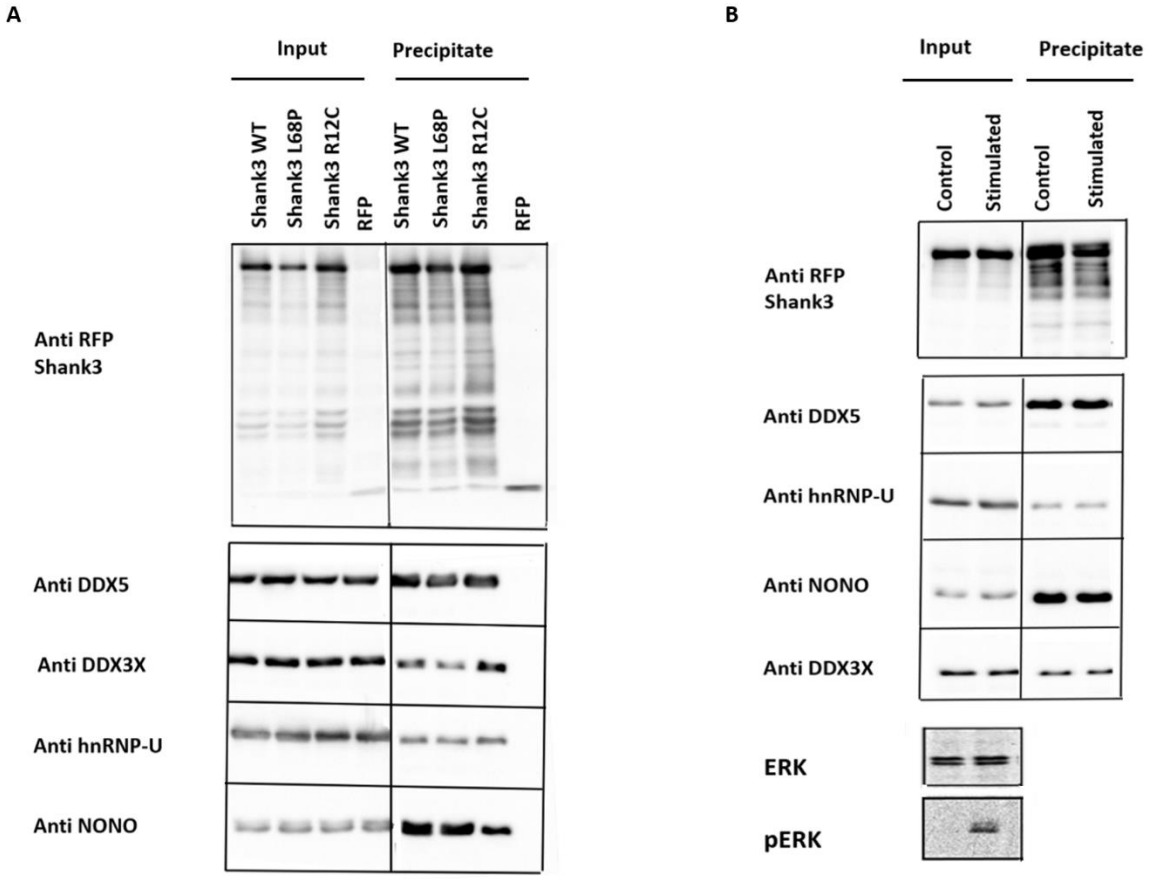

Figure 3.14 The effect of SPN domain mutations and interaction with Ras on Shank3- RNA binding protein interaction. A. 293T cells were transfected with RFP-tagged full length Shank3 WT and two mutant variants L68P and R12C. The endogenous RNA binding proteins were coprecipitated and detected using specific antibodies. The results show that L68P and R12C mutations in the SPN domain do not interfere with the interaction between Shank3 and RNA-binding proteins. **B.** The transfected 293T cells with Shank3 WT were overnight incubated in a serum starvation condition and on the following day one of the plates was stimulated using 10ng/µL of EGF 20 min before lysis. The result of co-precipitation of endogenous RNA-binding proteins with Shank3 WT do not show any significant difference after activating the endogenous Ras proteins in 293T cells, indicating that theses interactions are Ras-independent.

3.3.1.5 Brain extracted DDX5 binds to the Shank3 N-terminus fragment

Further on, to verify the interaction between Shank3 N-terminus and RNA binding proteins in the brain, I performed an affinity purification using a bacterially expressed His_6-SUMO fusion protein containing the SPN domain and the complete set of Ank repeats. This fragment had already been used for crystallization of the Shank3 N-terminus and can therefore be expected to fold properly. After

purification, the protein was immobilized by covalent coupling to sepharose beads and used as an affinity matrix for purifying the binding partners from a whole brain lysate. Here, Shank1 N-terminus fragment was also included due to the fact that Shank1 shares a similar N-terminal SPN-Ank domain with Shank3. His_6-SUMO expressed from the empty vector was used as control (figure 3.15).

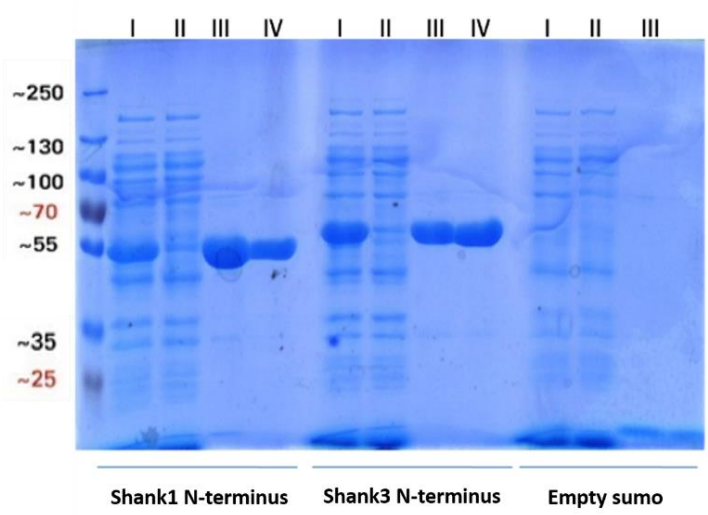

Figure 3.15 Purification of His_6-sumo-fusion proteins of the Shank3 and Shank1 N-termini. Fusion proteins of Shank1, Shank3, as well as SUMO alone (expressed from the empty vector) were expressed and purified as described in Materials and Methods. Samples from the purification procedure were analyzed by SDS-PAGE: Bacterial lysates before (I) and after (II) binding to Ni-NTA-agarose; (III) purified proteins obtained by Imidazol elution; and (IV) desalted protein which was used for immobilization to NHS sepharose. The gel was stained with coomassie blue.

Purification of brain proteins using this "sumo pulldown assay" show that among the RNA-binding proteins only endogenous DDX5 binds to the Shank3 and Shank1 N-terminus (figure 3.16 A). Further experiments using an isolated postsynaptic fraction of the WT mice brains showed that under basal conditions, DDX5 is not present in the postsynaptic density (figure 3.16 B).

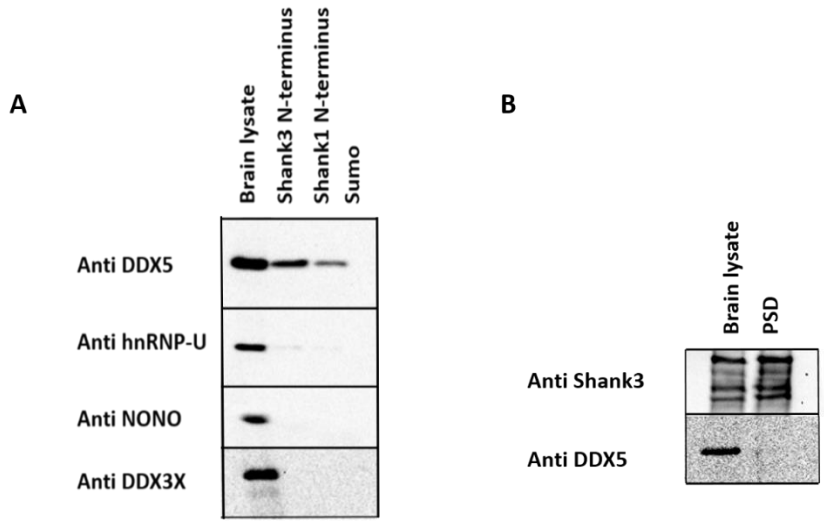

Figure 3.16 Interaction between Shank3 and RNA-binding proteins in the brain. A. The result of sumo purification using a Shank3 N-terminus fusion protein show that the brain extracted DDX5 is able to bind to Shank3 and Shank1 N-terminus whereas the other RNA-binding proteins fail to bind to do so. **B.** Using a DDX5 specific antibody, I investigated the presence of DDX5 in the whole brain lysate as well as an isolated postsynaptic density (PSD) fraction. The result shows under a normal condition DDX5 is not present in the PSD.

3.3.1.6 DDX5 shows a nuclear localization in neurons

To investigate the localization of DDX5 in the presence of Shank3 in neurons, I overexpressed GFP-Shank3 in primary cultured hippocampal neurons and used specific antibodies to detect endogenous DDX5. Here, I observed that in neurons DDX5 is completely recruited to the nucleus and colocalizes with Dapi (a marker for the nucleus) whereas overexpressed full length Shank3 is recruited to the dendritic spines, as seen before (figure 3.17).

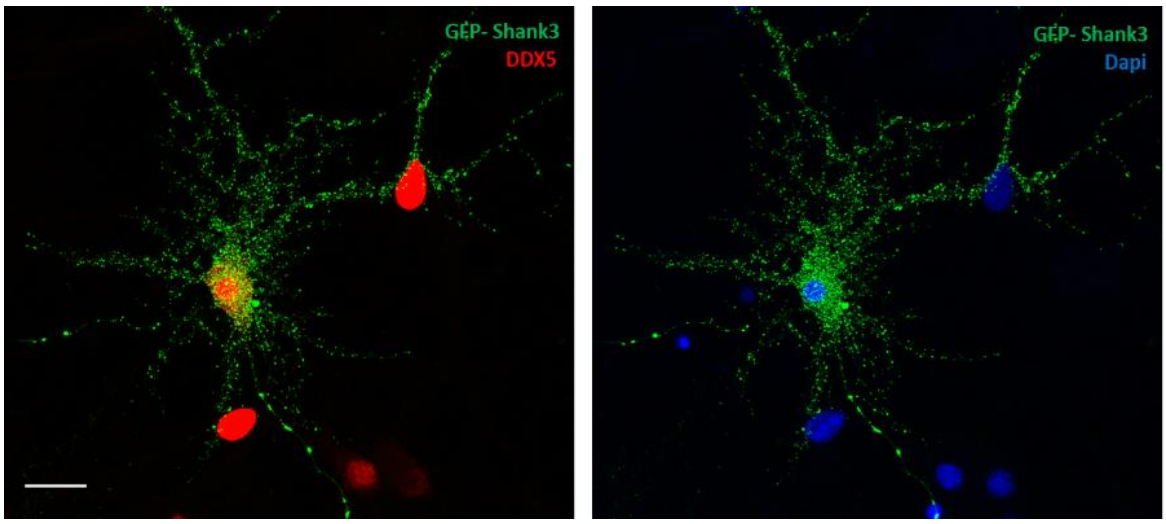

Figure 3.17 Different localization of Shank3 and DDX5 in neurons. Embryonic E18 rat hippocampal neurons were transfected with GFP-Shank3 (DIV 7) and fixed (DIV 14) and stained for endogenous DDX5 (red) and Dapi (blue). The result shows nuclear localization of DDX5 while overexpressed full length Shank3 shows punctate synaptic pattern (scale bar 20 µm).

It has been shown that some truncated variants of Shank3 found in patients with ASDs were localized in the nucleus. Also, through the alternative splicing, some of the Shank3 isoforms are most likely recruited to the nucleus (Grabrucker et al., 2014, Wang et al., 2014). On the other hand, an activity-dependent change in the composition of the postsynaptic density was reported that specifically increased the postsynaptic level of hnRNPs as well as DDX17 which is the paralog of DDX5 from the same family of RNA helicases (Zhang et al., 2012). Altogether, these data suggest that under basal conditions interaction of full length Shank3 (the Shank3a isoform as described in figure 1.6) with an RNA binding protein such as DDX5 is very unlikely, simply because these proteins are localized in distinct neuronal compartments and the conditions in which postsynaptic proteins and nuclear proteins can meet and interact with each other is still widely unclear.

3.3.2 Catenin proteins are the novel postsynaptic interaction partners of Shank3

In order to specifically target direct postsynaptic interaction partners of Shank3 N-terminus, an affinity purification was performed using a bacterially expressed His_6-SUMO fusion protein containing the SPN domain and the complete set of Ank repeats, as described above. His_6-SUMO protein expressed from the empty vector was used as negative control (figure 3.15). The Shank3 fusion protein was covalently

coupled to sepharose beads; these beads were then used as an affinity matrix for purification of putative binding partners from an isolated postsynaptic fraction from mouse brain after solubilization in DOC buffer. Purified proteins were again identified by mass spectrometry analysis at the UKE Core Facility for Mass Spectrometric Proteomics. The results revealed, among other proteins, six different members of the Catenin protein family as potential interaction partners for Shank3 (table 3.2).

Protein names	**Gene names**
Armadillo repeat protein deleted in velo-cardio-facial syndrome	*Arvcf*
14-3-3 protein sigma	*Sfn*
Catenin alpha-1	*Ctnna1*
Versican core protein	*Vcan*
Probable ubiquitin carboxyl-terminal hydrolase FAF-X	*Usp9x*
Arf-GAP with GTPase, ANK repeat and PH domain-containing protein 3	*Agap3*
Pancreatic alpha-amylase	*Amy2*
SH3 and multiple ankyrin repeat domains protein 3	*Shank3*
Catenin delta-2	*Ctnnd2*
Dynactin subunit 1	*Dctn1*
Myosin phosphatase Rho-interacting protein	*Mprip*
Cadherin-2	*Cdh2*
F-box only protein 41	*Fbxo41*
Catenin delta-1	*Ctnnd1*
Disks large-associated protein 4	*Dlgap4*
Synaptosomal-associated protein 47	*Snap47*
Claudin-11	*Cldn11*
Ras/Rap GTPase-activating protein SynGAP	*Syngap1*
Voltage-dependent N-type calcium channel subunit alpha-1B	*Cacna1b*
Arf-GAP with GTPase, ANK repeat and PH domain-containing protein 2	*Agap2*
Disks large homolog 3	*Dlg3*
SRC kinase signaling inhibitor 1	*Srcin1*
Catenin beta-1	*Ctnnb1*
Disks large homolog 4	*Dlg4*
Voltage-dependent R-type calcium channel subunit alpha-1E	*Cacna1e*
Catenin alpha-2	*Ctnna2*

Latrophilin-1	*Lphn1*
Sorbin and SH3 domain-containing protein 1	*Sorbs1*
Brain-specific angiogenesis inhibitor 2	*Bai2*

Table 3.2 Results of mass spectrometric analysis of Shank3 N-terminus postsynaptic interaction partners. The isolated postsynaptic fraction from mouse brain was subjected to affinity purification with either a His_6-SUMO/Shank3 N-terminal fusion protein or His_6-SUMO as negative control. Both sets of samples were analysed by mass spectrometry. The label free quantification (LFQ) intensity signals obtained from the negative control samples were subtracted from the LFQ intensity signals obtained from the Shank3 N-terminus purified samples. Partners with the highest residual LFQ intensity signals are listed in the table above. Proteins of the Catenin family are highlighted in yellow.

3.3.2.1 δ-Catenin is the interaction partner of the Shank3 N-terminus

Both β- and δ-Catenin had been shown before to be in a complex with Shank proteins. However, it was not clear whether these are direct interactions, which domains of Shank might be involved and what the functional consequences are (Quitsch et al., 2005, Qin et al., 2018). To further differentiate between different interacting proteins, I performed the sumo-pulldown experiment with 293T cells expressing different GFP-tagged variants of Catenin, as well as HCN1 and α-fodrin. Here, also a fusion protein encoding the Ank repeats only is included. The data indicate that δ-Catenin binds most specifically to SPN–Ank and Ank fusion proteins, in contrast to β-Catenin which appeared to bind quite weakly. α-Fodrin binds stronger when the inhibitory SPN domain is removed in agreement with previous data from our lab; (Mameza et al., 2013), whereas HCN1 does not bind at all under these conditions (figure 3.18).

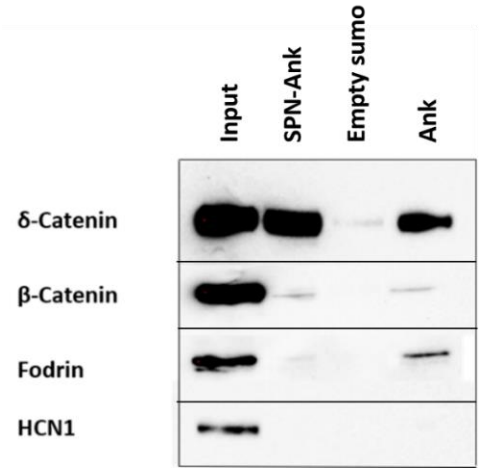

Figure 3.18 Sumo-pulldown of Ank interaction partners. 293T cells expressing GFP-tagged versions of the proteins indicated were lysed (Input samples) and subjected to a pulldown assay using immobilized fusion proteins of the complete Shank3 N-terminus (SPN-Ank), the SUMO control protein or the Ank repeats alone. δ-Catenin shows a strong specific binding to Shank3 N-terminus when compared to the other interaction partners.

3.3.2.2 Shank3 colocalizes with β-Catenin and δ-Catenin in 293T cells

Performing a colocalization assay in 293T cells showed both β-Catenin and δ-Catenin are highly co-localized with Shank3 but in different ways (figure 3.19). β-Catenin is known to function as a nuclear

protein and apparently targets Shank3 to the nucleus. δ-Catenin is membrane associated due to its palmitoylation and leads to partial translocation of Shank3 to the plasma membrane.

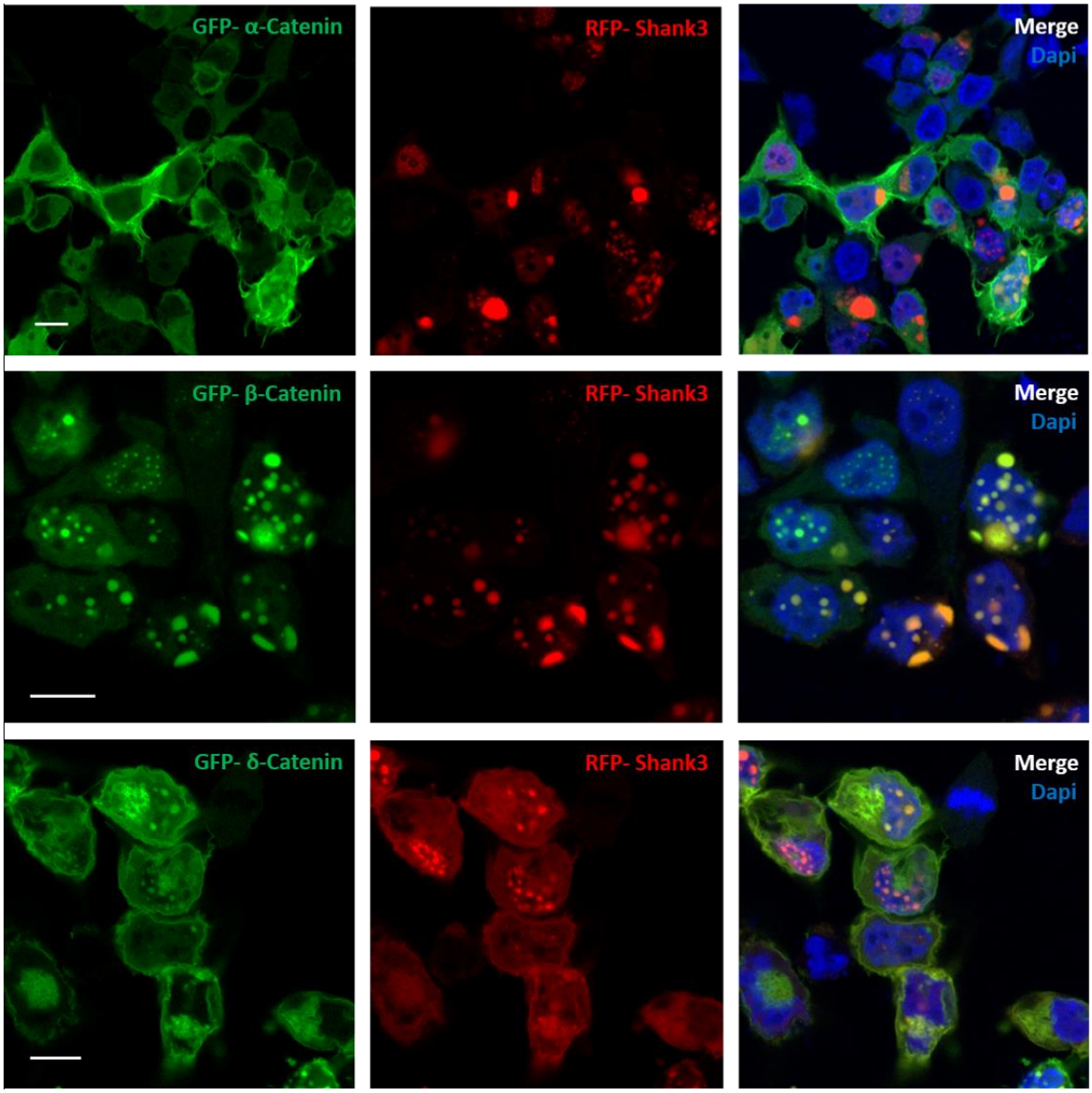

Figure 3.19 Colocalization assay in HEK cells. RFP-tagged Shank3 was co-expressed with GFP-tagged Catenin proteins in 293T cells, followed by fixation and confocal microscopic analysis. I observed (1) no significant overlap between α-Catenin and Shank3, with Shank3 presenting in large nuclear and cytosolic clusters, as described previously (Quitsch et al., 2005) (also see above NLS figure 3.11); (2) extensive colocalization of Shank3 and β-Catenin in nuclear clusters; and (3) extensive colocalization of δ-Catenin and Shank3 at the plasma membrane (but also in nuclear/ intracellular clusters). Blue: Dapi staining shows nucleus (scale bar 10µm).

3.3.2.3 Only β-Catenin and δ-Catenin bind to Shank3

Using co-expression/co-immunoprecipitation methods I compared the ability of three different members of the Catenin family (α-, β- and δ- Catenin) for binding to Shank3. The results showed that β-Catenin and δ-Catenin (but not α-Catenin) interact with full length Shank3 while only δ-Catenin binds

to the Shank3 N-terminus. This indicates that δ-Catenin is a novel interaction partner of the Shank3 N-terminus, and β-Catenin most likely binds to a domain other than the N-terminus (figure 3.20).

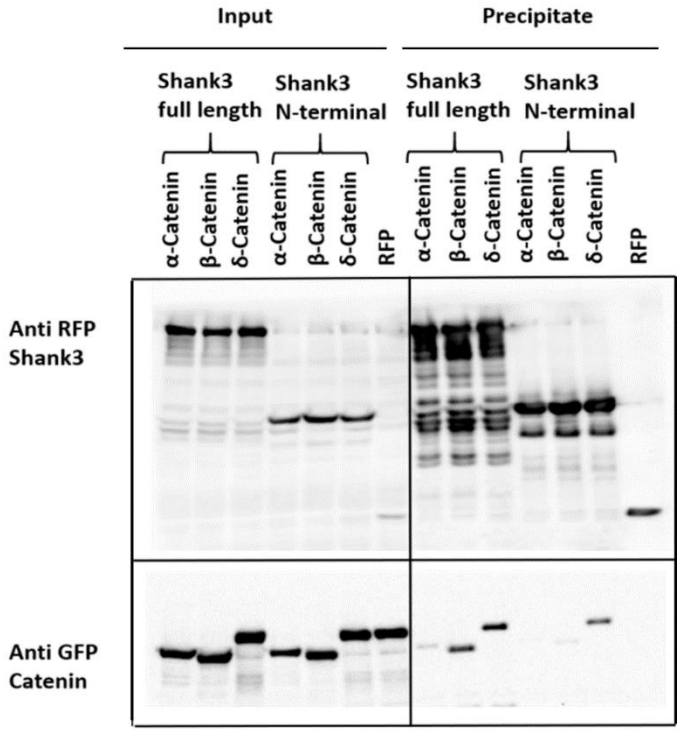

Figure 3.20 Interaction of Catenin proteins with Shank3. 293T cells co-expressing mRFP-Shank3 with GFP-tagged Catenin variants were lysed and subjected to immunoprecipitation using RFP-trap. The experiment shows that β- and δ-Catenin (but not α-Catenin) bind to full length Shank3, while only δ-Catenin binds to the Shank3 N-terminal fragment (SPN+Ank).

3.3.2.4 β-Catenin and δ-Catenin bind to distinct domains of Shank3

As these data indicated a differential mode for the interaction of Shank3 with different Catenins, I used a set of Shank3 deletion constructs to determine which domains of Shank3 are responsible for binding to these two proteins (figure 3.21). Again, by co-expression and co-immunoprecipitation, I confirmed that δ-Catenin binds to the N-terminal Ank repeats of Shank3. β-Catenin binds to the PDZ domain of Shank3, most likely through its C-terminal PDZ ligand motif (figure 3.21). Therefore, these results indicate that β-Catenin and δ-Catenin are novel interaction partners of Shank3 that bind to distinct domains of this protein.

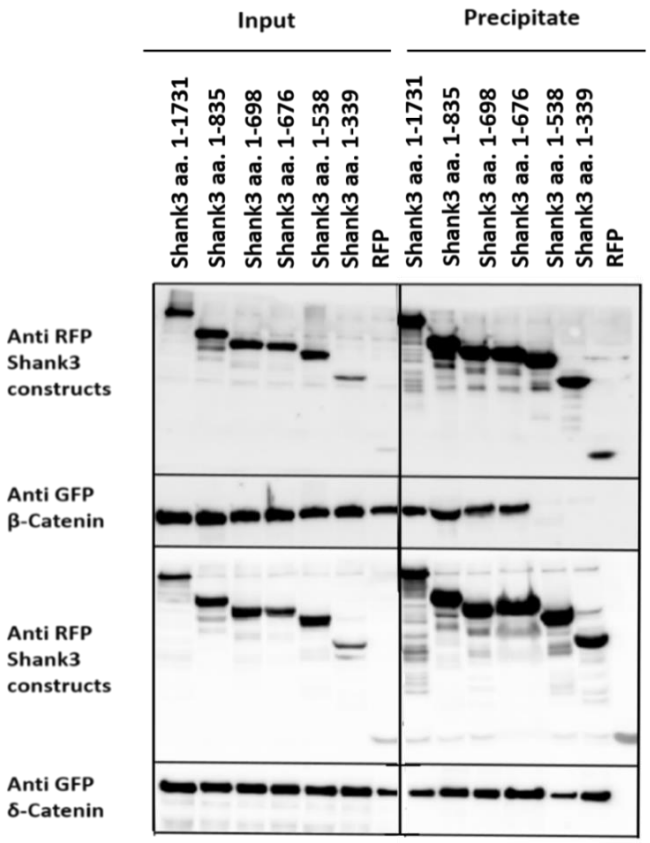

Figure 3.21 Mapping the binding sites for Catenin family members on Shank3. 293T cells co-expressing mRFP-Shank3 fragments with GFP-tagged Catenin proteins were lysed. The results of co-immunoprecipitation indicate that β-Catenin binding is dependent on the PDZ domain of Shank3, while δ-Catenin binds to all fragments of Shank3 tested, including the shortest truncated Shank3 protein which is the N-terminal part (SPN+Ank).

3.3.2.5 β-Catenin binds to the Shank3 PDZ domain via an internal PDZ ligand

SAPAP proteins (SAPAP1-4) are well-known interaction partners of Shank3 that bind to the PDZ domain (Naisbitt et al., 1999) (also: see above, figure 3.4). In a recent study an N-terminal extended PDZ domain including the linker region between PDZ and SH3 domain has been proposed as the SAPAP binding site on Shank3 which explains the strong interaction between Shank3 and SAPAP, compared to other ligands of the Shank3 PDZ domain (Zeng et al., 2016). To investigate whether this is also relevant for β-Catenin, I performed a coimmunoprecipitation assay using a Shank3 N-terminal fragment which contains the linker region but lacks the PDZ domain. The result showed that β-Catenin binds only to the PDZ fragment but not the linker region (figure 3.22 A).

In most cases a C-terminal PDZ ligand is responsible for making contact with the PDZ domain of the interaction partner (Lee and Zheng, 2010). Therefore, using both PDZ ligand mutant (T779A) and a PDZ ligand deletion construct of β-Catenin, I tried to map the binding site on β-Catenin (figure 3.22 B). Interestingly, after mutating or removing the C-terminal PDZ ligand of β-Catenin, the interaction with Shank3 seemed to be intact, meaning that the interaction between Shank3 PDZ domain and β-Catenin is most likely mediated by an internal PDZ ligand (figure 3.22 C).

A

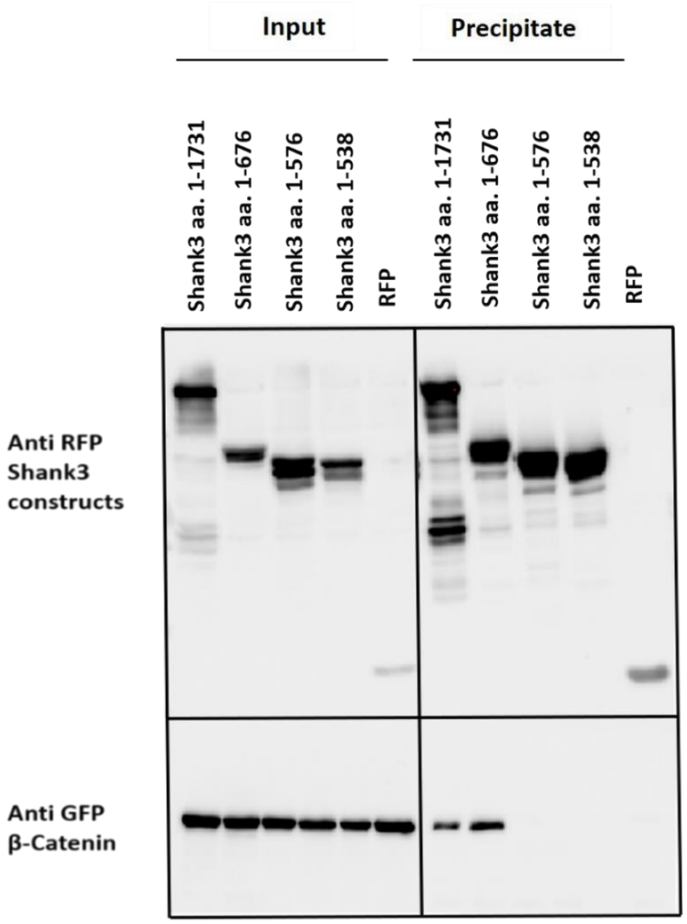

Figure 3.22 Mapping the binding sites on β-Catenin. A. 293T cells expressing GFP-tagged β-Catenin with RFP-tagged Shank3 fragments were lysed and subjected to immunoprecipitation using RFP trap. Input and precipitate samples were then analysed by Western blotting using RFP and GFP specific antibodies. The data confirm that unlike SAPAP protein, β-Catenin binds only to the PDZ domain of Shank3. **B.** Sequences of a canonical type I PDZ ligand and two different mutations introduced to destroy the PDZ ligand motif of β-catenin are indicated. X represents any amino acid, and Φ represents large hydrophobic amino acids. **C.** Coexpression of RFP-tagged Shank3 with GFP-tagged β-Catenin carrying C-terminal mutations, followed by coimmunprecipitation using GFP-trap, showed that mutation or deletion of the C-terminal PDZ ligand of β-Catenin does not interfere with the binding to the Shank3 PDZ domain, indicating that the interaction might be mediated by an internal PDZ ligand.

B

The canonical PDZ ligand	**X X X S/T X φ COO⁻**
β- Catenin C-terminal PDZ ligand	**W F D T D L COO⁻**
β- Catenin T779A	**W F D A D L COO⁻**
β- Catenin Δ PDZ ligand	**W F COO⁻**

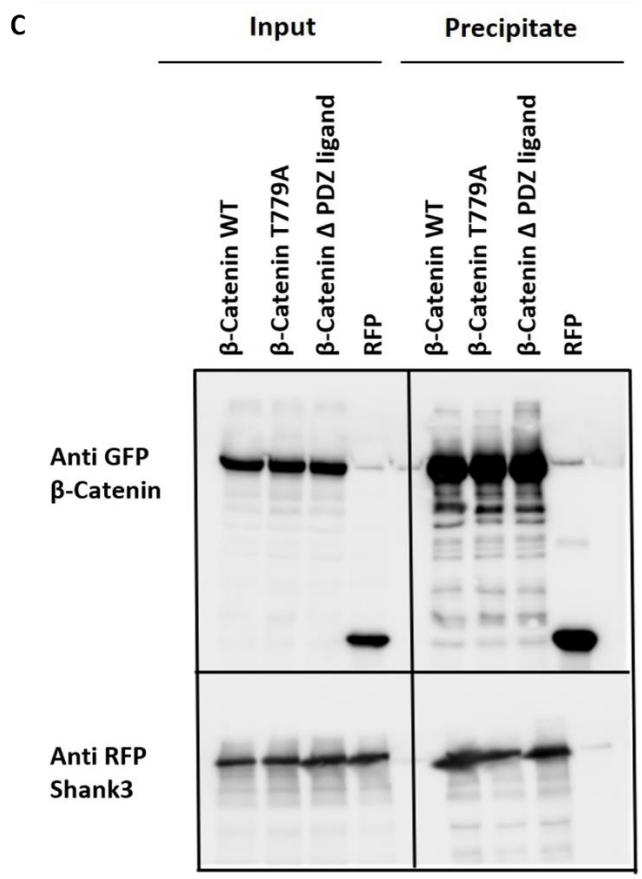

3.3.2.6 δ-Catenin binds to the Shank3 Ank domain via its Armadillo repeat domain

Mapping the binding site on δ-Catenin was performed using δ-Catenin deletion constructs that produce δ-Catenin fragments lacking different domains including the N-terminus, the Armadillo (Arm) repeat region or the C-terminal portion (figure 3.23 A). 293T cells were transfected with mRFP-Shank3 and different δ-Catenin deletion constructs. The result of coprecipitation of these truncated δ-Catenin proteins with Shank3 showed that with removing the Armadillo repeat region (mainly the first N-terminal Arm repeats), the interaction with Shank3 is strongly reduced, meaning that the Arm repeat region of δ-Catenin is a new interaction motif for the Shank3 Ank domain (figure 3.23 B).

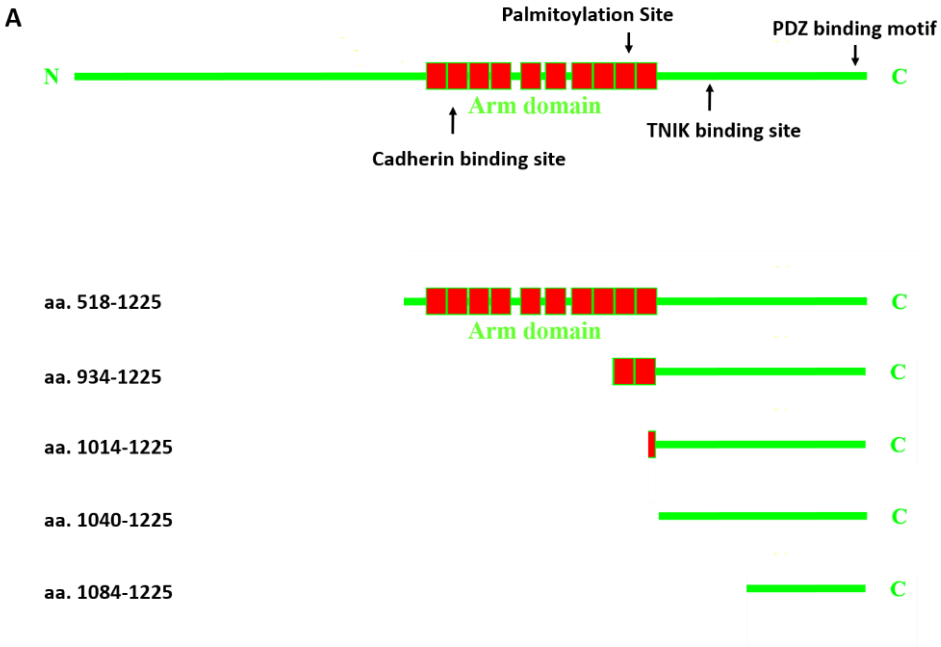

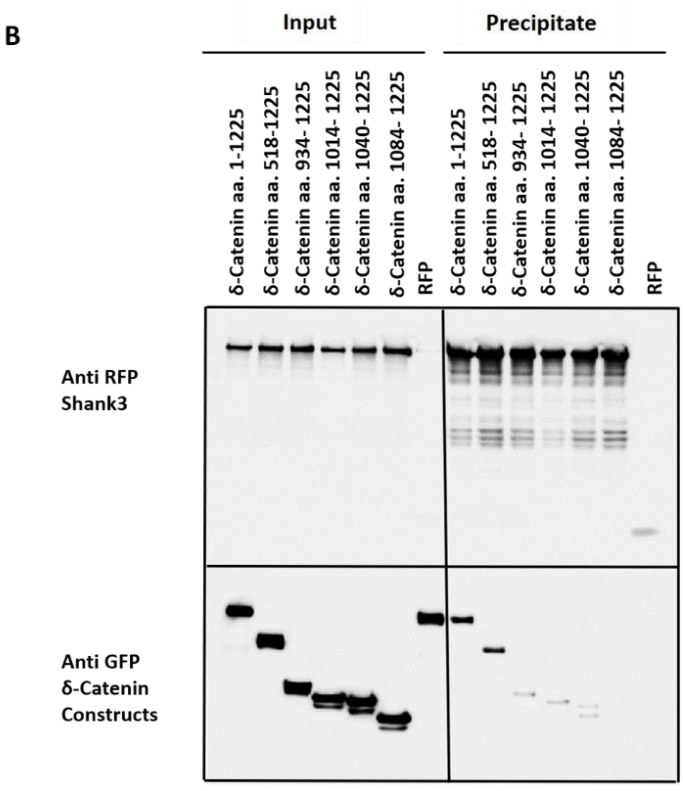

Figure 3.23 Mapping the binding sites on δ-Catenin. A. The domain structure of the full length δ-Catenin, and the truncated proteins used in this study. The binding site for N-Cadherin and the phosphorylation and palmitoylation sites are indicated by arrows. **B.** The result of coimmunoprecipitation of different truncated δ-Catenin proteins with full length Shank3 show that the Arm repeats bind to the Ank domain of Shank3.

3.3.2.7 β-Catenin and δ-Catenin colocalize with Shank3 in the dendritic spines

To investigate whether Catenin proteins colocalize with Shank3 in neurons, primary rat hippocampal neurons were transfected (DIV 7) with constructs coding for mRFP-Shank3 and GFP-tagged β-Catenin or δ-Catenin constructs. The neurons were fixed (DIV 14) and stained for dendritic marker Map2 and Dapi for staining the nucleus. The results of imaging show the colocalization of Shank3 with these two

proteins of Catenin family in the dendritic spine. However, in the neuron overexpressing β-Catenin a nuclear co-cluster of Shank3 and β-Catenin was observed (figure 3.24).

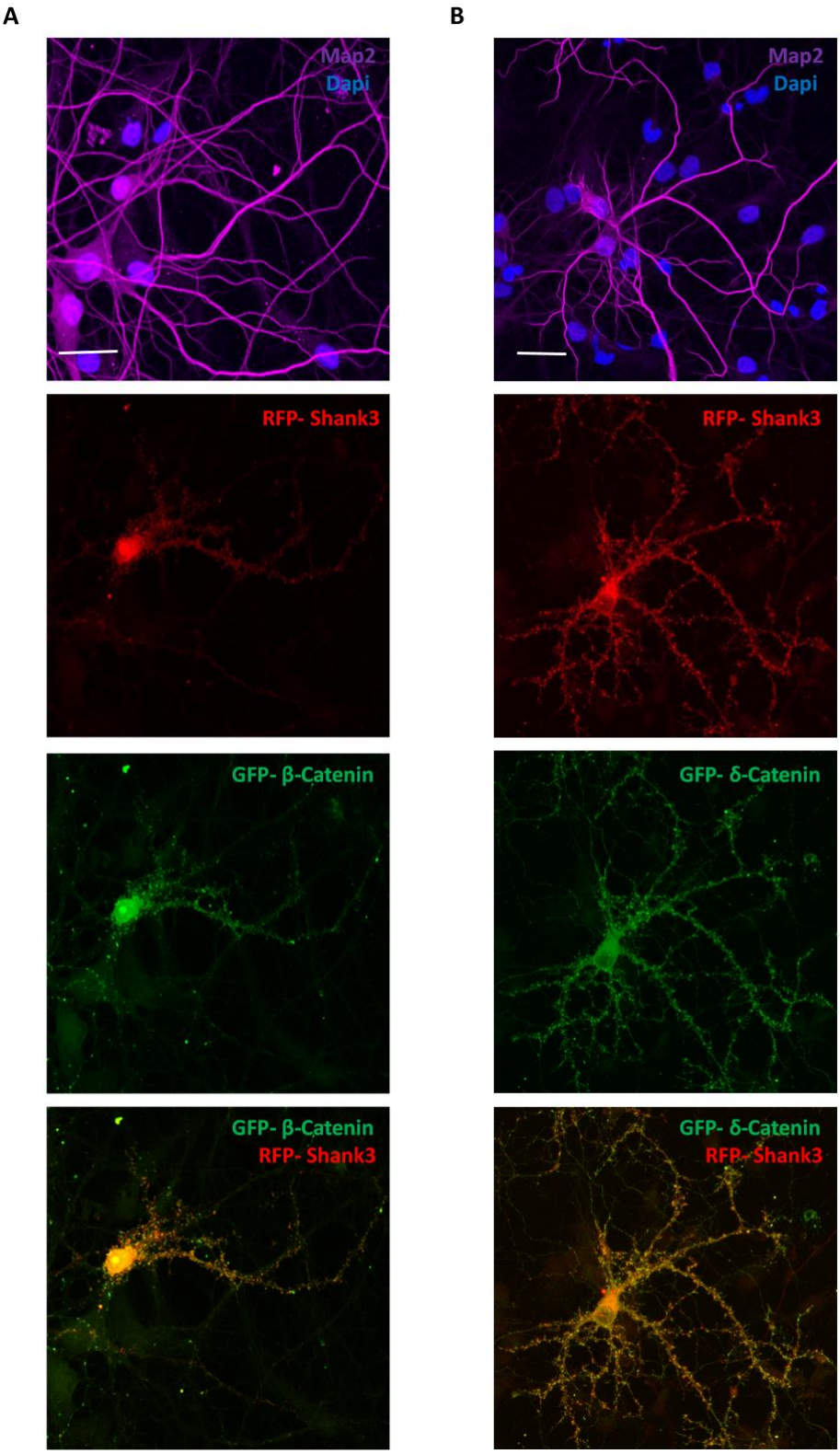

Figure 3.24 Colocalization assay in the neurons. Rat hippocampal neurons were transfected with mRFP-Shank3 with GFP tagged Catenin proteins and stained for Map2 (magenta) and Dapi (blue). **A.** δ-Catenin shows colocalization with Shank3 in in a punctate pattern along dendrites, indicative of a postsynaptic localization. **B.**

In addition to the colocalization of β-Catenin with Shank3 along dendrites, both proteins seem to colocalize in a nuclear cluster as well (scale bar 20 µm).

3.3.2.8 The SPN-Ras interaction does not affect the binding to Catenin proteins

Since I had previously observed that the activation of Ras in 293T cells affects the interactions of both PDZ and Ank domain interactions with SAPAP and Fodrin respectively, I asked whether this also includes the newly found interaction partners from the Catenin family that bind to either the PDZ or Ank domain of Shank3. An EGF stimulation assay was performed in 293T cells coexpressing mRFP-Shank3 with GFP-tagged Catenin proteins. Using 10 ng/µL EGF after an overnight starvation condition, 20 min before the cell lysis the MAPK pathway was activated and Shank3 was co-precipitated with the Catenin proteins in a GFP-trap experiment. Comparing the strength of the co-precipitated Shank3 bands before and after stimulation showed that the binding of Catenin proteins to the Shank3 is not affected by activation of endogenous Ras proteins in 293T cells (figure 3.25).

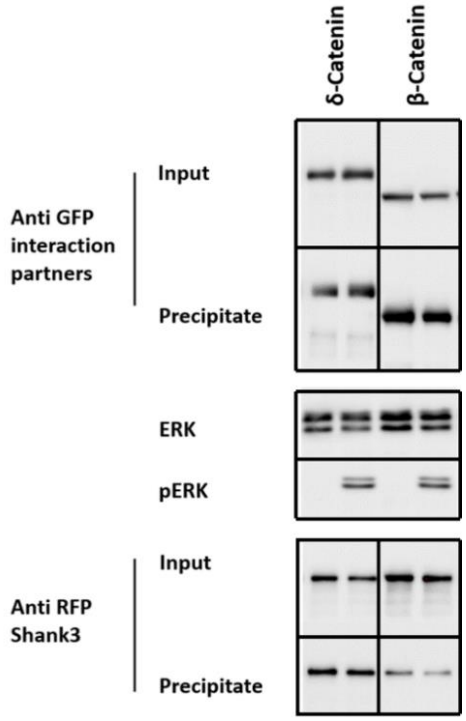

Figure 3.25 EGF stimulation assay. 293T cells overexpressing Shank3 together with β- or δ- Catenin were treated with 10ng/mL of EGF to activate the endogenous Ras proteins, followed by immunoprecipitation of GFP-tagged proteins using GFP trap. The quantification of Western Blot of input and precipitate samples showed that the interaction between Shank3 and the proteins of Catenin family is independent of Ras activation. Activation of the Ras pathway was verified by analysing cell lysates for active pERK.

3.3.2.9 The L68P mutation significantly improves binding to δ-Catenin

Since δ-Catenin binds to the Ank domain, I further aimed to determine whether ASD-related mutations in the Shank3 N-terminal affect binding of δ-Catenin. The results of a series of co-immunoprecipitation experiments using Shank3 constructs carrying patient mutations with δ-Catenin show that none of these mutations results in a loss of binding, but the L68P mutation significantly improves binding to δ-Catenin. The Shank1 protein also binds to δ-Catenin; this was expected based on the high similarity between the Shank1 and Shank3 N-termini which both include the SPN-Ank motifs (figure 3.26).

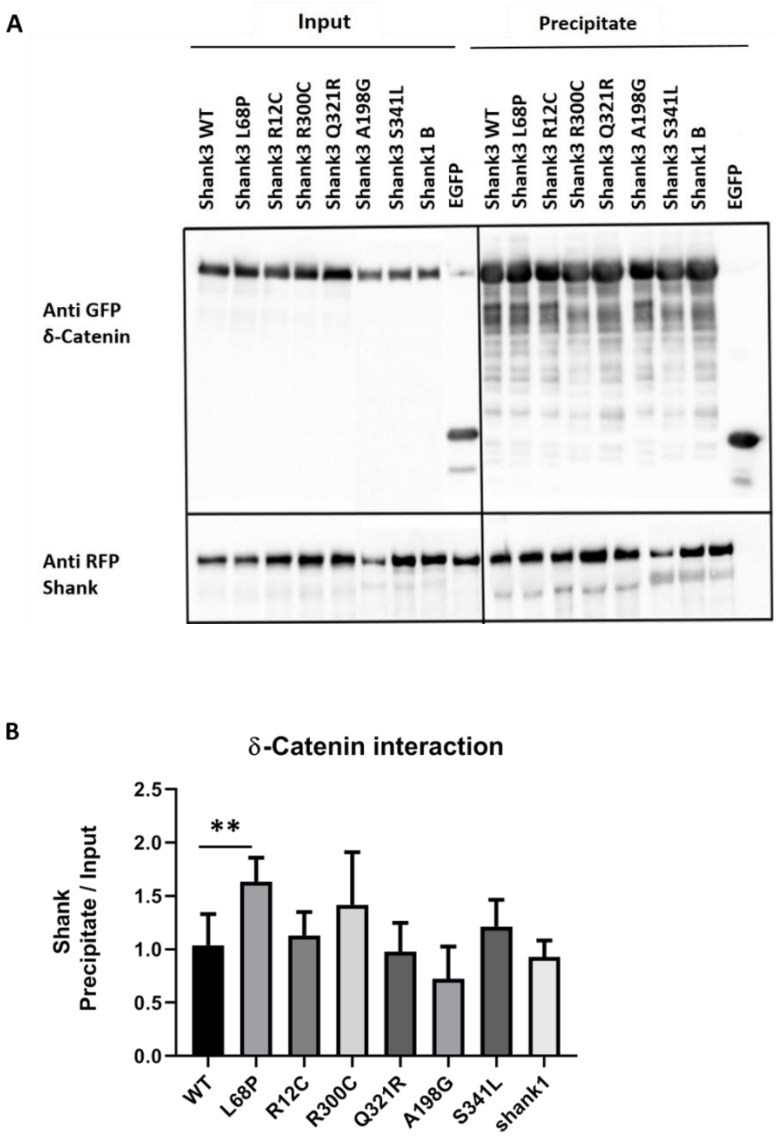

Figure 3.26 The effect of Shank3 N-terminus mutations on binding to δ-Catenin. A. Overexpressed Shank variants carrying ASD mutations were co-immunoprecipitated with δ-Catenin. **B.** The L68P mutation improves the binding of δ- Catenin to Shank3. Shank1 is also able to interact with δ-Catenin via its N-terminal domain (N= 4, one-way ANOVA with Dunnett's Test, **p= 0.001, mean ± SD).

3.3.2.10 The P141A mutation slightly increases the binding to δ-Catenin

One of the Shank3 N-terminal missense mutations which previously has not been functionally analysed is P141A. P141A is a *de novo* mutation found in an autistic patient (Boccuto et al., 2013). In the 3D structure of Shank3, P141 is situated in the contact surface between SPN domain and Ank (see figure 1.7). To clarify the effect of this ASD associated mutation on the interaction of the Shank3 Ank domain with δ-Catenin, I performed a co-expression/co-immunoprecipitation experiment using an RFP-tagged Shank3 P141A mutant variant as well as L68P variant comparing with WT Shank3 protein. Using the RFP trap matrix in this experiment also allowed me to verify the effect of the L68P mutation on the

interaction between Shank3 and δ-Catenin which previously has been obtained from GFP-trap experiments. The results of co-immunoprecipitation showed that the P141A mutation slightly increased the binding of δ-Catenin to the Ank domain of Shank3; however, this effect is not as strong as the effect of the L68P mutation that again reached the same strength as before (figure 3.27 A). Later, I checked the effect of P141A mutation also on the binding of Fodrin to the Ank domain of Shank3. A similar effect was observed, with a slight increase in the binding of Fodrin, whereas L68P very significantly improved the binding to Fodrin consistent with the results published by Mameza et al. in 2013 (Mameza et al., 2013) (figure 3.27 B).

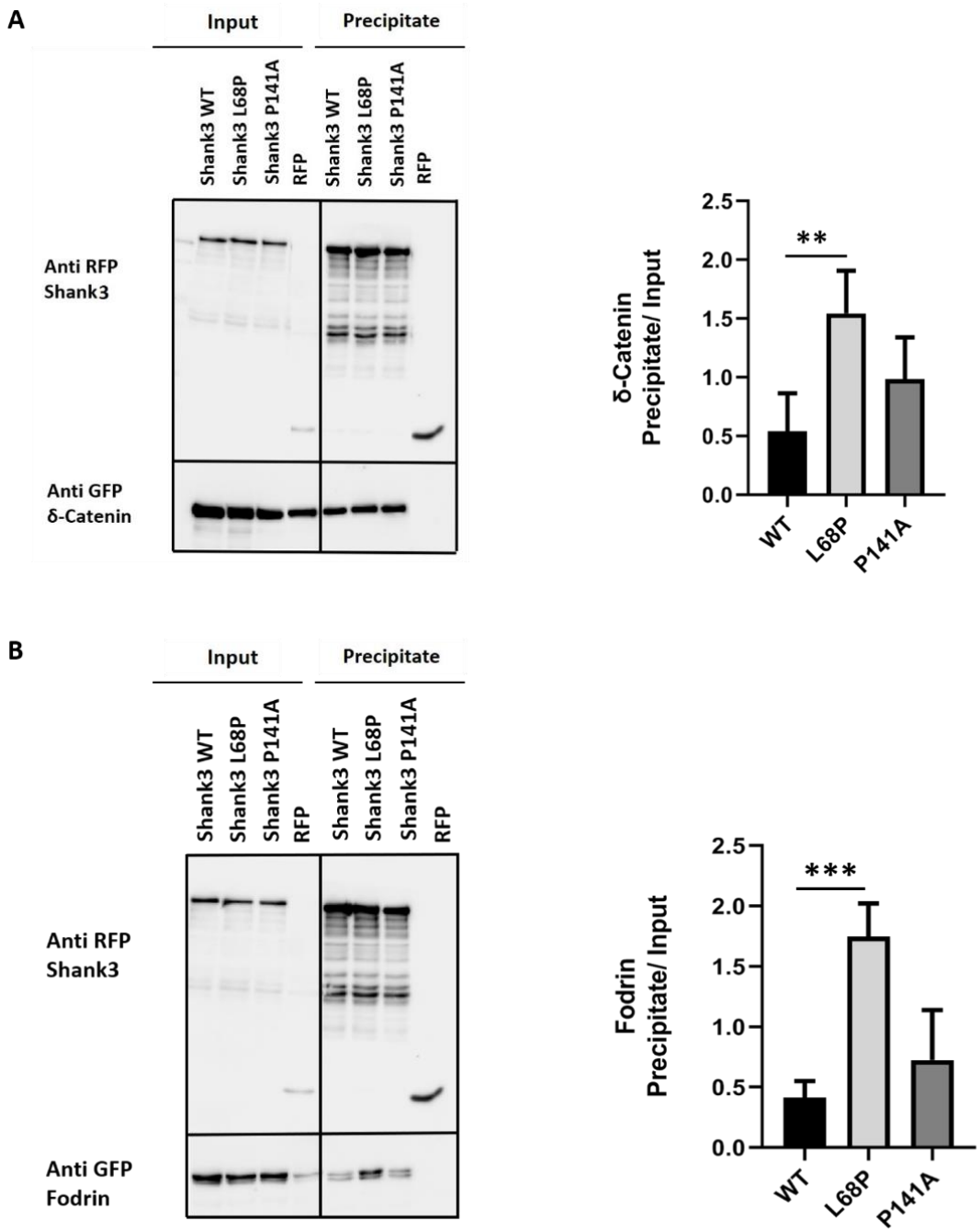

Figure 3.27 The effect of Shank3 P141A mutation on binding of Shank3 Ank domain to δ-Catenin and Fodrin. Overexpressed δ-Catenin (**A)** and Fodrin (**B)** were co-immunoprecipitated with Shank WT or variants carrying L68P and P141A mutations. The blots and representative graphs show that the *de novo* mutation P141A slightly (and non-significantly) improves the binding of both Ank interaction partners while the effect of L68P is highly significant in improving binding of both Ank domain interaction partners (N = 4, one-way ANOVA with Dunnett's Test, ***p= 0.0003, mean ± SD).

3.3.2.11 The L68P and P141A mutations affect the distribution pattern of the Shank3 N-terminus in U2OS cells

Interestingly, I observed that the overexpressed Shank3 N-terminal fragment carrying the P141A mutation often tends to aggregate in cells. I have previously observed a very similar pattern by L68P mutant variant of Shank3. To investigate the distribution pattern of these Shank3 mutant variants, I overexpressed the mRFP-tagged N-terminal fragments of Shank3 carrying either L68P or P141A mutations as well as WT N-terminal fragment in U2OS cells. The cells were fixed a day after transfection and stained for Dapi. The results of confocal imaging showed that the P141A mutant sometimes occurs in cytosolic clusters in an expression level - dependent manner; therefore it behaves very similar to the L68P mutant. At lower expression levels, P141A mutant Shank3 is found in a diffuse cytosolic pattern similar to the overexpressed WT fragment (figure 3.28). Because of the position of this mutation in Shank3 N-terminus, these results might indicate that P141A is able to transiently disrupt the intramolecular interaction between SPN and Ank domain and result in an open N-terminal conformation which then leads to increased interactions between Ank and its interaction partners as well as clustering in the cell very similar to L68P.

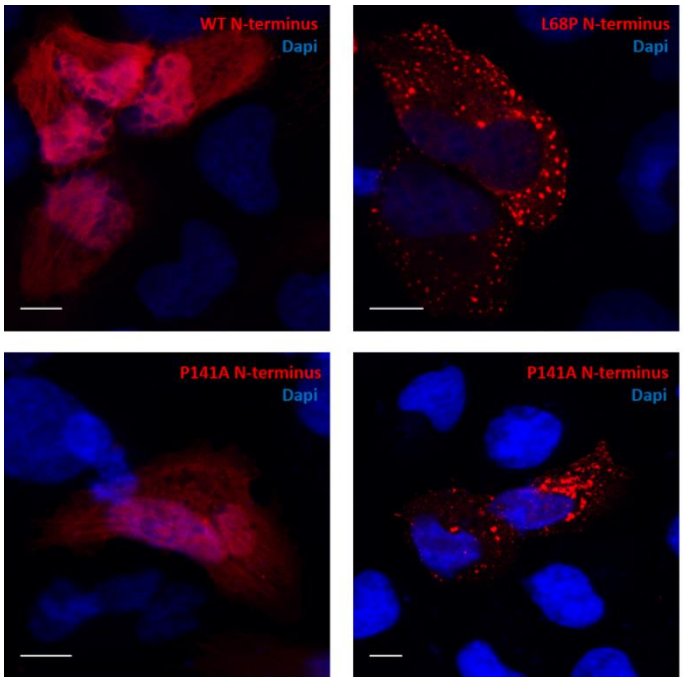

Figure 3.28 The effect of Shank3 mutations on the subcellular distribution of the Shank3 N-terminal fragments in U2OS cells. U2OS cells were transfected with Shank3 WT N-terminal fragment (aa. 1-339) or the N-terminal variants L68P or P141A and were fixed and stained for Dapi a day after transfection. The result of confocal imaging shows that the WT N-terminus shows a ubiquitous diffuse pattern in the cells whereas the L68P variant appears in cytosolic clusters. Interestingly, the P141A variant aggregates at high expression levels and leads to formation of protein clusters which are very similar to clusters observed with the L68P variant., At a lower expression level it shows a diffuse pattern very similar to the WT N-terminus (scale bar 10 µm).

3.3.2.12 δ-Catenin phosphorylation via TNIK does not affect its binding to Shank3

δ-Catenin has been reported as a neuronal TNIK substrate with multiple TNIK phosphorylation sites (Wang et al., 2016). To investigate the effect of TNIK phosphorylation on the interaction between Shank3 and δ-Catenin, I performed a co-expression/co-immunoprecipitation assay of Shank3 with δ-Catenin in the presence of either HA-tagged WT TNIK or a TNIK "kinase dead" mutant protein. Comparing the results of the co-precipitated GFP- δ-Catenin with mRFP-Shank3 protein showed that the presence of active WT TNIK does not change the state of interaction between Shank3 and δ-Catenin (figure 3.29). Therefore, it seems that the phosphorylation of δ-Catenin via TNIK in this condition most likely does not affect the interaction with Shank3.

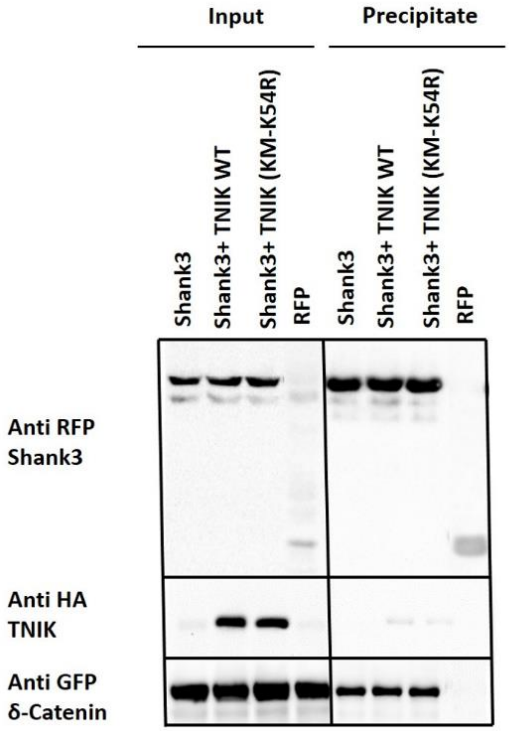

Figure 3.29 The effect of TNIK phosphorylation on Shank3-δ-Catenin interaction. 293T cells overexpressing GFP- δ-Catenin and mRFP-Shank3 without TNIK or in the presence of either HA-TNIK WT or the TNIK "kinase dead" mutant K54R were lysed. Co-immunoprecipitation was performed using RFP-trap beads. Comparing the amount of co-precipitated GFP-δ-Catenin in all three conditions showed that the presence of TNIK and most likely the phosphorylation of GFP- δ-Catenin via TNIK does not affect the interaction of GFP- δ-Catenin with Shank3.

3.3.2.13 The overexpressed δ-Catenin is colocalized with endogenous Shank3 in cultured neurons

Further, I investigate the localization of the overexpressed δ-Catenin in the presence of endogenous Shank3 proteins. The rat primary hippocampal neurons were transfected (DIV 7) with GFP δ-Catenin and a week later the neurons were fixed (DIV 14) and stained for endogenous Shank3 and Map2 dendritic marker. The result of confocal imaging showed that the overexpressed δ-Catenin highly colocalizes with endogenous Shank3 at the tip of dendritic spines (figure 3.30).

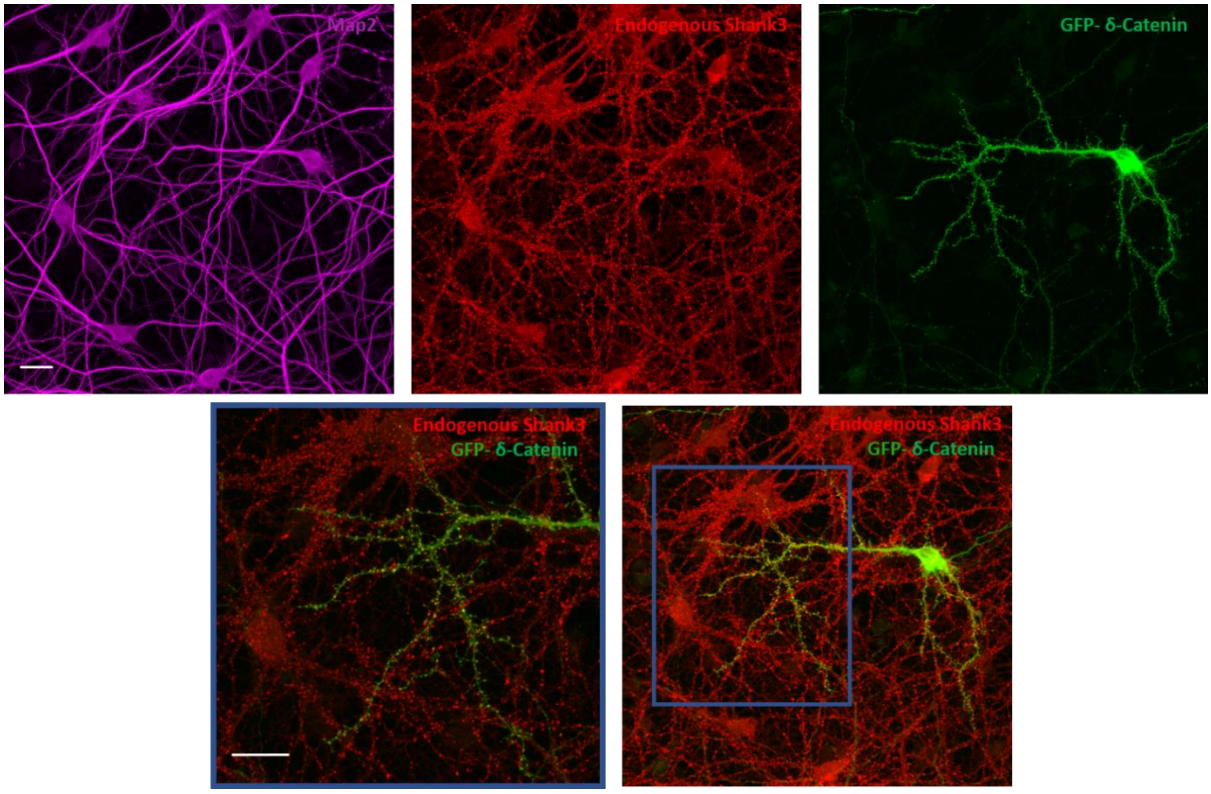

Figure 3.30 Colocalization of overexpressed δ-Catenin with endogenous Shank3 in the postsynaptic sites. An overview and a zoomed in image of a dendritic area of a neuron transfected with GFP- δ-Catenin (DIV 7) and stained for endogenous Shank3 (red) and Map2 (magenta). The overexpressed δ-Catenin in the primary hippocampal neurons is colocalized with endogenous Shank3 protein (scale bar 20µm).

3.3.2.14 Shank3 contributes to the postsynaptic targeting of δ-Catenin

To determine the *in vivo* relevance of the interaction between Shank3 and δ-Catenin, I took advantage of a KO mouse line lacking long (SPN+Ank domains containing) isoforms of Shank3 (Shank3a). I compared the isolated PSD fractions of Shank3 WT and KO mice (6 animal per each condition) by detecting δ-Catenin with a specific antibody. Here, I observed that the level of postsynaptic δ-Catenin is significantly reduced in the absence of Shank3a carrying the SPN+Ank repeats (figure 3.31 A). In agreement with our coimmunoprecipitation results, the postsynaptic localization of β-Catenin does not show dependency on Shank3 N-terminus and remains intact in the postsynaptic density of these Shank3a deficient mice (figure 3.31 B). Moreover, I compared the P2 fraction of the WT and Shank3 KO animals which contains the isolated membrane proteins of the brain. Here the level of membrane associated δ-Catenin is not different between Shank3 WT and KO animals. Altogether, these findings indicate that the general level of δ-Catenin is not affected by the absence of Shank3a. Instead, Shank3 might be involved in the postsynaptic trafficking or the stabilization of δ-Catenin at postsynaptic sites.

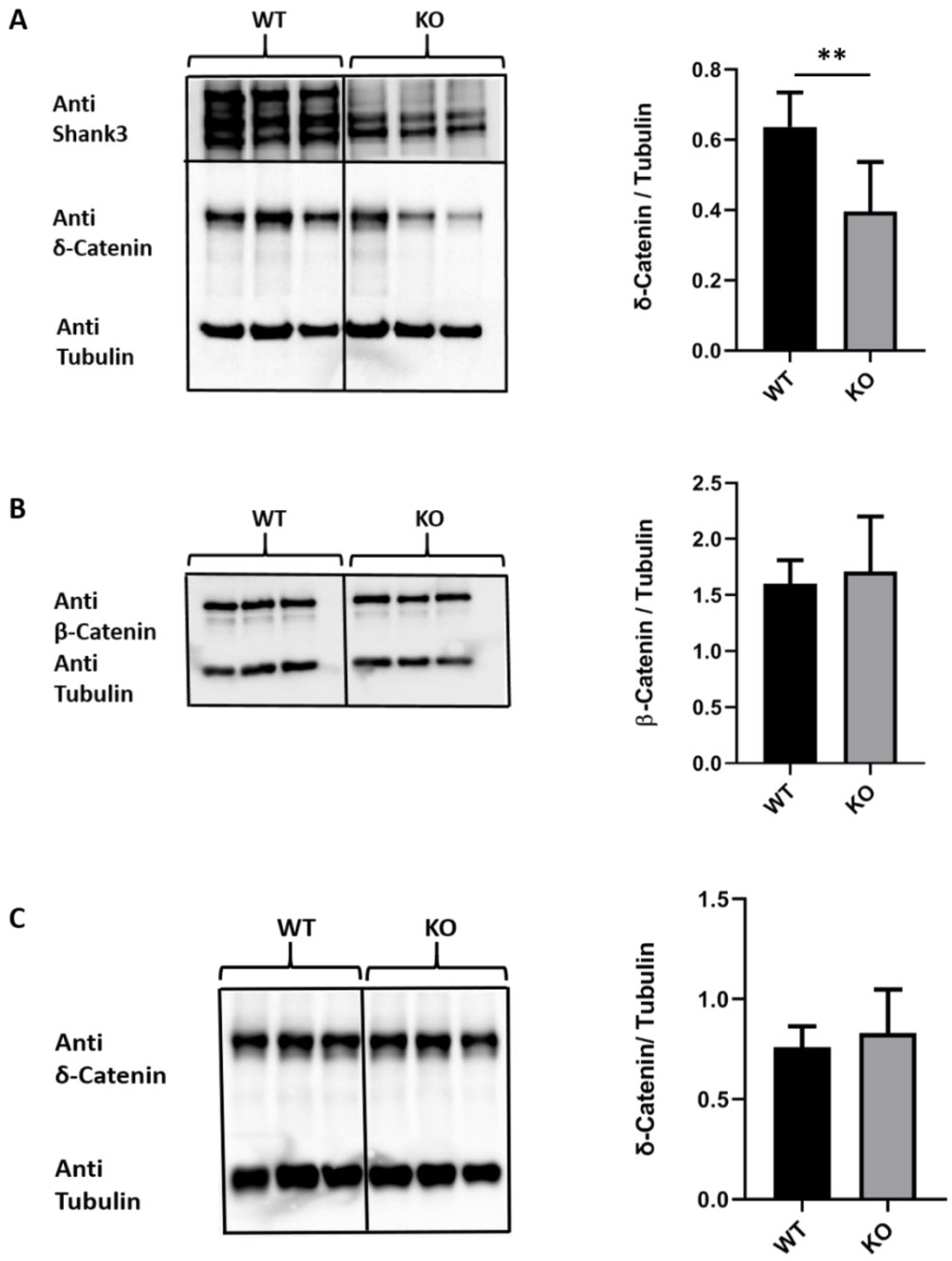

Figure 3.31 The level of Catenin proteins in the postsynaptic fraction of Shank3 KO mice. **A.** The PSD fractions from WT and KO mice lacking the larger SPN+Ank-containing isoforms of Shank3 were prepared and analyzed by Western Blotting using the antibodies indicated. δ-Catenin levels were quantified as the δ-Catenin/tubulin ratio. The two larger bands of Shank3 detected in the WT PSD samples are absent in the PSD of Shank3 KO mice, indicating the lack of larger isoforms of Shank3 containing N-terminal SPN+Ank domains. **B.** The postsynaptic localization of β-Catenin does not show any significant changes resulted from lacking Shank3 N-terminus. **C.** The level of δ-Catenin in the P2 fraction of Shank3 KO animals containing membrane associated proteins is not affected by the absence of Shank3 N-terminus (N= 6, unpaired T-test, **p= 0.004, mean ± SD).

3.3.2.15 N-Cadherin protein level is decreased in the postsynaptic fraction of Shank3 KO mice

It has been reported that the absence of δ-Catenin reduces the level of N-Cadherin (NCAD) at postsynaptic sites (Israely et al., 2004). One reason could be that because δ-Catenin reduces endocytosis of surface Cadherins, loss of δ-Catenin reduces Cadherin stability, thereby decreasing steady state levels (Davis et al., 2003, Xiao et al., 2003). To analyze whether Shank3, through its interaction with Catenins, contributes to the targeting of N-Cadherin to postsynaptic sites, I compared the isolated PSD fractions of Shank3 WT and KO mice (from the same animals used for previous experiments with β- and δ-Catenin). Using a specific antibody to detect N-Cadherin, here I showed that the level of postsynaptic N-Cadherin is slightly but not significantly reduced in the absence of the Shank3a isoform which carries the SPN+Ank domains (figure 3.32).

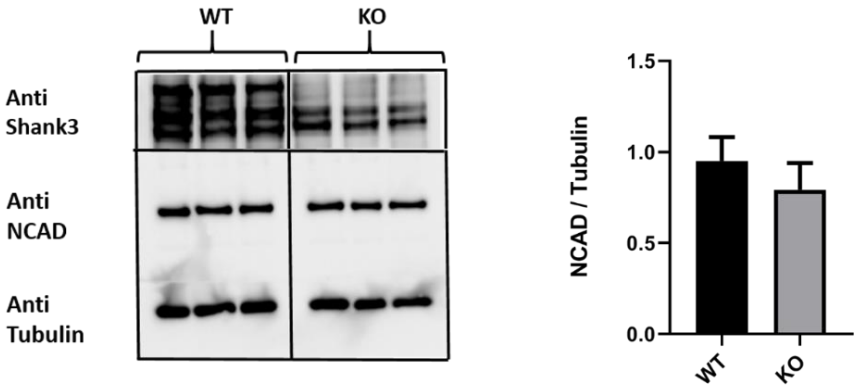

Figure 3.32 The level of N-Cadherin in the postsynaptic fraction of Shank3 KO mice. The level of N-Cadherin is slightly reduced in the postsynaptic fraction KO mice lacking the larger SPN-Ank-containing isoforms of Shank3 (N= 6, unpaired T-test, p= 0.07 mean ± SD).

Chapter 4

Discussion

4.1 Shank3 co-clusters with PSD95 in distinct nanodomains in the PSD

In 1999, Shank proteins were reported as a novel family of proteins which are specifically localized in excitatory synapses and highly enriched in the PSD. Shank directly interacts with SAPAP (GKAP), and as a major component of the PSD-95/ SAPAP/ Shank protein complex shows a high level of colocalization with various postsynaptic markers including PSD95 in cultured neurons (Naisbitt et al., 1999).

Among the various synaptic molecules, PSD95 (Post Synaptic Density protein 95) is one of the most well-studied proteins. PSD95 is an abundant scaffold protein of the PSD that has been regarded as a central player in the organization of the PSD core complex which is thought to be critical for synaptic development and transmission (Zhu et al., 2017, Broadhead et al., 2016, Chen et al., 2008). PSD95 forms complexes comprising glutamate receptors, ion channels, signalling enzymes and adhesion proteins in the PSD that are essential for controlling synaptic strength and plasticity in response to patterns of neural activity (Husi et al., 2000, Ferna´ndez et al., 2009).

Until recently, our knowledge of the postsynaptic density was limited to EM studies that described the PSD as an electron dense region in excitatory synapses. Likewise, the diffraction limited resolution of conventional light microscopy hindered us from resolving morphological details of the PSD. However, over the past few years, the advent and development of super-resolution nanoscopic techniques revolutionized our knowledge of the molecular architecture of synapses and sub-synaptic organisation of synaptic molecules (Broadhead et al., 2016, Dani et al., 2010, Frank and Grant, 2017, Wegner et al., 2018).

Electron microscopy first showed the distribution pattern of PSD95 with an orientation towards the synaptic membrane throughout the PSD (Chen et al., 2008, Petersen et al., 2003, Valtschanoff and Weinberg, 2001). Further on, super-resolution studies revealed that PSD95 is in fact organized into nanoclusters (NCs) of approximately 50–250 nm in diameter (MacGillavry et al., 2013, Nair et al., 2013, Fukata et al., 2013). Since PSD95 super-complexes are ~2 MDa in size (Husi and Grant, 2001), the PSD95 NCs might represent the local packing of dozens or hundreds of these complexes. These PSD95 nanodomains are building blocks underpinning the structure of the PSD that are also present *in vivo*. Some synapses contain multiple NCs suggesting that NCs may be subdomains of the PSD and their number is a determinant of the PSD size (Broadhead et al., 2016).

In 2013, using a combination of live cell, single molecule imaging and quantitative spatial analysis, McGillavry et al. showed that the four major PSD scaffold proteins Shank3, PSD95, SAPAP and Homer were each organized in distinctive ~80 nm ensembles able to undergo striking changes over time

(figure 4.1). While the spatial relation between different scaffold proteins within individual PSDs has not been measured, it is likely that through their interactions, different scaffold proteins accumulate in the same or interlinked domains (MacGillavry et al., 2013).

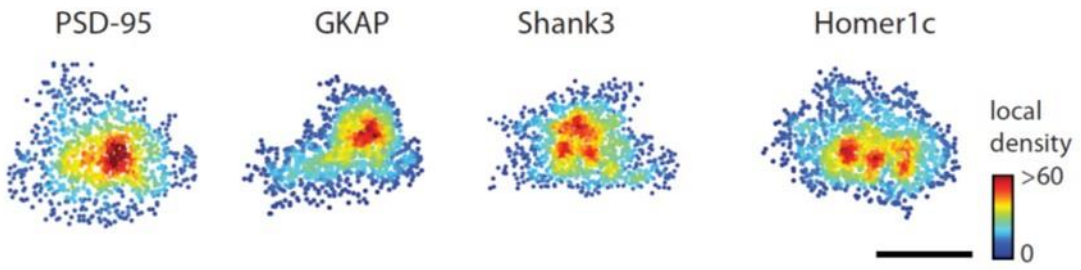

Figure 4.1 Scaffold molecules are organized in subsynaptic clusters. A. Examples of PSDs resolved with PALM for mEos2-tagged shrPSD-95, SAPAP (GKAP), shrShank3, and Homer1c. (Scale bar 200 nm) (shr: replacement construct). Adapted from (MacGillavry et al., 2013).

Here, I used super-resolution STED (STimulated Emission Depletion) nanoscopy to map the spatial distribution of Shank3 and PSD95 within single synapse at nanometer resolution. Despite the homogeneous distribution and colocalization of both proteins in confocal images, I observed that in fact these scaffold proteins are not homogeneously distributed but rather accumulate in subsynaptic nanoclusters; within the same synapse their signal intensity does not perfectly match with each other. Due to the fact that Shank3 and PSD95 do not interact directly in postsynaptic sites, I conclude that Shank3 and PSD95 accumulate in distinct, but closely associated nanodomains and SAPAP as a linker fills out the gap between their nanodomains in the postsynaptic density. Furthermore, I observed that the number, shape and position of both Shank3 and PSD95 nanodomains, as well as the arrangement of Shank3/PSD95 co-clusters differ from one synapse to another.

Durand et al. reported in 2012 that overexpression of Shank3 WT promotes spine maturation, and that some of the N-terminal missense mutations identified in ASD (R12C, R300C, Q321R) modify this function of Shank3 (Durand et al., 2012). Here, using STED imaging I investigated the effect of the L68P mutation in Shank3 on the organization of Shank3 nanodomains in the postsynaptic density. The results showed that the reported enlargement of spine heads due to overexpression of Shank3 WT might be a result of accumulation of larger number of nanoclusters in the postsynaptic density of neurons transfected with Shank3 WT compare to Shank3 L68P. I observed that both overexpressed WT and L68P mutant variants of Shank3 often tend to form mushroom spines with Y shape patterns of nanoclustering. It appeared that while overexpression of Shank3 WT increased the size of the spine and the number nanoclusters, the L68P mutant variant failed to do so. However, due to limited availability of the STED microscope, these data are not still statistically verified.

4.2 Shank3 is a downstream effector of Ras GTPases in the postsynaptic density

In 2017 we reported that the SPN domain is a novel binding motif for active GTPases of the Ras family. Solving the three-dimensional structure of the N-terminal portion of Shank3 (residues 1-348, including both the SPN and ARR domains) showed that the SPN domain adopts a ubiquitin like (Ubl) fold which is most similar to the so-called F0 domain of the focal adhesion protein Talin. Subsequent interaction studies confirmed that the SPN domain of Shank3 constitutes a high affinity binding site for several Ras family G-proteins, including H-Ras, KRas, Rap1a and Rap1b. The high affinity for both Rap1 and H-Ras (K_D values in the nM to low µM range) suggests that the interaction of Shank3 with Ras family members is biologically relevant. Importantly, both ASD-related mutations found in the Shank3 SPN domain, R12C and L68P, completely disrupted the binding of Ras and Rap proteins (Lilja et al., 2017).

The Ras family GTPases (Ras, Rap1, and Rap2) and their downstream effectors and signalling cascades control numerous physiological processes. At synapses, both Ras and Rap play regulatory roles with respect to synapse development and synaptic plasticity (Stornetta and Zhu, 2011, Lee et al., 2011) (figure 4.2).

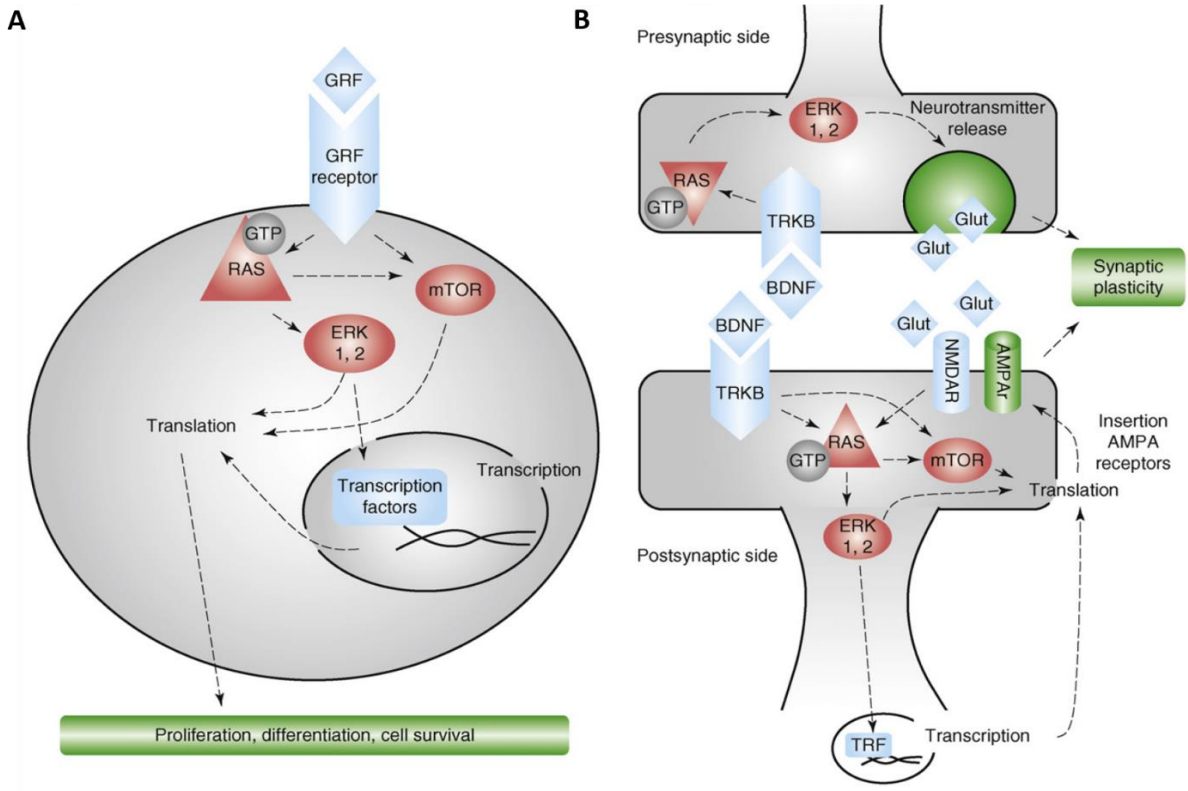

Figure 4.2. The output of extracellular signal regulated kinase (ERK) and mammalian target of rapamycin (mTOR) signaling in mitotic cells and neurons. A. In non-neuronal, mitotic cells, extracellular signals such as growth factors and cytokines induce proliferation, differentiation and cell cycle progression via activation of ERK and mTOR pathways. **B.** Neurons are mostly postmitotic, and the ERK and mTOR pathways are recruited for processes such as synaptic plasticity, important in memory formation. Adapted from (Krab et al., 2008).

In neurons, Ras and Rap are differentially activated by different forms of synaptic activity. LTP-inducing stimuli activate the Ras signalling pathway, that results in phosphorylation of AMPA receptors with long cytoplasmic termini and drive these receptors into synapses. LTD-inducing stimuli activate the Rap1 signalling pathway, which phosphorylates AMPA receptors with only short cytoplasmic tails and leads to synaptic removal of the receptors. Depotentiation-inducing stimuli activate the Rap2 signalling pathway, which dephosphorylates AMPA receptors with long cytoplasmic termini and triggers synaptic removal of the receptors (Thomas and Huganir, 2004, Tada and Sheng, 2006, Gu and Stornetta, 2007, Stornetta and Zhu, 2011).

The best characterized Ras signalling pathway is the RAS/MAPK signaling pathway which is initiated by activation of Ras through receptor tyrosine kinases such as the epidermal growth factor receptor (EGFR) and mediates the transmission of signals from cell surface receptors to cytoplasmic and nuclear effectors. Interestingly, this pathway has been reported as one of the commonly affected intracellular pathways in autistic patients (Faridar et al., 2014, Wennerberg et al., 2005, Colicelli, 2004, Repasky et al., 2004). In 2019 Wang et al. showed that ERK2, one of the MAP kinases which are downstream effector of Ras in this pathway, promotes polyubiquitination-dependent degradation of Shank3 via promoting its phosphorylation in three residues located in the C-terminal Prolin-rich region (Wang et al., 2019).

Here, I asked whether Ras proteins are able to influence the molecular interactions of Shank3. Therefore, in order to determine the effect of the SPN-Ras interaction on the Shank3 interaction with its synaptic interaction partners, I performed a series of stimulation assays using EGF to stimulate the endogenous epidermal growth factor receptor (EGFR) in 293T cells and activate the Ras/MAPK pathway. Evaluation of the strength of interaction in a coprecipitation assay of Shank3 with each individual interaction partner before and after activation of the MAPK pathway revealed that SAPAP1 is the interaction partner of Shank which is highly affected. Interestingly, SAPAP1 is the interaction partner of the Shank3 PDZ domain and according to the linear Shank3 protein sequence it is far away from the SPN domain. Activation of the Ras/MAPK pathway significantly decreased the interaction between Shank3 and SAPAP, but it was not clear whether this effect was an indirect effect of the activated MAPK pathway (such as phosphorylation by ERK) or whether it is directly mediated by binding of the Shank3 SPN domain to active Ras proteins. To clarify the role of the SPN domain, I compared the effect of EGF stimulation on SAPAP1 interaction with Shank3 WT and the two SPN mutant variants (L68P and R12C) which do not bind to small G-proteins of the Ras family. The result showed that, although the L68P variant showed a high variability, the interaction of both variants with SAPAP1 was not affected by stimulation of the MAPK pathway. These data suggest that activation of Ras strongly affects the interaction between Shank and SAPAP and that this effect is through the direct binding of Ras to the SPN domain.

SAPAP proteins are among the most abundant postsynaptic scaffolding proteins in the PSD that play an essential role in recruitment of Shank to excitatory synapses (Naisbitt et al., 1999, Sala et al., 2001, Romorini et al., 2004). Accordingly, the synaptic SAPAP protein level contributes to synaptogenesis and dendritic spine morphogenesis (Shin et al., 2012). It has been shown that more specifically, SAPAP1 mediates the interaction between Shank3 and PSD95 and these three proteins form large interaction complexes with each other in the postsynaptic density (Li et al., 2017). More recently, Coba et al. 2018 showed that the association between Shank3 and PSD95 is significantly reduced in SAPAP1 KO mice, while this impairment was not due to alterations in the levels of these proteins at the PSD and the interaction of Shank3 with the downstream component Homer1 was unaffected. These data

indicate that ablation of SAPAP1 disrupt the organization of the PSD by uncoupling its major scaffold proteins (Coba et al., 2018).

The Shank3-SAPAP interaction is mediated by the Shank3 PDZ domain binding to the PDZ ligand motif of SAPAP (Naisbitt et al., 1999, Boeckers et al., 1999). Recently, Zeng et al. discovered a novel binding site outside the canonical PDZ domain for SAPAP proteins. They showed that an N-terminal extended Shank3 PDZ domain (residues 533–665) as well as an N-terminally extended PDZ ligand motif containing the last 12 residues of SAPAP (residues 966–977) are responsible for the strong interaction between Shank3 and SAPAP (Zeng et al., 2016).

In 2012 Shin et al. showed that SAPAP levels at synapses are controlled through differential phosphorylation of SAPAP by different CaMKII isoforms. In a bidirectional regulatory mechanism, α-CaMKII activated upon NMDA receptor activation phosphorylates Serine-54 of SAPAP to induce poly-ubiquitination and degradation of SAPAP. In contrast, activation of β-CaMKII via L-type voltage-dependent calcium channels promote SAPAP recruitment by phosphorylating Serine-340 and Serine-384 residues, which uncouples SAPAP from the MyoVa motor complex. As a result of this regulation, over-excitation removes SAPAP from synapses via the ubiquitin-proteasome system, while inactivity induces synaptic accumulation of SAPAP at synapses of rat hippocampal neurons. Therefore, the turnover of SAPAP at synapses is required for the normal activity-dependent remodelling of PSD protein composition, as well as homeostatic synaptic scaling (Shin et al., 2012).

To clarify the relevance of the effect of active Ras on Shank3/SAPAP in synapses, I co-expressed HRas with Shank3 in cultured hippocampal neurons. In these experiments, Ras showed a membrane associated pattern along neuronal dendrite. Interestingly, Shank3 WT seemed to follow the pattern of Ras localization and highly colocalized with active Ras in dendrites. The L68P mutant variant of Shank3 did not show a strong colocalization with active Ras and remained clustered in the postsynaptic density, in agreement with its inability to bind to small G-proteins. Since it is known that Ras proteins activate their downstream effectors by recruitment to the plasma membrane (Simanshu et al., 2017), it seems that in the presence of GTP-bound Ras, Shank3 is no longer a part of the PSD core complex of PSD95/SAPAP/Shank and instead colocalizes with active Ras.

Despite the fact that a variety of factors, mainly the stimulators of receptor tyrosine kinases (RTKs), initiate Ras signalling pathways, the activation of Ras in the postsynaptic density is precisely regulated by SynGAP. SynGAP is a Ras GTPase activating protein (RasGAP), known as a CaMKII substrate, that promotes rapid hydrolysis of Ras bound GTP to GDP, leading to inactivation of Ras proteins (Chen et al., 1998, Carlisle et al., 2008, Oh et al., 2004).
SynGAP plays a critical role in neuronal development and synaptic plasticity, mostly because it couples NMDA receptor activation to downstream signaling pathways involved in LTP. It has been shown that through modulation of the Ras/MAPK pathway, SynGAP regulates the spine size as well as AMPA receptor recruitment to synapses during LTP (Komiyama et al., 2002, Kim et al., 2003, Scannevin and Huganir, 2000, Hell, 2014, Araki et al., 2015).

In this respect it is importnat that the activation of CaMKII through NMDAR-dependent calcium influx is required for the induction of LTP (Lisman et al., 2012). Upon LTP induction in hippocampal neurons, activation of CaMKII via the Ca^{+2} influx produced by activated NMDA receptors leads to phosphorylation of SynGAP. The phosphorylated SynGAP disperses from synapse and releases the

brake on the accumulation of active Ras. This would then lead to spine enlargement, AMPA receptor insertion and increased synaptic strength (Chen et al., 1998, Araki et al., 2015).

According to these data, I propose a model in which during LTP and through the NMDA receptor calcium influx, CamKII promotes phosphorylation and subsequent removal of SynGap from the synapse which then lead to the activation of Ras in the postsynaptic density. The active Ras binds to the SPN domain of Shank and results in weakening of Shank/SAPAP binding. Subsequently, Shank leaves the PSD95/SAPAP/Shank complex (figure 4.3). At the same time, alpha CaMKII activity leads to degradation of SAPAP. These two aspects of CamKII signalling might act synergistically to allow for restructuring of the PSD during LTP. Alternatively, this would allow neurons to weaken PSDs in periods of overexcitation. In this regard, the SPN mutations hinder synapses to manage over-excitation and therefore, contribute to synaptopathies such as ASDs.

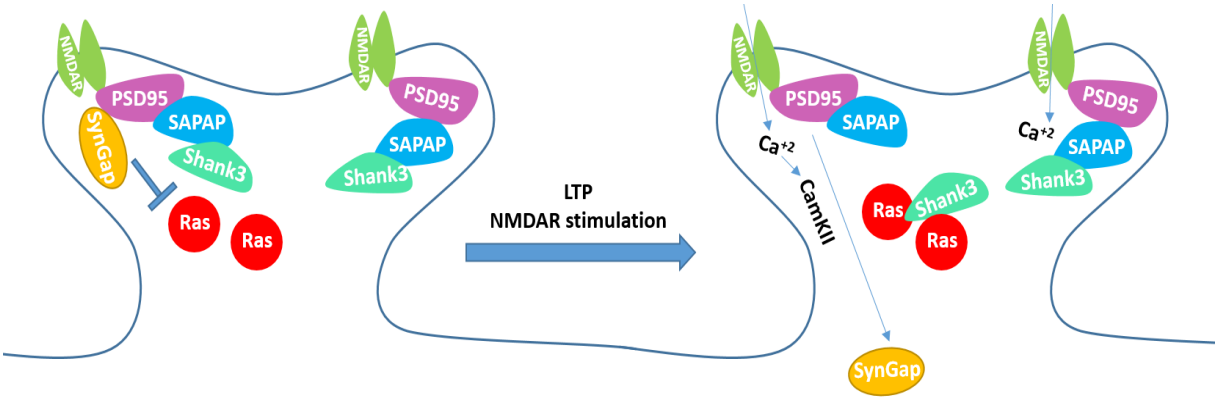

Figure 4.3 Schematic representation of the effect of Ras on Shank3 in the postsynaptic density. Activation of Ras during LTP results in dissociation of some of the Shank3 proteins from the postsynaptic core complex through weakening of the Shank3-SAPAP1 interaction.

4.3 Ras-SPN interaction might affect the conformation of the Shank3 N-terminus

Another interaction partner of Shank3 which was affected by activation of Ras signalling is Fodrin. However, the high variability in the observed increase in interaction with Shank3 results affected the significance of these data. Fodrin is one of the interaction partners of the Ank domain (Bockers et al., 2001). Based on the structural analysis of the Shank3 N-terminus, I expected that the Ank domain interaction partners show a higher sensitivity to changes in the SPN domain; in fact, it has already been shown in the case of the L68P mutation which improves binding of Ank interaction partners (Fodrin and Sharpin) to the Ank domain (Mameza et al., 2013).

The increase in binding of Fodrin to the Ank domain after stimulation of the Ras signalling was similar to the improvement of binding due to the L68P mutation. This could be an indication of conformational changes in the Shank3 N-terminus after binding to Ras. If the L68P mutant represents an open form of Shank3 N-terminal that exposes the Ank domain to its interaction partners, binding of active Ras to SPN domain might similarly result in a transient SPN-Ank separation and an open N-terminal conformation that upregulates Ank domain interactions. Therefore, to explore this hypothesis, I used a live FRET imaging combined with EGF stimulation to activate endogenous Ras proteins in 293T cells. For this, I expressed Shank3 N-terminal FRET constructs (WT, L68P and R12C) coding for amino acids 1- 339 of Shank3, including an N-terminal GFP and a C-terminal mCherry

sequence. I assumed that in an optimal condition (close distance and correct orientation) the energy-transfer will occur from the GFP donor to the mCherry acceptor and create an intramolecular fluorescence resonance energy transfer that can be detected and measured by the confocal microscopy. I compared the intensity of FRET signals before and after stimulation of WT, L68P and R12C variants of Shank3.

First, the appearance of a FRET signal in the cells expressing the Shank3 N-terminus showed that in a WT form and under basal conditions, the SPN and Ank domains are in fact close enough to permit the energy-transfer from the GFP (N-terminal to the SPN domain) to the mCherry (C-terminal to the Ank domain), as predicted from our 3D structure of the Shank3 N-terminal region (Lilja et al., 2017).

Further, comparing the intensity of FRET signals between the Shank3 WT N-terminus and the two SPN mutants showed that the L68P mutant shows a significantly reduced signal compared to the WT and the R12C mutant (which showed a very similar FRET signal to the WT). This strong reduction of FRET in the L68P form clearly indicates that, due to disruption of the SPN hydrophobic core by the L68P mutation, the N- and C-terminus of this Shank3 N-terminal fragment move away from each other and as a result the energy-transfer is no longer possible. Moreover, comparing the FRET signals before and after stimulation revealed that the cells transfected with the WT FRET construct in total showed around 2% signal decrease, whereas both L68P and R12C FRET signals remained quite stable during 20 min of imaging. This could indicate a conformational change in the Shank3 N-terminus due to the binding of the SPN domain to active Ras. Considering all data together, the FRET assay confirms that the L68P mutation leads to an open conformation of the Shank3 N-terminus and the R12C variant represent a closed N-terminus conformation, whereas the WT can be switched between open and closed conformation via binding to or separation from Ras respectively.

4.4 Shank3 is a negative regulator of the Rap1 signaling pathway

The ability of the SPN domain to bind active, GTP-bound small G-proteins might affect signal transduction at synapses in different ways. Shank3 could be a downstream effector of the Ras signaling pathway; alternatively, it could function to sequester active G-proteins, thus limiting their availability for other pathways. One of these pathways that could be regulated by Shank3 is the integrin activation pathway which requires active, GTP-bound Rap proteins. Rap1 plays a critical role in the final steps of integrin activation, where the active GTP bound Rap1 recruits RIAM and Talin to the plasma membrane to facilitate integrin activation (Calderwood et al., 2013).

To investigate the effect of Shank3 on this pathway, I targeted a well-known integrin function in the neurons, which is enhancing neurite outgrowth and filopodia formation (Plantman et al., 2008). By overexpressing Shank3 WT and the mutant L68P in the rat hippocampal neurons, I showed that the filopodia density in Shank3 L68P transfected neurons was significantly higher than the WT transfected neurons. These data suggest that Shank3 can act as a negative regulators of the integrin activation pathway where WT Shank3, but not the L68P mutant suppresses formation of filopodia by inhibiting integrin activity (Lilja et al., 2017) (figure 4.4).

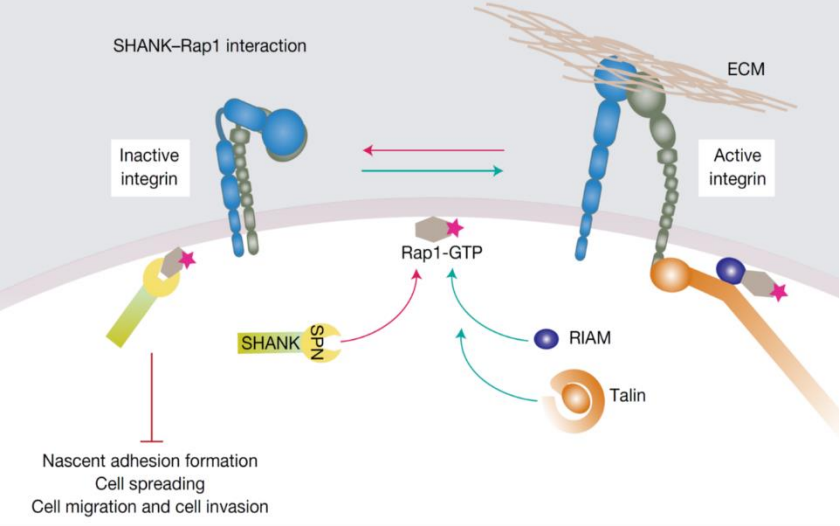

4.4 Schematic representation of Shank–Rap1-dependent integrin inhibition. In this model, we suggest that Shank sequesters active Rap1 and R-Ras via the SPN domain and thus limits their bioavailability at the plasma membrane. Eventually, this leads to inhibition of integrin activation through blocking the recruitment of RIAM and Talin to the plasma membrane. From (Lilja et al., 2017).

4.5 The Ank domain of Shank3 is a binding site for RNA-binding proteins

In search for new interaction partners of the Shank3 N-terminus, first I decided to use 293T cells and coprecipitate the endogenous interaction partners with the overexpressed Shank3 N-terminus, mainly because this approach allowed me to investigate the effect of co-expressed active small G-proteins on the putative interactions. Interestingly, about 90% of mRNAs expressed in the human brain are also expressed in 293T cells (Ascano et al., 2012). Neurons would be a better experimental system for finding interaction partners for a synaptic protein such as Shank, but the transfection rate in neurons is not high enough for performing a coimmunoprecipitation assay. Also, many of the actin binding proteins which shape dendritic spines are also present in tissue culture cells. Mass spectrometric analysis showed that the RNA binding proteins (RBPs), mainly from the two large families of heterogeneous nuclear ribonucleoproteins (hnRNPs) and DEAD box RNA helicases (DDX) were found to be in a complex with the N-terminus of Shank3.

The hnRNPs are RBPs involve in packing and stabilizing freshly transcribed pre-mRNAs, whereas DDX proteins function in most steps of the gene expression process such as transcription, mRNA processing and translation (Dardenne et al., 2014, Geuens et al., 2016, Ogilvie, 2003).

Results of co-precipitation of the endogenous RNA binding proteins with different expressed Shank3 variants including full length Shank3, SPN mutant variants and the deletion constructs confirmed that they all bind to the Ank domain of Shank3. Later on, by performing RNase digestion, I showed that the interaction of some of these proteins is RNA-dependent, whereas DDX5 and hnRNP-U remained bound to Shank3 after removing RNA from the experimental environment. Interestingly, performing a pulldown assay using a bacterially expressed Shank3 N-terminal fragment to precipitate brain-extracted RNA binding proteins, I showed that only DDX5 may interact with the isolated N-terminal fragment of Shank3.

A colocalization assay in the neurons showed that the endogenous DDX5 was completely recruited to the nucleus, whereas overexpressed full length Shank3 was recruited to the dendritic spines. Further, using a specific antibody to detect DDX5 in the isolated postsynaptic density revealed that under basal

condition DDX5 is not present in the PSD. Based on these observations which strongly indicate a different subcellular localization of Shank3 and DDX5, this question raised whether these two proteins can really find each other to interact in the neurons.
There are several proteins which shuttle from the synapses or PSD to the nucleus, and a few Shank3 interacting proteins such as Abi-1 have been previously reported to translocate from synapse to nucleus in an activity-dependent manner (Jordan and Kreutz, 2009, Proepper et al., 2007, Schmeisser et al., 2009). In 2014 Grabrucker et al. claimed that Shank3 also can undergo synapse-to-nucleus shuttling to influence the transcription levels of several target genes possibly via alteration of hnRNP complexes. However, it is still unclear if this is an isoform-specific effect or if Shank3 shuttles to the nucleus in a stimulus-specific manner (Grabrucker et al., 2014, Wang et al., 2014). At least two isoforms of Shank3 (figure 1.6) are likely to be constantly in the nucleus due to the presence of a nuclear localization signal and due to the lack of the synaptic targeting signal (a C-terminal domain including the Homer and Cortactin-binding sites and the SAM domain) which is necessary for synaptic localization of the Shank3 protein (Wang et al., 2014, Boeckers et al., 2005). Both of these isoforms contain the Ank domain, which is necessary for interaction with DDX5.
Furthermore, activity dependent changes in the composition of the PSD have been observed in a study by Zhang et al. in 2012 which implicates the presence of RNA-binding proteins at postsynaptic sites. In this study they showed that several RBPs including hnRNPs and DDX17 increased in abundance at synapses in response to synaptic activity (Zhang et al., 2012). Interestingly, DDX5 and DDX17 are highly conserved paralog proteins belonging to the family of DEAD box RNA helicase that share 90% identity (Dardenne et al., 2014, Ogilvie, 2003).
The dendritic trafficking of mRNAs in complex with RBPs has been identified as an important posttranscriptional process involved in the regulation of synaptic plasticity, and deletions or mutations of genes encoding RNA-binding proteins result in loss of synaptic plasticity and neuron function (Sephton and Yu, 2015, Tiruchinapalli et al., 2008). Recently, the protein JAKMIP1 has been shown in association with ribosomes and mRNP granules where it interacts with FMRP, PABPC1, and DDX5. Since mRNP granules are important for mRNA transport to synaptic sites, and for regulating the interaction between specific mRNAs and the translation machinery, these observations suggest that JAKMIP1 and DDX5 could also be involved in both processes (Berg et al., 2015).
Taken together, these data suggest that under certain conditions the RNA binding proteins could traffic to the postsynaptic density, or Shank3 could translocate to nucleus as it has been reported before, with respect to the Shank3 truncated variants (Grabrucker et al., 2014). Importantly, I showed here that the Ank domain of Shank3 is a binding site for RNA binding proteins and this might be strongly relevant for the nuclear Shank3 isoforms which all possess an Ank domain. In this way, Shank3 might get involved in the gene expression process through binding to RNA-binding proteins.

4.6 Catenins are the novel interaction partners of Shank3

In a second approach, I looked for direct interaction partners of Shank3 in postsynaptic density. This led me to the Catenin family of proteins. Catenins are a group of proteins which were first characterized as proteins associated with the cytoplasmic domains of Cadherins at cell-cell junctions. The Catenin family subdivides into four separate groups (β-Catenins, Plakophilin, α-Catenins and the p120 Catenin subfamily) that directly or indirectly link the transmembrane proteins of the Cadherin family to the cytoskeleton and function in cell-cell adhesion (Arikkath et al., 2008, McCrea and Gu,

2010, Ozawa et al., 1989, Zhao et al., 2011). All Catenins, except for members of the α-Catenin subfamily, possess a central Armadillo domain consisting of nine to twelve repeats (each of roughly 40 amino acids) of α-helical domains (figure 4.5). These repeats mediate various interactions in distinct intracellular compartments and associate β-Catenin or p120 subfamily members with Cadherins (Choi and Weis, 2005, Huber et al., 1997, Shapiro and Weis, 2009, McCrea and Gottardi, 2016).

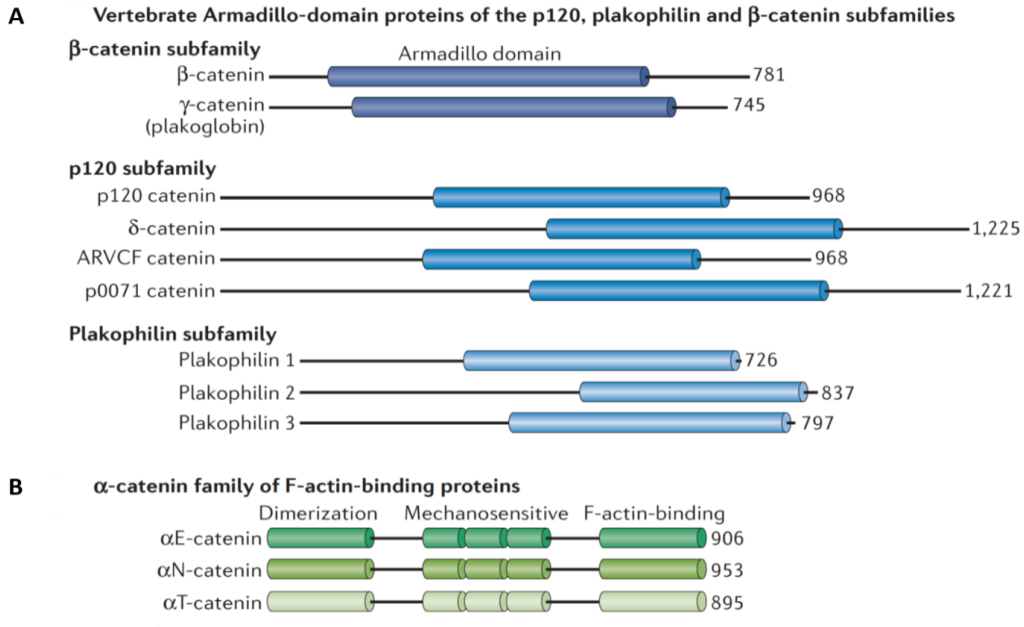

Figure 4.5 An overview of vertebrate Catenins. A. Vertebrate Catenins containing Armadillo domains were first identified at cell–cell contacts in association with classic Cadherins (β-Catenin and p120 Catenin subfamily members), or with desmosomal Cadherins (plakophilin Catenin subfamily members and γ-Catenin (plakoglobin)). **B.** α-Catenins are filamentous actin (F-actin)-binding proteins that are structurally related to vinculin. The N-terminal dimerization domain engages in mutually exclusive β-Catenin (heteromeric) or α-Catenin (homomeric) binding, whereas the central mechanosensitive and carboxy-terminal F-actin-binding domains are together composed of four to five α-helical bundles. From (McCrea and Gottardi, 2016).

Verification of my initial mass spectrometric results in tissue culture showed that β- and δ-Catenin (but not α-Catenin) can bind to Shank3. It is possible that these Catenin proteins are all in a complex together and therefore the interaction of only one of them (in this case δ-Catenin) with the isolated N-terminal fragment of Shank3 resulted in appearance of the other Catenins in the mass spectrometric results.

β-Catenin, the best-known Catenin protein as a key signal transducer of the canonical WNT pathway, is a multitasking protein involved in both cell adhesion and transcriptional regulation (Clevers and Nusse, 2012, Valenta et al., 2012). This nucleocytoplasmic shuttle protein consists of a central armadillo repeat domain (with 12 Arm repeats) flanked by N- and C-terminal regions (Huber et al., 1997, Pokutta and Weis, 2007). The C-terminal PDZ binding motif of β-Catenin mediates the linkage between Cadherins and PDZ domain-containing proteins in both pre- and postsynaptic sites. There, it is involved in presynaptic vesicle localization and regulating synaptic AMPA receptors. (Bamji et al., 2003, Okuda et al., 2007, Sun et al., 2009).

In addition to its well-studied role in Wnt signalling pathway, β-Catenin is involved in synaptic plasticity, with regulating both activity-dependent synaptic remodelling as well as gene transcription

(Maguschak and Ressler, 2008). It has been shown that neural activity alters the distribution of β-Catenin from dendritic shafts to spines in an NMDA-dependent manner, which coincides with an increase in the association of β-Catenin with Cadherin (Murase et al., 2002). Since the members of the α-Catenin family bind to Cadherins indirectly through β-Catenin, β-Catenin is also necessary to recruit α-Catenin to cell-cell contact sites and prevent the rapid degradation of the Cadherin cytoplasmic domain (Drees et al., 2005, Yamada et al., 2005, Huber and Weis, 2001). Ablation of postsynaptic β-Catenin decrease the number of mushroom spines and results in an increase in thin, elongated spines as well as a reduced synaptic AMPA responses (Okuda et al., 2007).

On the other hand, δ-Catenin is a neuron-specific Catenin belonging to the p120 subfamily which has been implicated in cell adhesion and dendritic branching. Its proper function is critical for normal cognitive function (Matter et al., 2009, Israely et al., 2004). δ-Catenin regulates the maintenance of dendrites and dendritic spines in mature cortex and as a part of synaptic adhesion complexes has a key role in spine growth, synaptic plasticity, and synapse morphogenesis during development (Lu et al., 1999, Kosik et al., 2005, Elia et al., 2006, Arikkath et al., 2009, Matter et al., 2009).

δ-Catenin shares a structural similarity with members of the β-Catenin family, with a central domain that includes ten armadillo repeats plus N- and C- terminal flanking sequences (Pokutta and Weis, 2007, McCrea and Park, 2007). In addition, the δ-Catenin C-terminus includes a four aa PDZ-binding motif which is the binding site for several PDZ containing proteins including erbin, densin-180, S-SCAM, PAPIN, ABP, and GRIP (Ide et al., 1999, Deguchi et al., 2000, Izawa et al., 2002, Laura et al., 2002). It has been shown that δ-Catenin-mediated regulation of spine density requires interactions mediated through its PDZ binding motif (Yuan et al., 2015, Arikkath et al., 2009, Arikkath and Reichardt, 2008, Kim et al., 2008).
The human δ-Catenin gene (*CTNND2*) has been mapped to chromosome 5p15.2 where a deletion causes the cri-du-chat syndrome (CDCS), a syndrome with severe cognitive and language impairments, motor delays, and behavioural problems (Medina et al., 2000). In 2008, a rare copy number variation was implicated in schizophrenia that disrupts the gene encoding δ-Catenin (Vrijenhoek et al., 2008). Recently, *CTNND2* has also been implicated as a novel autism gene as loss of function (deletions, unbalanced translocations) mutations in this gene result in severe autism (Turner et al., 2015).
Loss of δ-Catenin leads to a decrease in overall excitatory synapse density, as well as active synapses that expressed the GluA subunit of the AMPA receptors (Israely et al., 2004, Matter et al., 2009). δ-Catenin promotes surface expression of AMPA receptors and results in enhanced AMPA receptor-mediated synaptic currents (Silverman et al., 2007).

Both β- and δ-Catenin had been shown before to be in a complex with Shank proteins. However, it was not clear whether these are direct interactions, which domains of Shank might be involved and what the functional consequences are (Quitsch et al., 2005, Qin et al., 2018).
Here, I showed that in fact these two members of the Catenin family are able to directly interact with the Shank3 protein but do not share the same binding site. δ-Catenin is an interaction partner of the Ank domain, whereas β-Catenin binds to the PDZ domain. Mapping the binding site on Catenin proteins revealed that the Armadillo-repeat domain of δ-Catenin makes contact with the Shank3 Ank domain. β-Catenin binds to the PDZ domain of Shank3, but surprisingly, the C-terminal PDZ ligand of β-Catenin is not involved in binding to the PDZ domain of Shank3. Although the binding of many PDZ-containing proteins mostly occurs by recognition of the extreme C-terminus of the target protein, it

has been shown that some PDZ domains can also bind to internal sequences of target proteins (so called internal PDZ ligand; (Lee and Zheng, 2010)). Therefore, I suggest that the interaction between Shank3 and β-Catenin does not proceed through a canonical C-terminal PDZ ligand, but it is most likely through a putative internal PDZ ligand.

The results of a colocalization assay showed that these two Catenin proteins highly colocalize with Shank3 in 293T cells as well as neurons. Although in neurons β- and δ-Catenin colocalize with Shank3 in the dendritic spines, in 293T cells they show a slightly different pattern of colocalization. Shank3 and β-Catenin were colocalized mostly inside nuclear clusters, whereas δ-Catenin colocalizes with Shank3 not only in the nucleus but even stronger at the plasma membrane, suggesting that δ-Catenin reduces Shank3 clustering in the nucleus and recruits Shank3 to the plasma membrane.

Since the focus of my study was on the Shank3 N-terminus, and δ-Catenin very specifically binds to the Ank domain, I aimed to investigate the effect of seven ASD-associated missense mutations in the Shank3 N-terminus on the interaction between Shank3 and δ-Catenin. Interestingly, the results of coexpression/coimmunoprecipitation assays revealed that the L68P mutation in the Shank3 SPN domain significantly improves the binding of δ-Catenin to the Ank domain of Shank. This result is consistent with the previously published effect of the L68P mutation in upregulating the interaction of the Ank domainwith its partners Fodrin and Sharpin. Another mutation that increased the binding of δ-Catenin to the Shank3 Ank domain was the *de novo* mutation P141A (Boccuto et al., 2013) which has not been functionally analyzed before. Furthermore, I showed that this mutation also improves the binding of Fodrin to the Ank domain. Intriguingly, the overexpressed P141A protein (N-terminal fragment only) in 293T cells tends to form aggregates at high expression levels, whereas at lower levels it looks very similar to the homogenously diffuse appearance of overexpressed WT N-terminus. Due to the fact that this mutation occurs in the contact surface of SPN and Ank, the results might indicate that the P141A mutation partially disrupts the intramolecular interaction between SPN and Ank. This results in upregulating Ank domain interactions and formation of protein aggregates, similar to the L68P mutation.

In 2016 Wang et al. reported δ-Catenin as a neuronal substrate for the kinase TNIK. TNIK is a serine/threonine kinase highly expressed in the brain and enriched in the postsynaptic density of excitatory synapses which has been implicated as a risk factor for psychiatric disorders. Identification of multiple TNIK phosphorylation sites of δ-Catenin suggests their phosphorylation by TNIK is particularly important in synaptic adhesion, and synaptic plasticity (Wang et al., 2016). Therefore, to investigate whether δ-Catenin phosphorylation via TNIK affects the binding to Shank3, I used the WT TNIK coexpressed with Shank3 and δ-Catenin and compared the results to the condition with an overexpressed kinase dead variant of TNIK. The results showed that the presence of an active TNIK, does not change the interaction between Shank3 and δ-Catenin.
Very recently, a study revealed a β-Catenin dependent mechanism underlying the social deficits linked to Shank3 deficiency. In this study, Qin et al. showed that the level of global Histone H3 acetylation in the frontal cortex of Shank3+/ΔC mice was significantly lower than that of WT mice. These mice express a C-terminally deleted Shank3, with a reduced expression of full-length Shank3 and loss of synaptic localization of the truncated Shank3 protein. Interestingly, they observed that in prefrontal cortex of these mice the level of synaptic β-Catenin was decreased whereas the nuclear β-Catenin fraction showed a significant increase. According to these results, they suggested that *Shank3*

deficiency induces the redistribution of β-Catenin from synapses to the nucleus, leading to upregulation of histone deacetylase 2 (*HDAC2)* and social deficits (Qin et al., 2018).

To examine the effect of the Shank3 N-terminus on the postsynaptic localization of Catenins, I compared the δ-Catenin content of the isolated postsynaptic density fraction of Shank3 WT mice to the postsynaptic density isolated from Shank3 KO mice which lack the largest isoforms of Shank3 containing the N-terminal Ank and SPN domains. Interestingly, I found that the level of postsynaptic δ-Catenin in Shank3 KO mice is significantly reduced while the postsynaptic localization of β-Catenin was not affected. This indicates that there are sufficient levels of Shank3 proteins containing a PDZ domain in the PSD of these mice, but not of Shank3 proteins containing SPN and Ank domains. Therefore, I conclude that Shank3 is crucially involved in the postsynaptic localization and stabilization of δ-Catenin, where the Shank3 KO mice lacking Shank3 N-terminus results in loss of postsynaptic δ-Catenin.

Catenins are best known to interact with the cytoplasmic tail of transmembrane Cadherin proteins. Cadherins are Ca^{2+}-dependent cell adhesion molecules present in sites of contact between cells, including adherens junctions and synapses (Pokutta and Weis, 2007). The distal region of Cadherin cytoplasmic domains binds to β-Catenin, whereas the membrane proximal region contains a binding site for members of the p120ctn family including δ-Catenin. N-Cadherin is the most widely distributed neuronal Cadherin that is localized at pre- and postsynaptic compartments in a complex with Catenins and modifies adhesive contacts, activates signal transduction pathways, and regulate synapses formation and plasticity (Arikkath et al., 2008, Brigidi and Bamji, 2011).

It has been shown that p120ctn family members, including δ-Catenin and p120ctn, reduce endocytosis of surface Cadherins. As a result, the absence of δ-Catenin likely reduces Cadherin stability, which could be the mechanism underlying the decreased level of N-Cadherin in δ-Catenin null mice (Davis et al., 2003, Israely et al., 2004, Xiao et al., 2003).
Therefore, I asked whether the postsynaptic level of N-Cadherin is also affected in Shank3 KO mice. Comparing PSD of Shank3 WT and KO mice showed a slight reduction in the postsynaptic levels of N-Cadherin in the KO mice, which was however not statically significant. Although, probably due to a compensatory effect of other Catenins such as β-Catenin and p120 Catenin present in the postsynaptic density, the level of postsynaptic N-Cadherin is not dramatically reduced in the Shank3 KO mice, this reduction might indicate a mechanism in which Shank3 N-terminus regulates synapse formation through controlling synaptic level of N-Cadherin proteins. N-Cadherin regulates AMPA receptor trafficking by increasing surface expression of AMPA receptors in neurons and as a key transmembrane, cell-adhesion molecule in synaptic sites plays an important role in synapse formation and synaptic plasticity (Mysore et al., 2008, Nuriya and Huganir, 2006, Tanaka et al., 2000, Bozdagi et al., 2000).

A study by Brigidi et al. in 2014 revealed that the postsynaptic localization of δ-Catenin is dependent on palmitoylation via the palmitoyl-acyl transferase DHHC5 in an activity-dependent manner. Under basal conditions, DHHC5 is bound to PSD-95 and Fyn kinase, and is stabilized at the synaptic membrane whereas DHHC5's substrate, δ-Catenin, is highly localized to dendritic shafts. Neuronal activity disrupts DHHC5/PSD-95/Fyn kinase complexes, promotes DHHC5 endocytosis, its translocation to dendritic shafts and its association with δ-Catenin. Following DHHC5-mediated palmitoylation of δ-Catenin, DHHC5 and δ-Catenin are trafficked together back into spines where δ-Catenin increases

Cadherin stabilization and recruitment of AMPA receptors to the synaptic membrane (Brigidi et al., 2014).
So far, it is not clear whether the Shank3/ δ-Catenin interaction is activity dependent. Comparing the P2 fraction of Shank3 WT and KO mice showed that there is no significant difference between the δ-Catenin content of membrane fractions between WT and KO animals. This result indicates that total δ-Catenin protein content in the Shank3 KO mice is not changed but either the postsynaptic trafficking or stabilization of the δ-Catenin protein in the postsynaptic sites might be affected by the lack of interaction with Shank3. Despite the ability of Shank1 to interact with δ-Catenin, I observed that the presence of Shank1 in the postsynaptic density of Shank3 KO mice is not sufficient to rescue the loss of postsynaptic δ-Catenin.

4.7 Conclusion and final remarks

This study provides new information about the regulatory effect of the Shank3 N-terminus in synaptogenesis, and in the development of ASDs. STED imaging showed co-clustering of Shank3 with PSD95 in the nanoscale organization of postsynaptic density. SAPAP proteins function as key factors to assemble postsynaptic PSD95/SAPAP/Shank core complex by mediating the indirect binding of Shank proteins to PSD95. Further, activation of Ras/MAPK pathway in the cells and overexpression of active Ras in neurons showed a significant negative effect on the Shank3-SAPAP interaction which subsequently caused separation of Shank from the synaptic core complex and colocalization with active Ras. This effect turned out to be mediated by SPN domain following the interaction of the Shank3 SPN domain with active Ras. Additional experiments revealed that Shank3 is not only a part of a synaptic Ras dependent signalling pathway which is disrupted by mutations in the N-terminal part of Shank3, but it also negatively regulates some of the pathways which require small G-proteins. Overexpressed Shank3 WT supressed filopodia formation and neurite outgrowth by sequestering active Rap1 and inhibiting the integrin activation pathway.
The results of FRET analysis revealed that the L68P mutation leads to a constitutive open conformation due to an unfolded SPN domain and R12C shows a closed conformation of the Shank3 N-terminus in which SPN domain is not able to interact with active Ras, whereas the WT Shank3 represent an intermediate state between L68P and R12C that can switch from closed to open conformation through binding to Ras.
I showed that the Ank domain of Shank3 is a high affinity binding site for the RNA binding proteins, namely DDX5 and hnRNP-U, which might be functionally relevant in a Shank3 isoform-dependent manner. Regardless of RNA-binding proteins, here, I added two novel proteins to the list of Shank3 interaction partners (figure 4.6). Two members of the Catenin family, β-Catenin and δ-Catenin directly interact with Shank3 at postsynaptic sites. However, they target distinct binding domains on Shank3. β-Catenin binds to the PDZ domain of Shank3 most likely through a putative internal PDZ ligand, whereas δ-Catenin binds to the Shank3 Ank domain via its Armadillo-repeat domain. Shank3 seems to be crucially involved in the postsynaptic localization and stabilization of Catenin proteins, as I showed in this study that the KO of Shank3 proteins containing an N-terminal Ank domain results in loss of postsynaptic δ-Catenin. Furthermore, the lack of postsynaptic Shank3 results in loss of postsynaptic β-Catenin (reported in (Qin et al., 2018)). The absence of the Shank3 SPN and Ank domains also causes slight reduction of postsynaptic N-Cadherin proteins (most likely via a δ-Catenin-dependent

mechanism), suggesting that Shank3 might regulate the synapse formation as well as synaptic plasticity via controlling the level of postsynaptic N-Cadherins.
Interestingly, missense mutations in the SPN domain, as well as SPN domain interactions with the small G-proteins of Ras family, strongly influence the Ank domain as well as Shank3 protein function. The interaction of Shank3 with δ-Catenin is significantly increased due to the ASD associated mutation of Shank3 SPN domain, L68P. Taken together, I conclude that the Shank3 N-terminus has an essential role in the proper functioning of synapses, while its proper functioning is highly regulated by the specific connection between the SPN domain and the Ank repeat region.

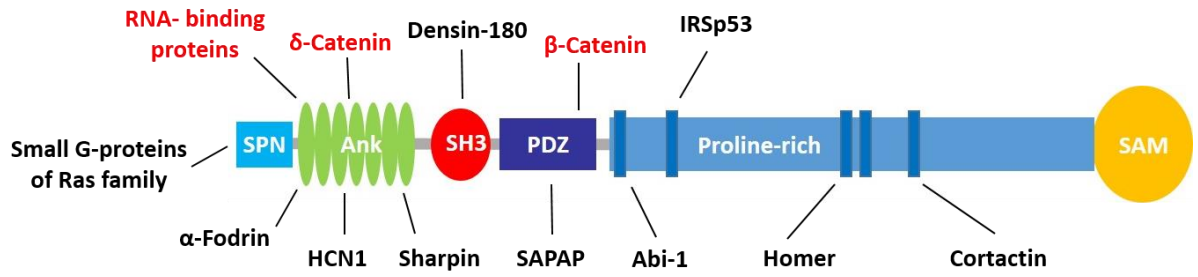

Figure 4.6 Shank3 binding domains and interaction partners. The proteins indicated in black are the previously known interaction partners of Shank3 which have been used in this study. The proteins indicated in red are the novel interaction partners of Shank3 found in this study.

References

ARAKI, Y., ZENG, M., ZHANG, M. & HUGANIR, R. L. 2015. Rapid dispersion of SynGAP from synaptic spines triggers AMPA receptor insertion and spine enlargement during LTP. *Neuron,* 85**,** 173-189.

ARIKKATH, J., ISRAELY, I., TAO, Y., MEI, L., LIU, X. & REICHARDT, L. F. 2008. Erbin controls dendritic morphogenesis by regulating localization of delta-catenin. *J Neurosci,* 28**,** 7047-56.

ARIKKATH, J., PENG, I. F., NG, Y. G., ISRAELY, I., LIU, X., ULLIAN, E. M. & REICHARDT, L. F. 2009. Delta-catenin regulates spine and synapse morphogenesis and function in hippocampal neurons during development. *J Neurosci,* 29**,** 5435-42.

ARIKKATH, J. & REICHARDT, L. F. 2008. Cadherins and catenins at synapses: roles in synaptogenesis and synaptic plasticity. *Trends in Neurosciences,* 31**,** 487-494.

ARONS, M. H., THYNNE, C. J., GRABRUCKER, A. M., LI, D., SCHOEN, M., CHEYNE, J. E., BOECKERS, T. M., MONTGOMERY, J. M. & GARNER, C. C. 2012. Autism-Associated Mutations in ProSAP2/Shank3 Impair Synaptic Transmission and Neurexin-Neuroligin-Mediated Transsynaptic Signaling. *Journal of Neuroscience,* 32**,** 14966-14978.

ASCANO, M., MUKHERJEE, N., BANDARU, P., MILLER, J. B., NUSBAUM, J. D., CORCORAN, D. L., LANGLOIS, C., MUNSCHAUER, M., DEWELL, S., HAFNER, M., WILLIAMS, Z., OHLER, U. & TUSCHL, T. 2012. FMRP targets distinct mRNA sequence elements to regulate protein expression. *Nature,* 492**,** 382.

BAILEY, C. H., KANDEL, E. R. & HARRIS, K. M. 2015. Structural Components of Synaptic Plasticity and Memory Consolidation. *Cold Spring Harb Perspect Biol,* 7**,** a021758.

BAMJI, S. X., SHIMAZU, K., KIMES, N., HUELSKEN, J., BIRCHMEIER, W., LU, B. & REICHARDT, L. F. 2003. Role of β-Catenin in Synaptic Vesicle Localization and Presynaptic Assembly. *Neuron,* 40**,** 719-731.

BANERJEE, S., RIORDAN, M. & BHAT, M. A. 2014. Genetic aspects of autism spectrum disorders: insights from animal models. *Front Cell Neurosci,* 8**,** 58.

BARON, M. K., BOECKERS, T. M., VAIDA, B., FAHAM, S., GINGERY, M., SAWAYA, M. R., SALYER, D., GUNDELFINGER, E. D. & BOWIE, J. U. 2006. An Architectural Framework That May Lie at the Core of the Postsynaptic Density. *Science,* 311**,** 531.

BERG, J. M., LEE, C., CHEN, L., GALVAN, L., CEPEDA, C., CHEN, J. Y., PENAGARIKANO, O., STEIN, J. L., LI, A., OGURO-ANDO, A., MILLER, J. A., VASHISHT, A. A., STARKS, M. E., KITE, E. P., TAM, E., GDALYAHU, A., AL-SHARIF, N. B., BURKETT, Z. D., WHITE, S. A., FEARS, S. C., LEVINE, M. S., WOHLSCHLEGEL, J. A. & GESCHWIND, D. H. 2015. JAKMIP1, a Novel Regulator of Neuronal Translation, Modulates Synaptic Function and Autistic-like Behaviors in Mouse. *Neuron,* 88**,** 1173-1191.

BERKEL, S., MARSHALL, C. R., WEISS, B., HOWE, J., ROETH, R., MOOG, U., ENDRIS, V., ROBERTS, W., SZATMARI, P., PINTO, D., BONIN, M., RIESS, A., ENGELS, H., SPRENGEL, R., SCHERER, S. W. & RAPPOLD, G. A. 2010. Mutations in the SHANK2 synaptic scaffolding gene in autism spectrum disorder and mental retardation. *Nat Genet,* 42**,** 489-91.

BOCCUTO, L., LAURI, M., SARASUA, S. M., SKINNER, C. D., BUCCELLA, D., DWIVEDI, A., ORTESCHI, D., COLLINS, J. S., ZOLLINO, M., VISCONTI, P., DUPONT, B., TIZIANO, D., SCHROER, R. J., NERI, G., STEVENSON, R. E., GURRIERI, F. & SCHWARTZ, C. E. 2013. Prevalence of SHANK3 variants in patients with different subtypes of autism spectrum disorders. *Eur J Hum Genet,* 21**,** 310-6.

BOCKERS, T. M., MAMEZA, M. G., KREUTZ, M. R., BOCKMANN, J., WEISE, C., BUCK, F., RICHTER, D., GUNDELFINGER, E. D. & KREIENKAMP, H. J. 2001. Synaptic scaffolding proteins in rat brain. Ankyrin repeats of the multidomain Shank protein family interact with the cytoskeletal protein alpha-fodrin. *J Biol Chem,* 276**,** 40104-12.

BOCKMANN, J., KREUTZ, M. R., GUNDELFINGER, E. D. & BÖCKERS, T. M. 2002. ProSAP/Shank postsynaptic density proteins interact with insulin receptor tyrosine kinase substrate IRSp53. *Journal of Neurochemistry,* 83**,** 1013-1017.

BOECKERS, T. M., KREUTZ, M. R., WINTER, C., ZUSCHRATTER, W., SMALLA, K.-H., SANMARTI-VILA, L., WEX, H., LANGNAESE, K., BOCKMANN, J., GARNER, C. C. & GUNDELFINGER, E. D. 2001. Proline-rich synapse-associated protein-1/cortactin binding protein 1 (ProSAP1/CortBP1) is a PDZ-domain protein highly enriched in the postsynaptic density. *Annals of Anatomy - Anatomischer Anzeiger,* 183**,** 101.

BOECKERS, T. M., LIEDTKE, T., SPILKER, C., DRESBACH, T., BOCKMANN, J., KREUTZ, M. R. & GUNDELFINGER, E. D. 2005. C-terminal synaptic targeting elements for postsynaptic density proteins ProSAP1/Shank2 and ProSAP2/Shank3. *J Neurochem,* 92**,** 519-24.

BOECKERS, T. M., WINTER, C., SMALLA, K.-H., KREUTZ, M. R., BOCKMANN, J., SEIDENBECHER, C., GARNER, C. C. & GUNDELFINGER, E. D. 1999. Proline-Rich Synapse-Associated Proteins ProSAP1 and ProSAP2 Interact with Synaptic Proteins of the SAPAP/GKAP Family. *Biochemical and Biophysical Research Communications,* 264**,** 247-252.

BONAGLIA, M. C., GIORDA, R., MANI, E., ACETI, G., ANDERLID, B. M., BARONCINI, A., PRAMPARO, T. & ZUFFARDI, O. 2006. Identification of a recurrent breakpoint within the SHANK3 gene in the 22q13.3 deletion syndrome. *J Med Genet,* 43**,** 822-8.

BONANSCO, C. & FUENZALIDA, M. 2016. Plasticity of Hippocampal Excitatory-Inhibitory Balance: Missing the Synaptic Control in the Epileptic Brain. *Neural plasticity,* 2016**,** 8607038-8607038.

BOURGERON, T. 2009. A synaptic trek to autism. *Curr Opin Neurobiol,* 19**,** 231-4.

BOURNE, J. N. & HARRIS, K. M. 2011. Coordination of size and number of excitatory and inhibitory synapses results in a balanced structural plasticity along mature hippocampal CA1 dendrites during LTP. *Hippocampus,* 21**,** 354-373.

BOZDAGI, O., SAKURAI, T., PAPAPETROU, D., WANG, X., DICKSTEIN, D. L., TAKAHASHI, N., KAJIWARA, Y., YANG, M., KATZ, A. M., SCATTONI, M. L., HARRIS, M. J., SAXENA, R., SILVERMAN, J. L., CRAWLEY, J. N., ZHOU, Q., HOF, P. R. & BUXBAUM, J. D. 2010. Haploinsufficiency of the autism-associated Shank3 gene leads to deficits in synaptic function, social interaction, and social communication. *Mol Autism,* 1**,** 15.

BOZDAGI, O., SHAN, W., TANAKA, H., BENSON, D. L. & HUNTLEY, G. W. 2000. Increasing Numbers of Synaptic Puncta during Late-Phase LTP: N-Cadherin Is Synthesized, Recruited to Synaptic Sites, and Required for Potentiation. *Neuron,* 28**,** 245-259.

BRIGIDI, G. S. & BAMJI, S. X. 2011. Cadherin-catenin adhesion complexes at the synapse. *Curr Opin Neurobiol,* 21**,** 208-14.

BRIGIDI, G. S., SUN, Y., BECCANO-KELLY, D., PITMAN, K., MOBASSER, M., BORGLAND, S. L., MILNERWOOD, A. J. & BAMJI, S. X. 2014. Palmitoylation of delta-catenin by DHHC5 mediates activity-induced synapse plasticity. *Nat Neurosci,* 17**,** 522-32.

BROADHEAD, M. J., HORROCKS, M. H., ZHU, F., MURESAN, L., BENAVIDES-PICCIONE, R., DEFELIPE, J., FRICKER, D., KOPANITSA, M. V., DUNCAN, R. R., KLENERMAN, D., KOMIYAMA, N. H., LEE, S. F. & GRANT, S. G. 2016. PSD95 nanoclusters are postsynaptic building blocks in hippocampus circuits. *Sci Rep,* 6**,** 24626.

CALDERWOOD, D. A., CAMPBELL, I. D. & CRITCHLEY, D. R. 2013. Talins and kindlins: partners in integrin-mediated adhesion. *Nat Rev Mol Cell Biol,* 14**,** 503-17.

CARLISLE, H. J., MANZERRA, P., MARCORA, E. & KENNEDY, M. B. 2008. SynGAP Regulates Steady-State and Activity-Dependent Phosphorylation of Cofilin. *The Journal of Neuroscience,* 28**,** 13673.

CHEN, H.-J., ROJAS-SOTO, M., OGUNI, A. & KENNEDY, M. B. 1998. A Synaptic Ras-GTPase Activating Protein (p135 SynGAP) Inhibited by CaM Kinase II. *Neuron,* 20**,** 895-904.

CHEN, X., WINTERS, C., AZZAM, R., LI, X., GALBRAITH, J. A., LEAPMAN, R. D. & REESE, T. S. 2008. Organization of the core structure of the postsynaptic density. *Proceedings of the National Academy of Sciences,* 105**,** 4453.

CHKLOVSKII, D. B. 2004. Synaptic connectivity and neuronal morphology: two sides of the same coin. *Neuron,* 43**,** 609-17.

CHOI, H.-J. & WEIS, W. I. 2005. Structure of the Armadillo Repeat Domain of Plakophilin 1. *Journal of Molecular Biology,* 346**,** 367-376.

CLEMENT, J. P., ACETI, M., CRESON, T. K., OZKAN, E. D., SHI, Y., REISH, N. J., ALMONTE, A. G., MILLER, B. H., WILTGEN, B. J., MILLER, C. A., XU, X. & RUMBAUGH, G. 2012. Pathogenic SYNGAP1 mutations impair cognitive development by disrupting maturation of dendritic spine synapses. *Cell,* 151**,** 709-723.

CLEVERS, H. & NUSSE, R. 2012. Wnt/β-Catenin Signaling and Disease. *Cell,* 149**,** 1192-1205.

COBA, M. P., RAMAKER, M. J., HO, E. V., THOMPSON, S. L., KOMIYAMA, N. H., GRANT, S. G. N., KNOWLES, J. A. & DULAWA, S. C. 2018. Dlgap1 knockout mice exhibit alterations of the postsynaptic density and selective reductions in sociability. *Scientific Reports,* 8**,** 2281.

COLICELLI, J. 2004. Human RAS Superfamily Proteins and Related GTPases. *Science's STKE,* 2004**,** re13.

DANI, A., HUANG, B., BERGAN, J., DULAC, C. & ZHUANG, X. 2010. Superresolution Imaging of Chemical Synapses in the Brain. *Neuron,* 68**,** 843-856.

DARDENNE, E., POLAY ESPINOZA, M., FATTET, L., GERMANN, S., LAMBERT, M. P., NEIL, H., ZONTA, E., MORTADA, H., GRATADOU, L., DEYGAS, M., CHAKRAMA, F. Z., SAMAAN, S., DESMET, F. O., TRANCHEVENT, L. C., DUTERTRE, M., RIMOKH, R., BOURGEOIS, C. F. & AUBOEUF, D. 2014. RNA helicases DDX5 and DDX17 dynamically orchestrate transcription, miRNA, and splicing programs in cell differentiation. *Cell Rep,* 7**,** 1900-13.

DAVIS, M. A., IRETON, R. C. & REYNOLDS, A. B. 2003. A core function for p120-catenin in cadherin turnover. *J Cell Biol,* 163**,** 525-34.

DEGUCHI, M., IIZUKA, T., HATA, Y., NISHIMURA, W., HIRAO, K., YAO, I., KAWABE, H. & TAKAI, Y. 2000. PAPIN: A NOVEL MULTIPLE PSD-95/Dlg-A/ZO-1 PROTEIN INTERACTING WITH NEURAL PLAKOPHILIN-RELATED Armadillo REPEAT PROTEIN/δ-CATENIN AND p0071. *Journal of Biological Chemistry,* 275**,** 29875-29880.

DIERING, G. H. & HUGANIR, R. L. 2018. The AMPA Receptor Code of Synaptic Plasticity. *Neuron,* 100**,** 314-329.

DREES, F., POKUTTA, S., YAMADA, S., NELSON, W. J. & WEIS, W. I. 2005. Alpha-catenin is a molecular switch that binds E-cadherin-beta-catenin and regulates actin-filament assembly. *Cell,* 123**,** 903-15.

DU, Y., WEED, S. A., XIONG, W.-C., MARSHALL, T. D. & PARSONS, J. T. 1998. Identification of a Novel Cortactin SH3 Domain-Binding Protein and Its Localization to Growth Cones of Cultured Neurons. *Molecular and Cellular Biology,* 18**,** 5838.

DURAND, C. M., BETANCUR, C., BOECKERS, T. M., BOCKMANN, J., CHASTE, P., FAUCHEREAU, F., NYGREN, G., RASTAM, M., GILLBERG, I. C., ANCKARSATER, H., SPONHEIM, E., GOUBRAN-BOTROS, H., DELORME, R., CHABANE, N., MOUREN-SIMEONI, M. C., DE MAS, P., BIETH, E., ROGE, B., HERON, D., BURGLEN, L., GILLBERG, C., LEBOYER, M. & BOURGERON, T. 2007. Mutations in the gene encoding the synaptic scaffolding protein SHANK3 are associated with autism spectrum disorders. *Nat Genet,* 39**,** 25-7.

DURAND, C. M., PERROY, J., LOLL, F., PERRAIS, D., FAGNI, L., BOURGERON, T., MONTCOUQUIOL, M. & SANS, N. 2012. SHANK3 mutations identified in autism lead to modification of dendritic spine morphology via an actin-dependent mechanism. *Mol Psychiatry,* 17**,** 71-84.

ELIA, L. P., YAMAMOTO, M., ZANG, K. & REICHARDT, L. F. 2006. p120 catenin regulates dendritic spine and synapse development through Rho-family GTPases and cadherins. *Neuron,* 51**,** 43-56.

FARIDAR, A., JONES-DAVIS, D., RIDER, E., LI, J., GOBIUS, I., MORCOM, L., RICHARDS, L. J., SEN, S. & SHERR, E. H. 2014. Mapk/Erk activation in an animal model of social deficits shows a possible link to autism. *Molecular Autism,* 5**,** 57.

FERNA´NDEZ, E., COLLINS, M. O., UREN, R. T., KOPANITSA, M. V., KOMIYAMA, N. H., CRONING, M. D. R., ZOGRAFOS, L., ARMSTRONG, J. D., CHOUDHARY, J. S. & GRANT, S. G. 2009. Targeted

tandem affinity purification of PSD-95 recovers core postsynaptic complexes and schizophrenia susceptibility proteins. *Molecular Systems Biology,* 5.

FOGARTY, M. J., KANJHAN, R., BELLINGHAM, M. C. & NOAKES, P. G. 2016. Glycinergic Neurotransmission: A Potent Regulator of Embryonic Motor Neuron Dendritic Morphology and Synaptic Plasticity. *J Neurosci,* 36**,** 80-7.

FRANK, R. A. & GRANT, S. G. 2017. Supramolecular organization of NMDA receptors and the postsynaptic density. *Curr Opin Neurobiol,* 45**,** 139-147.

FRANZE, K. & GUCK, J. 2010. The biophysics of neuronal growth. *Reports on Progress in Physics,* 73.

FUKATA, Y., DIMITROV, A., BONCOMPAIN, G., VIELEMEYER, O., PEREZ, F. & FUKATA, M. 2013. Local palmitoylation cycles define activity-regulated postsynaptic subdomains. *The Journal of Cell Biology,* 202**,** 145.

GAUTHIER, J., CHAMPAGNE, N., LAFRENIERE, R. G., XIONG, L., SPIEGELMAN, D., BRUSTEIN, E., LAPOINTE, M., PENG, H., COTE, M., NOREAU, A., HAMDAN, F. F., ADDINGTON, A. M., RAPOPORT, J. L., DELISI, L. E., KREBS, M. O., JOOBER, R., FATHALLI, F., MOUAFFAK, F., HAGHIGHI, A. P., NERI, C., DUBE, M. P., SAMUELS, M. E., MARINEAU, C., STONE, E. A., AWADALLA, P., BARKER, P. A., CARBONETTO, S., DRAPEAU, P., ROULEAU, G. A. & TEAM, S. D. 2010. De novo mutations in the gene encoding the synaptic scaffolding protein SHANK3 in patients ascertained for schizophrenia. *Proc Natl Acad Sci U S A,* 107**,** 7863-8.

GAUTHIER, J., SPIEGELMAN, D., PITON, A., LAFRENIERE, R. G., LAURENT, S., ST-ONGE, J., LAPOINTE, L., HAMDAN, F. F., COSSETTE, P., MOTTRON, L., FOMBONNE, E., JOOBER, R., MARINEAU, C., DRAPEAU, P. & ROULEAU, G. A. 2009. Novel de novo SHANK3 mutation in autistic patients. *Am J Med Genet B Neuropsychiatr Genet,* 150B**,** 421-4.

GESCHWIND, D. H. 2009. Advances in autism. *Annu Rev Med,* 60**,** 367-80.

GEUENS, T., BOUHY, D. & TIMMERMAN, V. 2016. The hnRNP family: insights into their role in health and disease. *Hum Genet,* 135**,** 851-67.

GRABRUCKER, A. M. 2014. A role for synaptic zinc in ProSAP/Shank PSD scaffold malformation in autism spectrum disorders. *Developmental neurobiology,* 74**,** 136-146.

GRABRUCKER, S., PROEPPER, C., MANGUS, K., ECKERT, M., CHHABRA, R., SCHMEISSER, M. J., BOECKERS, T. M. & GRABRUCKER, A. M. 2014. The PSD protein ProSAP2/Shank3 displays synapto-nuclear shuttling which is deregulated in a schizophrenia-associated mutation. *Exp Neurol,* 253**,** 126-37.

GRANT, S. G. 2012. Synaptopathies: diseases of the synaptome. *Curr Opin Neurobiol,* 22**,** 522-9.

GU, Y. & STORNETTA, R. L. 2007. Synaptic plasticity, AMPA-R trafficking, and Ras-MAPK signaling. *Acta Pharmacologica Sinica,* 28**,** 928.

GUILMATRE, A., HUGUET, G., DELORME, R. & BOURGERON, T. 2014. The emerging role of SHANK genes in neuropsychiatric disorders. *Dev Neurobiol,* 74**,** 113-22.

HAN, K.-S., COOKE, S. F. & XU, W. 2017. Experience-Dependent Equilibration of AMPAR-Mediated Synaptic Transmission during the Critical Period. *Cell Reports,* 18**,** 892-904.

HAN, K., HOLDER JR, J. L., SCHAAF, C. P., LU, H., CHEN, H., KANG, H., TANG, J., WU, Z., HAO, S., CHEUNG, S. W., YU, P., SUN, H., BREMAN, A. M., PATEL, A., LU, H.-C. & ZOGHBI, H. Y. 2013. SHANK3 overexpression causes manic-like behaviour with unique pharmacogenetic properties. *Nature,* 503**,** 72.

HASSANI NIA, F. & KREIENKAMP, H. J. 2018. Functional Relevance of Missense Mutations Affecting the N-Terminal Part of Shank3 Found in Autistic Patients. *Front Mol Neurosci,* 11**,** 268.

HELL, J. W. 2014. CaMKII: claiming center stage in postsynaptic function and organization. *Neuron,* 81**,** 249-65.

HUBER, A. H., NELSON, W. J. & WEIS, W. I. 1997. Three-Dimensional Structure of the Armadillo Repeat Region of β-Catenin. *Cell,* 90**,** 871-882.

HUBER, A. H. & WEIS, W. I. 2001. The Structure of the β-Catenin/E-Cadherin Complex and the Molecular Basis of Diverse Ligand Recognition by β-Catenin. *Cell,* 105**,** 391-402.

HUGUET, G., EY, E. & BOURGERON, T. 2013. The genetic landscapes of autism spectrum disorders. *Annu Rev Genomics Hum Genet,* 14**,** 191-213.

HUSI, H. & GRANT, S. G. N. 2001. Isolation of 2000-kDa complexes of N-methyl-d-aspartate receptor and postsynaptic density 95 from mouse brain. *Journal of Neurochemistry,* 77**,** 281-291.

HUSI, H., WARD, M. A., CHOUDHARY, J. S., BLACKSTOCK, W. P. & GRANT, S. G. N. 2000. Proteomic analysis of NMDA receptor–adhesion protein signaling complexes. *Nature Neuroscience,* 3**,** 661.

IDE, N., HATA, Y., DEGUCHI, M., HIRAO, K., YAO, I. & TAKAI, Y. 1999. Interaction of S-SCAM with Neural Plakophilin-RelatedArmadillo-Repeat Protein/δ-Catenin. *Biochemical and Biophysical Research Communications,* 256**,** 456-461.

ISRAELY, I., COSTA, R. M., XIE, C. W., SILVA, A. J., KOSIK, K. S. & LIU, X. 2004. Deletion of the neuron-specific protein delta-catenin leads to severe cognitive and synaptic dysfunction. *Curr Biol,* 14**,** 1657-63.

IZAWA, I., NISHIZAWA, M., OHTAKARA, K. & INAGAKI, M. 2002. Densin-180 interacts with delta-catenin/neural plakophilin-related armadillo repeat protein at synapses. *J Biol Chem,* 277**,** 5345-50.

JAMAIN, S., QUACH, H., BETANCUR, C., RASTAM, M., COLINEAUX, C., GILLBERG, I. C., SODERSTROM, H., GIROS, B., LEBOYER, M., GILLBERG, C., BOURGERON, T. & PARIS AUTISM RESEARCH INTERNATIONAL SIBPAIR, S. 2003. Mutations of the X-linked genes encoding neuroligins NLGN3 and NLGN4 are associated with autism. *Nat Genet,* 34**,** 27-9.

JORDAN, B. A. & KREUTZ, M. R. 2009. Nucleocytoplasmic protein shuttling: the direct route in synapse-to-nucleus signaling. *Trends Neurosci,* 32**,** 392-401.

KELLEHER, R. J., 3RD, GEIGENMULLER, U., HOVHANNISYAN, H., TRAUTMAN, E., PINARD, R., RATHMELL, B., CARPENTER, R. & MARGULIES, D. 2012. High-throughput sequencing of mGluR signaling pathway genes reveals enrichment of rare variants in autism. *PLoS One,* 7**,** e35003.

KIM, H., HAN, J.-R., PARK, J., OH, M., JAMES, S. E., CHANG, S., LU, Q., LEE, K. Y., KI, H., SONG, W.-J. & KIM, K. 2008. δ-Catenin-induced Dendritic Morphogenesis: AN ESSENTIAL ROLE OF p190RhoGEF INTERACTION THROUGH AKT1-MEDIATED PHOSPHORYLATION. *Journal of Biological Chemistry,* 283**,** 977-987.

KIM, J. H., LEE, H.-K., TAKAMIYA, K. & HUGANIR, R. L. 2003. The Role of Synaptic GTPase-Activating Protein in Neuronal Development and Synaptic Plasticity. *The Journal of Neuroscience,* 23**,** 1119.

KOMIYAMA, N. H., WATABE, A. M., CARLISLE, H. J., PORTER, K., CHARLESWORTH, P., MONTI, J., STRATHDEE, D. J. C., CARROLL, C. M., MARTIN, S. J., MORRIS, R. G. M., DELL, T. J. & GRANT, S. G. N. 2002. SynGAP Regulates ERK/MAPK Signaling, Synaptic Plasticity, and Learning in the Complex with Postsynaptic Density 95 and NMDA Receptor. *The Journal of Neuroscience,* 22**,** 9721.

KOSIK, K. S., DONAHUE, C. P., ISRAELY, I., LIU, X. & OCHIISHI, T. 2005. δ-Catenin at the synaptic–adherens junction. *Trends in Cell Biology,* 15**,** 172-178.

KOUSER, M., SPEED, H. E., DEWEY, C. M., REIMERS, J. M., WIDMAN, A. J., GUPTA, N., LIU, S., JARAMILLO, T. C., BANGASH, M., XIAO, B., WORLEY, P. F. & POWELL, C. M. 2013. Loss of predominant Shank3 isoforms results in hippocampus-dependent impairments in behavior and synaptic transmission. *J Neurosci,* 33**,** 18448-68.

KRAB, L. C., GOORDEN, S. M. & ELGERSMA, Y. 2008. Oncogenes on my mind: ERK and MTOR signaling in cognitive diseases. *Trends Genet,* 24**,** 498-510.

LAURA, R. P., WITT, A. S., HELD, H. A., GERSTNER, R., DESHAYES, K., KOEHLER, M. F. T., KOSIK, K. S., SIDHU, S. S. & LASKY, L. A. 2002. The Erbin PDZ Domain Binds with High Affinity and Specificity to the Carboxyl Termini of δ-Catenin and ARVCF. *Journal of Biological Chemistry,* 277**,** 12906-12914.

LEBLOND, C. S., NAVA, C., POLGE, A., GAUTHIER, J., HUGUET, G., LUMBROSO, S., GIULIANO, F., STORDEUR, C., DEPIENNE, C., MOUZAT, K., PINTO, D., HOWE, J., LEMIERE, N., DURAND, C. M.,

GUIBERT, J., EY, E., TORO, R., PEYRE, H., MATHIEU, A., AMSELLEM, F., RASTAM, M., GILLBERG, I. C., RAPPOLD, G. A., HOLT, R., MONACO, A. P., MAESTRINI, E., GALAN, P., HERON, D., JACQUETTE, A., AFENJAR, A., RASTETTER, A., BRICE, A., DEVILLARD, F., ASSOULINE, B., LAFFARGUE, F., LESPINASSE, J., CHIESA, J., RIVIER, F., BONNEAU, D., REGNAULT, B., ZELENIKA, D., DELEPINE, M., LATHROP, M., SANLAVILLE, D., SCHLUTH-BOLARD, C., EDERY, P., PERRIN, L., TABET, A. C., SCHMEISSER, M. J., BOECKERS, T. M., COLEMAN, M., SATO, D., SZATMARI, P., SCHERER, S. W., ROULEAU, G. A., BETANCUR, C., LEBOYER, M., GILLBERG, C., DELORME, R. & BOURGERON, T. 2014. Meta-analysis of SHANK Mutations in Autism Spectrum Disorders: a gradient of severity in cognitive impairments. *PLoS Genet,* 10**,** e1004580.

LEE, H.-J. & ZHENG, J. J. 2010. PDZ domains and their binding partners: structure, specificity, and modification. *Cell Communication and Signaling,* 8**,** 8.

LEE, K. J., HOE, H. S. & PAK, D. T. 2011. Plk2 Raps up Ras to subdue synapses. *Small GTPases,* 2**,** 162-166.

LEPETA, K., LOURENCO, M. V., SCHWEITZER, B. C., MARTINO ADAMI, P. V., BANERJEE, P., CATUARA-SOLARZ, S., DE LA FUENTE REVENGA, M., GUILLEM, A. M., HAIDAR, M., IJOMONE, O. M., NADORP, B., QI, L., PERERA, N. D., REFSGAARD, L. K., REID, K. M., SABBAR, M., SAHOO, A., SCHAEFER, N., SHEEAN, R. K., SUSKA, A., VERMA, R., VICIDOMINI, C., WRIGHT, D., ZHANG, X. D. & SEIDENBECHER, C. 2016. Synaptopathies: synaptic dysfunction in neurological disorders - A review from students to students. *J Neurochem,* 138**,** 785-805.

LEVINSON, J. N. & EL-HUSSEINI, A. 2005. Building excitatory and inhibitory synapses: balancing neuroligin partnerships. *Neuron,* 48**,** 171-4.

LI, J., ZHANG, W., YANG, H., HOWRIGAN, D. P., WILKINSON, B., SOUAIAIA, T., EVGRAFOV, O. V., GENOVESE, G., CLEMENTEL, V. A., TUDOR, J. C., ABEL, T., KNOWLES, J. A., NEALE, B. M., WANG, K., SUN, F. & COBA, M. P. 2017. Spatiotemporal profile of postsynaptic interactomes integrates components of complex brain disorders. *Nature Neuroscience,* 20**,** 1150.

LILJA, J., ZACHARCHENKO, T., GEORGIADOU, M., JACQUEMET, G., DE FRANCESCHI, N., PEUHU, E., HAMIDI, H., POUWELS, J., MARTENS, V., NIA, F. H., BEIFUSS, M., BOECKERS, T., KREIENKAMP, H. J., BARSUKOV, I. L. & IVASKA, J. 2017. SHANK proteins limit integrin activation by directly interacting with Rap1 and R-Ras. *Nat Cell Biol,* 19**,** 292-305.

LIM, S., NAISBITT, S., YOON, J., HWANG, J.-I., SUH, P.-G., SHENG, M. & KIM, E. 1999. Characterization of the Shank Family of Synaptic Proteins: MULTIPLE GENES, ALTERNATIVE SPLICING, AND DIFFERENTIAL EXPRESSION IN BRAIN AND DEVELOPMENT. *Journal of Biological Chemistry,* 274**,** 29510-29518.

LIM, S., SALA, C., YOON, J., PARK, S., KURODA, S., SHENG, M. & KIM, E. 2001. Sharpin, a novel postsynaptic density protein that directly interacts with the shank family of proteins. *Mol Cell Neurosci,* 17**,** 385-97.

LIN, A. W. & MAN, H. Y. 2013. Ubiquitination of neurotransmitter receptors and postsynaptic scaffolding proteins. *Neural Plast,* 2013**,** 432057.

LISMAN, J., YASUDA, R. & RAGHAVACHARI, S. 2012. Mechanisms of CaMKII action in long-term potentiation. *Nat Rev Neurosci,* 13**,** 169-82.

LU, Q., PAREDES, M., MEDINA, M., ZHOU, J., CAVALLO, R., PEIFER, M., ORECCHIO, L. & KOSIK, K. S. 1999. δ-catenin, an Adhesive Junction–associated Protein Which Promotes Cell Scattering. *The Journal of Cell Biology,* 144**,** 519–532.

MACGILLAVRY, H. D., SONG, Y., RAGHAVACHARI, S. & BLANPIED, T. A. 2013. Nanoscale scaffolding domains within the postsynaptic density concentrate synaptic AMPA receptors. *Neuron,* 78**,** 615-22.

MAGUSCHAK, K. A. & RESSLER, K. J. 2008. Beta-catenin is required for memory consolidation. *Nat Neurosci,* 11**,** 1319-26.

MAKINO, H. & MALINOW, R. 2009. AMPA Receptor Incorporation into Synapses during LTP: The Role of Lateral Movement and Exocytosis. *Neuron,* 64**,** 381-390.

MAMEZA, M. G., DVORETSKOVA, E., BAMANN, M., HONCK, H. H., GULER, T., BOECKERS, T. M., SCHOEN, M., VERPELLI, C., SALA, C., BARSUKOV, I., DITYATEV, A. & KREIENKAMP, H. J. 2013. SHANK3 gene mutations associated with autism facilitate ligand binding to the Shank3 ankyrin repeat region. *J Biol Chem,* 288**,** 26697-708.

MANGUS, K., JANNETTI, L., ECKERT, M., CHHABRA, R., GRABRUCKER, S., GRABRUCKER, A. M., EHRET, G., GAUB, S., SCHMEISSER, M. J., PFAENDER, S., BOECKERS, T. M., KREUTZ, M. R., REDDY, P. P. & RANKOVIC, V. 2013. Zinc deficiency dysregulates the synaptic ProSAP/Shank scaffold and might contribute to autism spectrum disorders. *Brain,* 137**,** 137-152.

MARTELLA, G., MERINGOLO, M., TROBIANI, L., DE JACO, A., PISANI, A. & BONSI, P. 2018. The neurobiological bases of autism spectrum disorders: the R451C-neuroligin 3 mutation hampers the expression of long-term synaptic depression in the dorsal striatum. *Eur J Neurosci,* 47**,** 701-708.

MATTER, C., PRIBADI, M., LIU, X. & TRACHTENBERG, J. T. 2009. Delta-catenin is required for the maintenance of neural structure and function in mature cortex in vivo. *Neuron,* 64**,** 320-7.

MCCREA, P. D. & GOTTARDI, C. J. 2016. Beyond beta-catenin: prospects for a larger catenin network in the nucleus. *Nat Rev Mol Cell Biol,* 17**,** 55-64.

MCCREA, P. D. & GU, D. 2010. The catenin family at a glance. *J Cell Sci,* 123**,** 637-42.

MCCREA, P. D. & PARK, J. I. 2007. Developmental functions of the P120-catenin sub-family. *Biochim Biophys Acta,* 1773**,** 17-33.

MCWILLIAMS, R. R., GIDEY, E., FOUASSIER, L., WEED, S. A. & DOCTOR, R. B. 2004. Characterization of an ankyrin repeat-containing Shank2 isoform (Shank2E) in liver epithelial cells. *The Biochemical journal,* 380**,** 181-191.

MEDINA, M., MARINESCU, R. C., OVERHAUSER, J. & KOSIK, K. S. 2000. Hemizygosity of delta-catenin (CTNND2) is associated with severe mental retardation in cri-du-chat syndrome. *Genomics,* 63**,** 157-64.

MEYER, D., BONHOEFFER, T. & SCHEUSS, V. 2014. Balance and stability of synaptic structures during synaptic plasticity. *Neuron,* 82**,** 430-43.

MEYER, G., VAROQUEAUX, F., NEEB, A., OSCHLIES, M. & BROSE, N. 2004. The complexity of PDZ domain-mediated interactions at glutamatergic synapses: a case study on neuroligin. *Neuropharmacology,* 47**,** 724-733.

MOESSNER, R., MARSHALL, C. R., SUTCLIFFE, J. S., SKAUG, J., PINTO, D., VINCENT, J., ZWAIGENBAUM, L., FERNANDEZ, B., ROBERTS, W., SZATMARI, P. & SCHERER, S. W. 2007. Contribution of SHANK3 mutations to autism spectrum disorder. *Am J Hum Genet,* 81**,** 1289-97.

MURASE, S., MOSSER, E. & SCHUMAN, E. M. 2002. Depolarization Drives β-Catenin into Neuronal Spines Promoting Changes in Synaptic Structure and Function. *Neuron,* 35**,** 91-105.

MYSORE, S. P., TAI, C.-Y. & SCHUMAN, E. M. 2008. N-cadherin, spine dynamics, and synaptic function. *Frontiers in neuroscience,* 2**,** 168-175.

NAIR, D., HOSY, E., PETERSEN, J. D., CONSTALS, A., GIANNONE, G., CHOQUET, D. & SIBARITA, J. B. 2013. Super-resolution imaging reveals that AMPA receptors inside synapses are dynamically organized in nanodomains regulated by PSD95. *J Neurosci,* 33**,** 13204-24.

NAISBITT, S., KIM, E., TU, J. C., XIAO, B., SALA, C., VALTSCHANOFF, J., WEINBERG, R. J., WORLEY, P. F. & SHENG, M. 1999. Shank, a Novel Family of Postsynaptic Density Proteins that Binds to the NMDA Receptor/PSD-95/GKAP Complex and Cortactin. *Neuron,* 23**,** 569-582.

NIMCHINSKY, E. A., SABATINI, B. L. & SVOBODA, K. 2002. Structure and Function of Dendritic Spines. *Annual Review of Physiology,* 64**,** 313-353.

NURIYA, M. & HUGANIR, R. L. 2006. Regulation of AMPA receptor trafficking by N-cadherin. *Journal of Neurochemistry,* 97**,** 652-661.

OGILVIE, V. C. 2003. The highly related DEAD box RNA helicases p68 and p72 exist as heterodimers in cells. *Nucleic Acids Research,* 31**,** 1470-1480.

OH, J. S., MANZERRA, P. & KENNEDY, M. B. 2004. Regulation of the Neuron-specific Ras GTPase-activating Protein, synGAP, by Ca2+/Calmodulin-dependent Protein Kinase II. *Journal of Biological Chemistry,* 279**,** 17980-17988.

OKUDA, T., YU, L. M. Y., CINGOLANI, L. A., KEMLER, R. & GODA, Y. 2007. β-Catenin regulates excitatory postsynaptic strength at hippocampal synapses. *PNAS,* 104**,** 13479–13484.

OZAWA, M., BARIBAULT, H. & KEMLER, R. 1989. The cytoplasmic domain of the cell adhesion molecule uvomorulin associates with three independent proteins structurally related in different species. *The EMBO Journal,* 8**,** 1 711 - 1717.

PECA, J., FELICIANO, C., TING, J. T., WANG, W., WELLS, M. F., VENKATRAMAN, T. N., LASCOLA, C. D., FU, Z. & FENG, G. 2011. Shank3 mutant mice display autistic-like behaviours and striatal dysfunction. *Nature,* 472**,** 437-42.

PETERSEN, J. D., CHEN, X., VINADE, L., DOSEMECI, A., LISMAN, J. E. & REESE, T. S. 2003. Distribution of Postsynaptic Density (PSD)-95 and Ca²⁺/Calmodulin-Dependent Protein Kinase II at the PSD. *The Journal of Neuroscience,* 23**,** 11270.

PLANTMAN, S., PATARROYO, M., FRIED, K., DOMOGATSKAYA, A., TRYGGVASON, K., HAMMARBERG, H. & CULLHEIM, S. 2008. Integrin-laminin interactions controlling neurite outgrowth from adult DRG neurons in vitro. *Mol Cell Neurosci,* 39**,** 50-62.

POKUTTA, S. & WEIS, W. I. 2007. Structure and mechanism of cadherins and catenins in cell-cell contacts. *Annu Rev Cell Dev Biol,* 23**,** 237-61.

PROEPPER, C., JOHANNSEN, S., LIEBAU, S., DAHL, J., VAIDA, B., BOCKMANN, J., KREUTZ, M. R., GUNDELFINGER, E. D. & BOECKERS, T. M. 2007. Abelson interacting protein 1 (Abi-1) is essential for dendrite morphogenesis and synapse formation. *EMBO J,* 26**,** 1397-409.

QIN, L., MA, K., WANG, Z. J., HU, Z., MATAS, E., WEI, J. & YAN, Z. 2018. Social deficits in Shank3-deficient mouse models of autism are rescued by histone deacetylase (HDAC) inhibition. *Nat Neurosci,* 21**,** 564-575.

QUITSCH, A., BERHORSTER, K., LIEW, C. W., RICHTER, D. & KREIENKAMP, H. J. 2005. Postsynaptic shank antagonizes dendrite branching induced by the leucine-rich repeat protein Densin-180. *J Neurosci,* 25**,** 479-87.

RAMIRO-CORTÉS, Y., HOBBISS, A. F. & ISRAELY, I. 2013. Synaptic competition in structural plasticity and cognitive function. *Philosophical transactions of the Royal Society of London. Series B, Biological sciences,* 369**,** 20130157-20130157.

REPASKY, G. A., CHENETTE, E. J. & DER, C. J. 2004. Renewing the conspiracy theory debate: does Raf function alone to mediate Ras oncogenesis? *Trends in Cell Biology,* 14**,** 639-647.

ROMORINI, S., PICCOLI, G., JIANG, M., GROSSANO, P., TONNA, N., PASSAFARO, M., ZHANG, M. & SALA, C. 2004. A functional role of postsynaptic density-95-guanylate kinase-associated protein complex in regulating Shank assembly and stability to synapses. *J Neurosci,* 24**,** 9391-404.

RUBENSTEIN, J. L. R. & MERZENICH, M. M. 2003. Model of autism: increased ratio of excitation/inhibition in key neural systems. *Genes, Brain and Behavior,* 2**,** 255-267.

SALA, C., PIËCH, V., WILSON, N. R., PASSAFARO, M., LIU, G. & SHENG, M. 2001. Regulation of Dendritic Spine Morphology and Synaptic Function by Shank and Homer. *Neuron,* 31**,** 115-130.

SCANNEVIN, R. H. & HUGANIR, R. L. 2000. Postsynaptic organisation and regulation of excitatory synapses. *Nature Reviews Neuroscience,* 1**,** 133.

SCHMEISSER, M. J., GRABRUCKER, A. M., BOCKMANN, J. & BOECKERS, T. M. 2009. Synaptic Cross-talk between N-Methyl-d-aspartate Receptors and LAPSER1-β-Catenin at Excitatory Synapses. *Journal of Biological Chemistry,* 284**,** 29146-29157.

SCHUMMERS, J., MARIÑO, J. & SUR, M. 2002. Synaptic Integration by V1 Neurons Depends on Location within the Orientation Map. *Neuron,* 36**,** 969-978.

SEPHTON, C. F. & YU, G. 2015. The function of RNA-binding proteins at the synapse: implications for neurodegeneration. *Cell Mol Life Sci,* 72**,** 3621-35.

SHAPIRO, L. & WEIS, W. I. 2009. Structure and Biochemistry of Cadherins and Catenins. *Cold Spring Harb Perspect Biol*.

SHENG, M. & HOOGENRAAD, C. C. 2007. The postsynaptic architecture of excitatory synapses: a more quantitative view. *Annu Rev Biochem,* 76**,** 823-47.

SHENG, M. & KIM, E. 2000. The Shank family of scaffold proteins. *Journal of Cell Science,* 113**,** 1851.

SHENG, M. & KIM, E. 2011. The postsynaptic organization of synapses. *Cold Spring Harb Perspect Biol,* 3.

SHIN, S. M., ZHANG, N., HANSEN, J., GERGES, N. Z., PAK, D. T., SHENG, M. & LEE, S. H. 2012. GKAP orchestrates activity-dependent postsynaptic protein remodeling and homeostatic scaling. *Nat Neurosci,* 15**,** 1655-66.

SILVERMAN, J. B., RESTITUITO, S., LU, W., LEE-EDWARDS, L., KHATRI, L. & ZIFF, E. B. 2007. Synaptic anchorage of AMPA receptors by cadherins through neural plakophilin-related arm protein AMPA receptor-binding protein complexes. *J Neurosci,* 27**,** 8505-16.

SIMANSHU, D. K., NISSLEY, D. V. & MCCORMICK, F. 2017. RAS Proteins and Their Regulators in Human Disease. *Cell,* 170**,** 17-33.

SOLTAU, M., RICHTER, D. & KREIENKAMP, H.-J. 2002. The Insulin Receptor Substrate IRSp53 Links Postsynaptic shank1 to the Small G-Protein cdc42. *Molecular and Cellular Neuroscience,* 21**,** 575-583.

STORNETTA, R. L. & ZHU, J. J. 2011. Ras and Rap signaling in synaptic plasticity and mental disorders. *Neuroscientist,* 17**,** 54-78.

SÜDHOF, T. C. 2008. Neuroligins and neurexins link synaptic function to cognitive disease. *Nature,* 455**,** 903.

SUN, Y., AIGA, M., YOSHIDA, E., HUMBERT, P. O. & BAMJI, S. X. 2009. Scribble Interacts with β-Catenin to Localize Synaptic Vesicles to Synapses. *Molecular Biology of the Cell,* 20**,** 3390-3400.

TADA, T. & SHENG, M. 2006. Molecular mechanisms of dendritic spine morphogenesis. *Current Opinion in Neurobiology,* 16**,** 95-101.

TANAKA, H., SHAN, W., PHILLIPS, G. R., ARNDT, K., BOZDAGI, O., SHAPIRO, L., HUNTLEY, G. W., BENSON, D. L. & COLMAN, D. R. 2000. Molecular Modification of N-Cadherin in Response to Synaptic Activity. *Neuron,* 25**,** 93-107.

TATAVARTY, V., TORRADO PACHECO, A., LIN, H., MISKA, N. J., HENGEN, K. B., WAGNER, F. F. & TURRIGIANO, G. G. 2018. Autism-associated Shank3 is essential for homeostatic plasticity and neuronal circuit stability. *bioRxiv***,** 365445.

THOMAS, G. M. & HUGANIR, R. L. 2004. MAPK cascade signalling and synaptic plasticity. *Nature Reviews Neuroscience,* 5**,** 173.

TIRUCHINAPALLI, D. M., CARON, M. G. & KEENE, J. D. 2008. Activity-dependent expression of ELAV/Hu RBPs and neuronal mRNAs in seizure and cocaine brain. *Journal of Neurochemistry,* 107**,** 1529-1543.

TORO, R., KONYUKH, M., DELORME, R., LEBLOND, C., CHASTE, P., FAUCHEREAU, F., COLEMAN, M., LEBOYER, M., GILLBERG, C. & BOURGERON, T. 2010. Key role for gene dosage and synaptic homeostasis in autism spectrum disorders. *Trends Genet,* 26**,** 363-72.

TU, J. C., XIAO, B., NAISBITT, S., YUAN, J. P., PETRALIA, R. S., BRAKEMAN, P., DOAN, A., AAKALU, V. K., LANAHAN, A. A., SHENG, M. & WORLEY, P. F. 1999. Coupling of mGluR/Homer and PSD-95 Complexes by the Shank Family of Postsynaptic Density Proteins. *Neuron,* 23**,** 583-592.

TURNER, T. N., SHARMA, K., OH, E. C., LIU, Y. P., COLLINS, R. L., SOSA, M. X., AUER, D. R., BRAND, H., SANDERS, S. J., MORENO-DE-LUCA, D., PIHUR, V., PLONA, T., PIKE, K., SOPPET, D. R., SMITH, M. W., CHEUNG, S. W., MARTIN, C. L., STATE, M. W., TALKOWSKI, M. E., COOK, E., HUGANIR, R., KATSANIS, N. & CHAKRAVARTI, A. 2015. Loss of delta-catenin function in severe autism. *Nature,* 520**,** 51-6.

VALENTA, T., HAUSMANN, G. & BASLER, K. 2012. The many faces and functions of beta-catenin. *EMBO J,* 31**,** 2714-36.

VALTSCHANOFF, J. G. & WEINBERG, R. J. 2001. Laminar Organization of the NMDA Receptor Complex within the Postsynaptic Density. *The Journal of Neuroscience,* 21**,** 1211.

VAN SPRONSEN, M. & HOOGENRAAD, C. C. 2010. Synapse pathology in psychiatric and neurologic disease. *Curr Neurol Neurosci Rep,* 10**,** 207-14.

VERPELLI, C., DVORETSKOVA, E., VICIDOMINI, C., ROSSI, F., CHIAPPALONE, M., SCHOEN, M., DI STEFANO, B., MANTEGAZZA, R., BROCCOLI, V., BOCKERS, T. M., DITYATEV, A. & SALA, C. 2011. Importance of Shank3 protein in regulating metabotropic glutamate receptor 5 (mGluR5) expression and signaling at synapses. *J Biol Chem,* 286**,** 34839-50.

VRIJENHOEK, T., BUIZER-VOSKAMP, J. E., VAN DER STELT, I., STRENGMAN, E., GENETIC, R., OUTCOME IN PSYCHOSIS, C., SABATTI, C., GEURTS VAN KESSEL, A., BRUNNER, H. G., OPHOFF, R. A. & VELTMAN, J. A. 2008. Recurrent CNVs disrupt three candidate genes in schizophrenia patients. *Am J Hum Genet,* 83**,** 504-10.

WANG, L., ADAMSKI, C. J., BONDAR, V. V., CRAIGEN, E., COLLETTE, J. R., PANG, K., HAN, K., JAIN, A., Y. JUNG, S., LIU, Z., SIFERS, R. N., HOLDER, J. L. & ZOGHBI, H. Y. 2019. A kinome-wide RNAi screen identifies ERK2 as a druggable regulator of Shank3 stability. *Molecular Psychiatry*.

WANG, Q., AMATO, S. P., RUBITSKI, D. M., HAYWARD, M. M., KORMOS, B. L., VERHOEST, P. R., XU, L., BRANDON, N. J. & EHLERS, M. D. 2016. Identification of Phosphorylation Consensus Sequences and Endogenous Neuronal Substrates of the Psychiatric Risk Kinase TNIK. *J Pharmacol Exp Ther,* 356**,** 410-23.

WANG, X., MCCOY, P. A., RODRIGUIZ, R. M., PAN, Y., JE, H. S., ROBERTS, A. C., KIM, C. J., BERRIOS, J., COLVIN, J. S., BOUSQUET-MOORE, D., LORENZO, I., WU, G., WEINBERG, R. J., EHLERS, M. D., PHILPOT, B. D., BEAUDET, A. L., WETSEL, W. C. & JIANG, Y. H. 2011. Synaptic dysfunction and abnormal behaviors in mice lacking major isoforms of Shank3. *Hum Mol Genet,* 20**,** 3093-108.

WANG, X., XU, Q., BEY, A. L., LEE, Y. & JIANG, Y.-H. 2014. Transcriptional and functional complexity of Shank3 provides a molecular framework to understand the phenotypic heterogeneity of SHANK3 causing autism and Shank3 mutant mice. *Molecular Autism,* 5**,** 30.

WEGNER, W., MOTT, A. C., GRANT, S. G. N., STEFFENS, H. & WILLIG, K. I. 2018. In vivo STED microscopy visualizes PSD95 sub-structures and morphological changes over several hours in the mouse visual cortex. *Sci Rep,* 8**,** 219.

WENNERBERG, K., ROSSMAN, K. L. & DER, C. J. 2005. The Ras superfamily at a glance. *J Cell Sci,* 118**,** 843-6.

WOOLFREY, K. M., SRIVASTAVA, D. P., PHOTOWALA, H., YAMASHITA, M., BARBOLINA, M. V., CAHILL, M. E., XIE, Z., JONES, K. A., QUILLIAM, L. A., PRAKRIYA, M. & PENZES, P. 2009. Epac2 induces synapse remodeling and depression and its disease-associated forms alter spines. *Nat Neurosci,* 12**,** 1275-84.

WU, H. & PARSONS, J. T. 1993. Cortactin, an 80/85-kilodalton pp60src substrate, is a filamentous actin-binding protein enriched in the cell cortex. *The Journal of Cell Biology,* 120**,** 1417.

XIAO, B., TU, J. C., PETRALIA, R. S., YUAN, J. P., DOAN, A., BREDER, C. D., RUGGIERO, A., LANAHAN, A. A., WENTHOLD, R. J. & WORLEY, P. F. 1998. Homer Regulates the Association of Group 1 Metabotropic Glutamate Receptors with Multivalent Complexes of Homer-Related, Synaptic Proteins. *Neuron,* 21**,** 707-716.

XIAO, K., ALLISON, D. F., BUCKLEY, K. M., KOTTKE, M. D., VINCENT, P. A., FAUNDEZ, V. & KOWALCZYK, A. P. 2003. Cellular levels of p120 catenin function as a set point for cadherin expression levels in microvascular endothelial cells. *J Cell Biol,* 163**,** 535-45.

YAMADA, S., POKUTTA, S., DREES, F., WEIS, W. I. & NELSON, W. J. 2005. Deconstructing the cadherin-catenin-actin complex. *Cell,* 123**,** 889-901.

YI, F., DANKO, T., BOTELHO, S. C., PATZKE, C., PAK, C., WERNIG, M. & SUDHOF, T. C. 2016. Autism-associated SHANK3 haploinsufficiency causes Ih channelopathy in human neurons. *Science,* 352**,** aaf2669.

YUAN, L., SEONG, E., BEUSCHER, J. L. & ARIKKATH, J. 2015. δ-Catenin Regulates Spine Architecture via Cadherin and PDZ-dependent Interactions. *THE JOURNAL OF BIOLOGICAL CHEMISTRY* 290**,** 10947–10957.

ZENG, M., SHANG, Y., GUO, T., HE, Q., YUNG, W. H., LIU, K. & ZHANG, M. 2016. A binding site outside the canonical PDZ domain determines the specific interaction between Shank and SAPAP and their function. *Proc Natl Acad Sci U S A,* 113**,** E3081-90.

ZHANG, G., NEUBERT, T. A. & JORDAN, B. A. 2012. RNA binding proteins accumulate at the postsynaptic density with synaptic activity. *J Neurosci,* 32**,** 599-609.

ZHAO, Z. M., REYNOLDS, A. B. & GAUCHER, E. A. 2011. The evolutionary history of the catenin gene family during metazoan evolution. *BMC Evol Biol,* 11**,** 198.

ZHOU, Q., HOMMA, K. J. & POO, M.-M. 2004. Shrinkage of Dendritic Spines Associated with Long-Term Depression of Hippocampal Synapses. *Neuron,* 44**,** 749-757.

ZHU, J., ZHOU, Q., SHANG, Y., LI, H., PENG, M., KE, X., WENG, Z., ZHANG, R., HUANG, X., LI, S. S. C., FENG, G., LU, Y. & ZHANG, M. 2017. Synaptic Targeting and Function of SAPAPs Mediated by Phosphorylation-Dependent Binding to PSD-95 MAGUKs. *Cell Reports,* 21**,** 3781-3793.

ZITZER, H., HÖNCK, H.-H., BÄCHNER, D., RICHTER, D. & KREIENKAMP, H.-J. 1999. Somatostatin Receptor Interacting Protein Defines a Novel Family of Multidomain Proteins Present in Human and Rodent Brain. *Journal of Biological Chemistry,* 274**,** 32997-33001.

Appendix I

pmRFP-Shank3 plasmid map

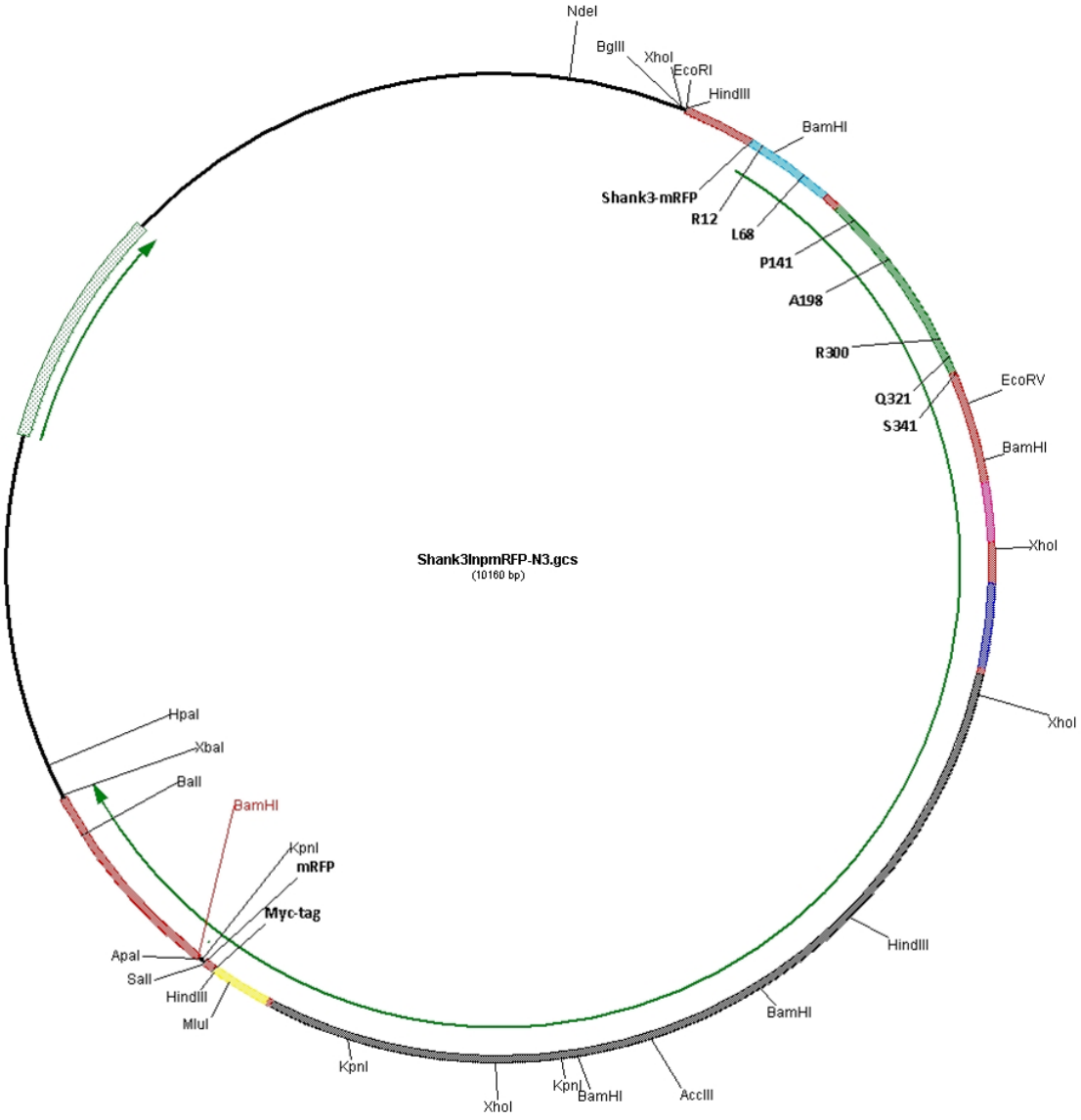

Appendix II

pHAGE-EGFP-Shank3 plasmid map

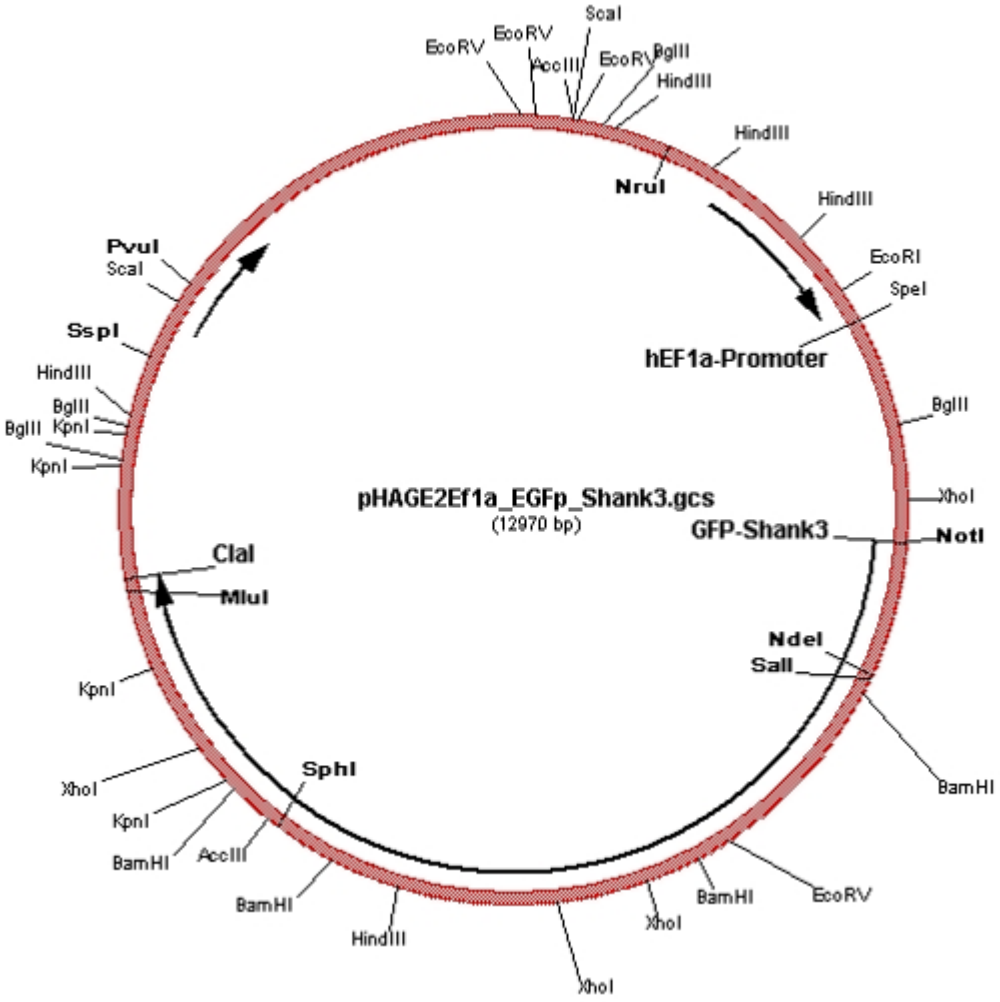

Appendix III

pEGFP-δ-Catenin plasmid map

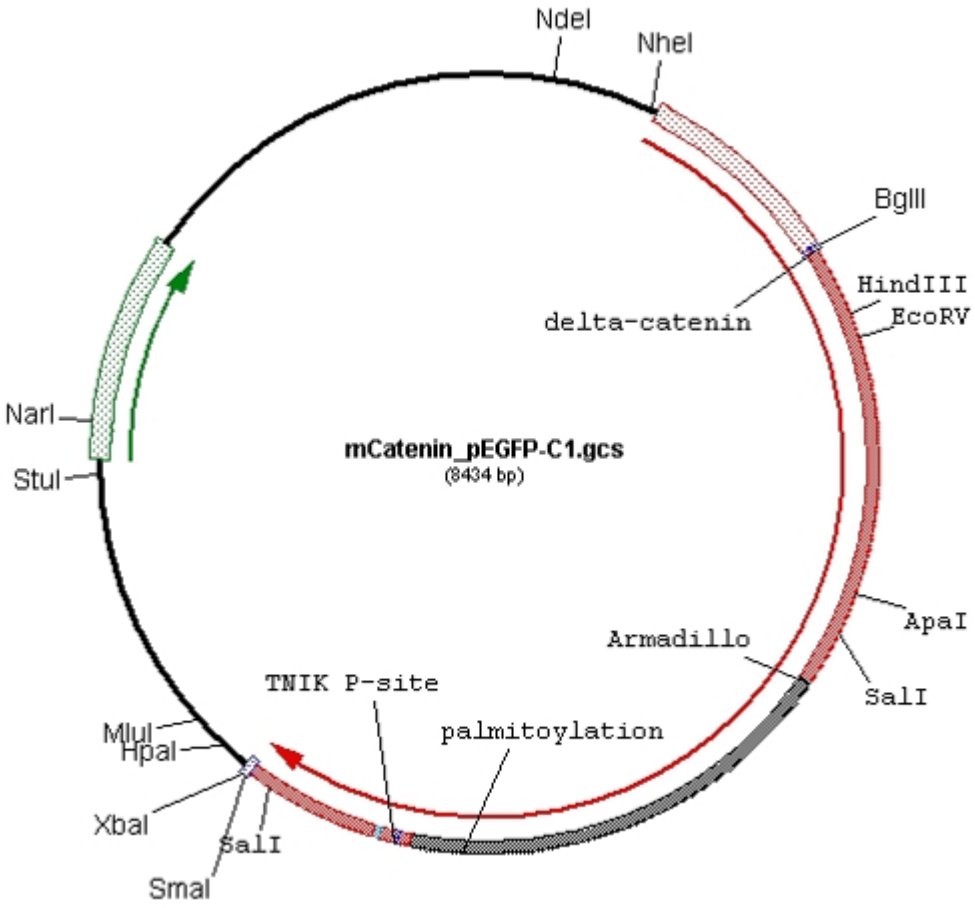

Appendix IV

pEmerald-β-Catenin plasmid map

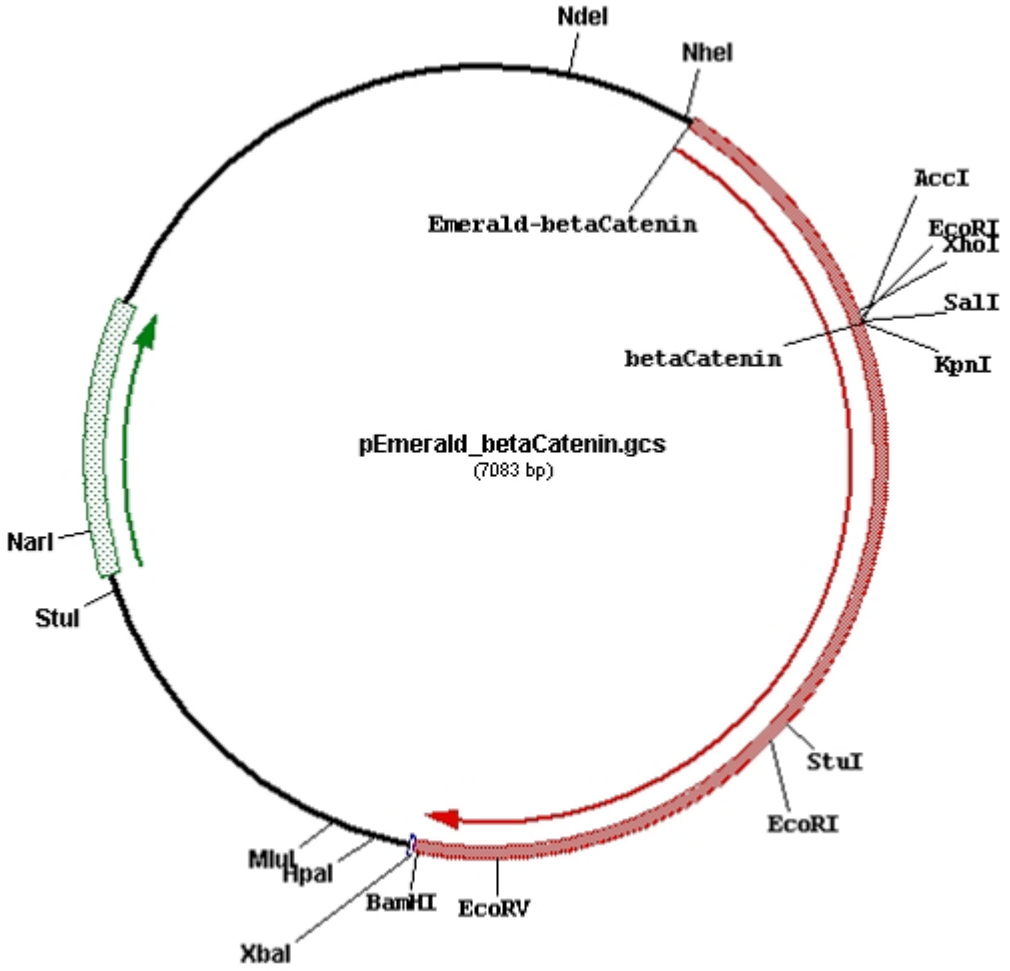

Eidesstattliche Versicherung
Declaration on oath

Hiermit erkläre ich an Eides statt, dass ich die vorliegende Dissertationsschrift selbst verfasst und keine anderen als die angegebenen Quellen und Hilfsmittel benutzt habe.
I hereby declare, on oath, that I have written the present dissertation by my own and have not used other than the acknowledged resources and aids.

Hamburg, den 19.02.2019 **Unterschrift**

Acknowledgments

I thank God for being present in every moment of my life and helping me to pass through all the difficulties and challenges in my life.

Thanks to my family for their love and eternal support from Iran.

My heartfelt gratitude to my supervisor Prof. Hans-Jürgen Kreienkamp for all his supports and for his trust in me that let me grow and find myself as a scientist in his lab.

Many thanks to my dear friend and colleague Edward Pan for his unwavering support throughout all these years.

Thanks to Victoria Martens for being my best friend and partner on the Shank project.

Thanks to Hans-Hinnrich Hönck for his admirable technical assistance.

Thanks to all who contributed to this work with their support, to Dr. Antonio Virgilio Failla and Dr. Bernd Zobiak from the UKE Microscopic Imaging Facility, to the UKE Core Facility for Mass Spectrometric Proteomics, and to our international collaborators: Dr. Igor Barsukov and Prof. Johanna Ivaska.

Thanks to Sabine Fleischer and Katja Husen from the ZMNH.

Thanks to the whole Institute of Human Genetics for accepting me in their team and for providing a friendly atmosphere throughout these years.

Thanks to the DAAD for the financial support and providing an opportunity for me to carry out my research in Germany.

This work is dedicated to my parents for giving me life and for their unconditional love.

Lebenslauf entfällt aus datenschutzrechtlichen Gründen.

UKE HAMBURG

Institut für Humangenetik

Universitätsklinikum Hamburg-Eppendorf | Martinistraße 52 | 20246 Hamburg
Institut für Humangenetik

Prof. Dr. Christian Kubisch
Direktor

Zentrum für Geburtshilfe, Kinder- und Jugendmedizin

Martinistraße 52
20246 Hamburg

Yingzhou Édward Pan
PhD student
Gebäude Nord 27, Raum 01.038
Telefon: +49 (0) 40 7410-54395
Fax: +49 (0) 40 7410-55138
Kreienkamp@uke.de
www.uke.de

Hamburg, 19.02.2019

To whom it may concern.

This is to certify:

1. that I am a citizen of Canada and that I am a native English speaker.

2. that the PhD thesis ("Autism-associated mutations interfere with the function of the Shank3 N-terminus in postsynaptic signaling pathways") written by my colleague, Fatemeh Hassani Nia, is written in correct English.

Sincerely Yours,

Edward Pan

(Yingzhou Edward Pan)